2-1-2006

Report on Field Measurements and Uncontrolled Load Testing of the Lehigh River Bridge (SR-33)

Robert J. Connor

Justin R. McCarthy

Report on Field Measurements and Uncontrolled Load Testing of the Lehigh River Bridge (SR-33)

Phase II

FINAL REPORT

by

Robert J. Connor

and

Justin R. McCarthy

ATLSS Report No. 06-12

February 2006

ATLSS is a National Center for Engineering Research on Advanced Technology for Large Structural Systems

117 ATLSS Drive
Bethlehem, PA 18015-4729

Phone: (610) 758-3525
Fax: (610) 758-5902

www.atlss.lehigh.edu
Email: inatl@lehigh.edu

Report on Field Measurements and Uncontrolled Load Testing of the Lehigh River Bridge (SR-33)

Phase II

FINAL REPORT

by

Robert J. Connor
Research Engineer
ATLSS Engineering Research Center

and

Justin R. McCarthy
Graduate Research Assistant
ATLSS Engineering Research Center

ATLSS Report No. 06-12

February 2006

ATLSS is a National Center for Engineering Research on Advanced Technology for Large Structural Systems

117 ATLSS Drive
Bethlehem, PA 18015-4729

Phone: (610) 758-3525
Fax: (610) 758-5902

www.atlss.lehigh.edu
Email: inatl@lehigh.edu

Table of Contents

LIST OF TABLES

Chapter Six

LIST OF FIGURES

Chapter Four

1.0 Introduction

This Final Report discusses the findings of the long-term monitoring and uncontrolled live load testing of the SR-33 truss bridge as of March 21, 2005. The bridge carries traffic over the Lehigh River, the Lehigh Canal, and a double set of Norfolk Southern railroad tracks. A view of the bridge looking northeast is shown in Figure 1.1. The purpose of the testing was to study the overall influence of temperature on the truss, determine the long-term effects of concrete creep and shrinkage on the instrumented members, and verify the behavior of selected truss members under vehicular live load. Additional instrumentation of the bridge was installed in July 2003 and vehicular live load data were collected for periods of time throughout 2004 and 2005.

Figure 1.1: Photograph of the SR-33 Lehigh River Bridge looking northeast at the west face of the bridge

The bridge is a four-span continuous haunched steel deck truss that is fully composite with the reinforced concrete deck. The main truss members (i.e., upper chords, lower chords and diagonals) are fabricated from structural steel plates into box or "H" shapes. The steel stringers, sway bracing, and cross bracing members are all rolled "W" shapes. The bridge is unique in that the reinforced concrete deck is not only composite with the longitudinal stringers and transverse floorbeams, but also with the upper chord members of the truss. It is the only fully composite deck truss bridge in Pennsylvania and quite possibly in the United States. An elevation view of the bridge with sequence of concrete deck pours is shown in Figure 1.2 and a typical cross-section at midspan of the main river span is shown in Figure 1.3.

All instrumentation and testing was conducted by personnel from Lehigh University's Center for Advanced Technology for Large Structural Systems (ATLSS), located in Bethlehem, PA.

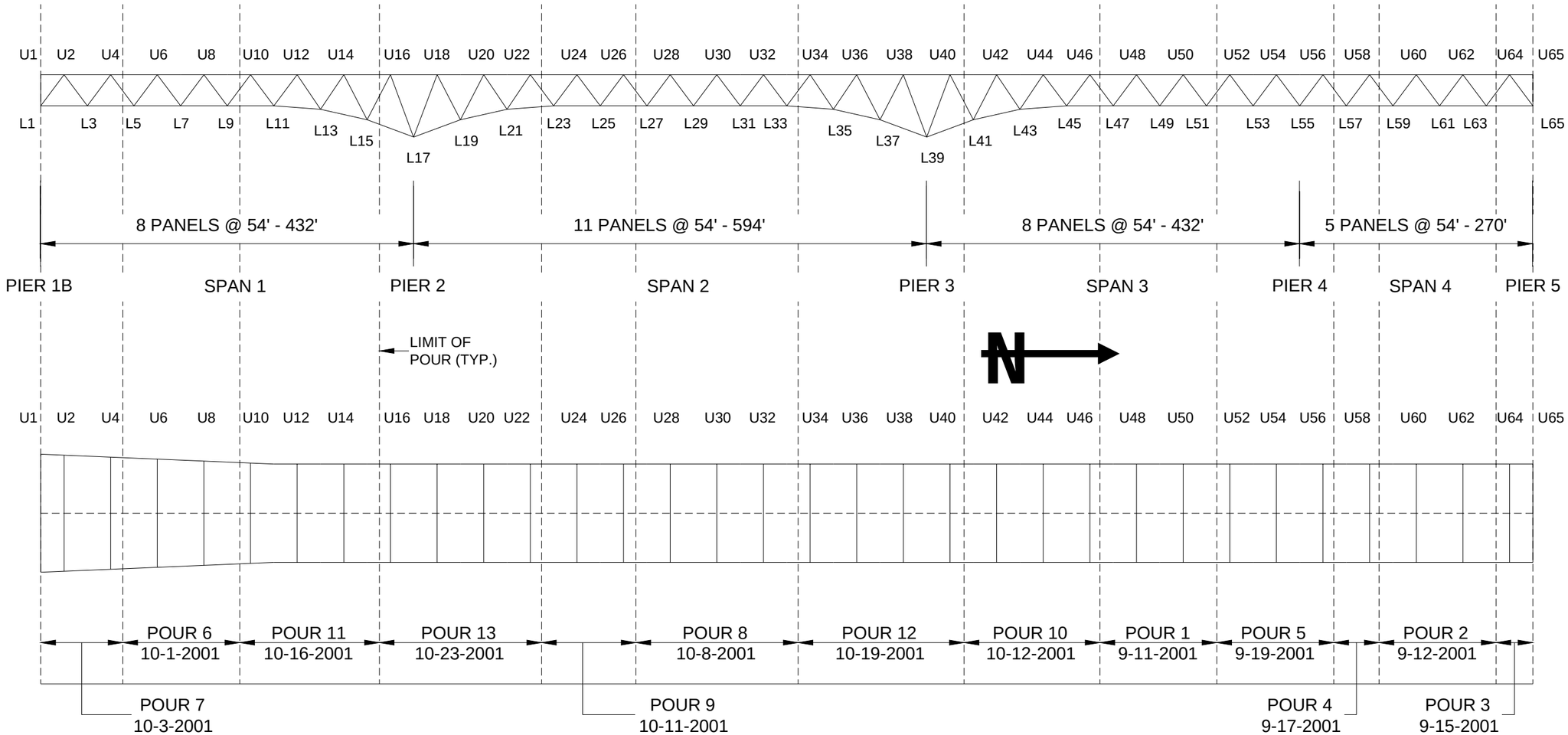

See pages 27-37 and 42-43 for gage locations

Figure 1.2 - Elevation view of Lehigh River Bridge and illustration of deck pours

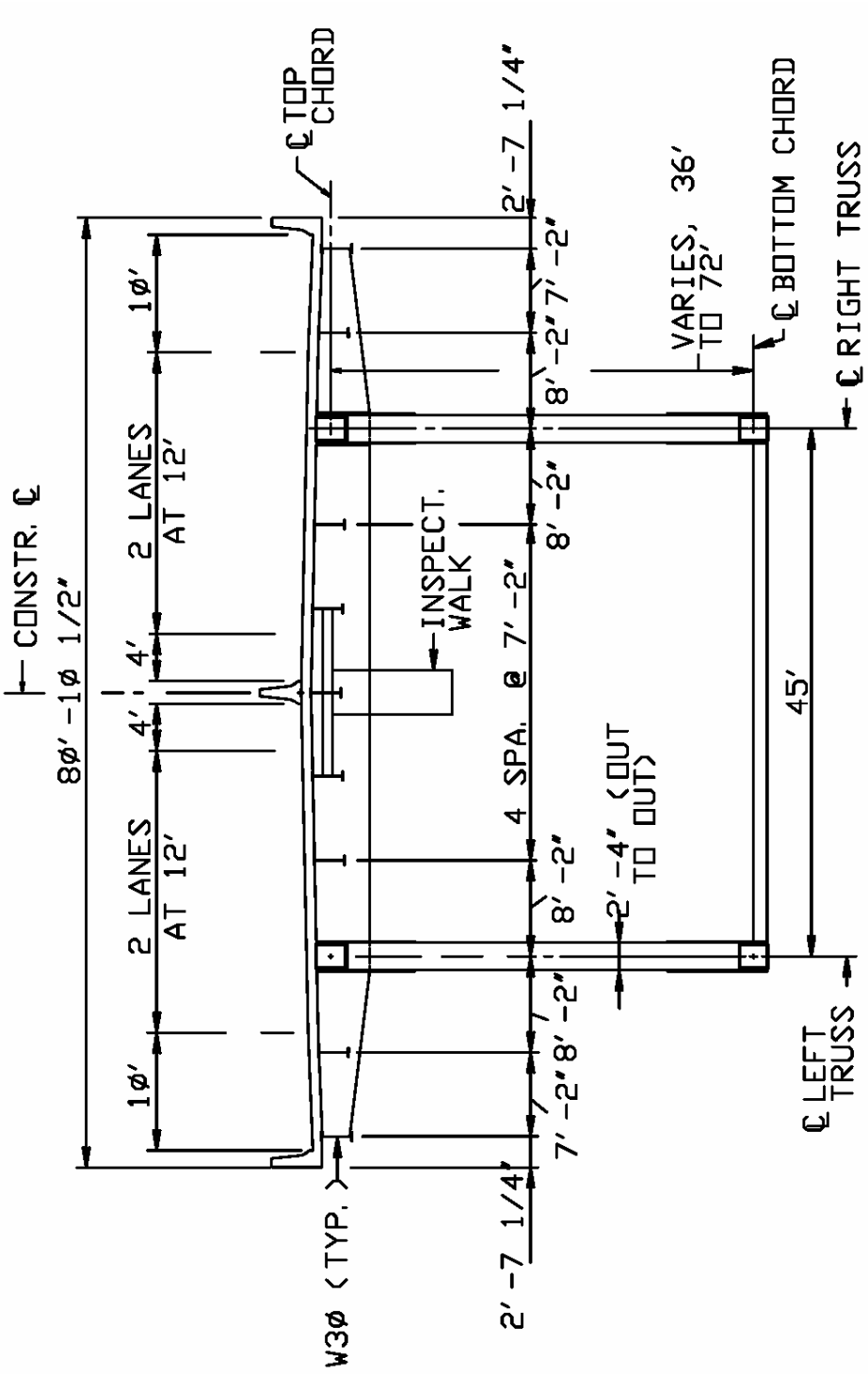

Figure 1.3: Typical cross-section of bridge at midspan

2.0 Summary of Previous (Phase I) Work

Instrumentation of Phase I of the project began in May of 2001. Selected members were chosen to monitor the effects of strain and temperature changes before and after deck placement and response during construction. The response of the truss to controlled live load testing conducted in January 2002, was also studied. A summary of these findings is presented in the following sections. A more detailed discussion of the Phase I work can be found in ATLSS Report 02-07 "Report on Field Measurements and Controlled Load Testing of the Lehigh River Bridge (SR-33)" (Connor and Santosuosso, 2002).

2.1 Monitoring During Construction

2.1.1 Effect of Temperature Changes Before Deck Placement

As previously stated in ATLSS Report 02-07, vibrating wire strain gages were used to measure the long-term changes in strain on selected truss members and within the reinforced concrete deck. A more detailed discussion of the instrumentation and data acquisition system is included in Section 3.0 of this report.

Figure 2.1 shows the comparison of measured temperatures on the east upper chord (U16-U18 East). The figure shows that the temperature of the upper chord remained fairly uniform within the member. The bottom gage remained cooler by only a few degrees. Similar temperature distributions were observed for both upper chords.

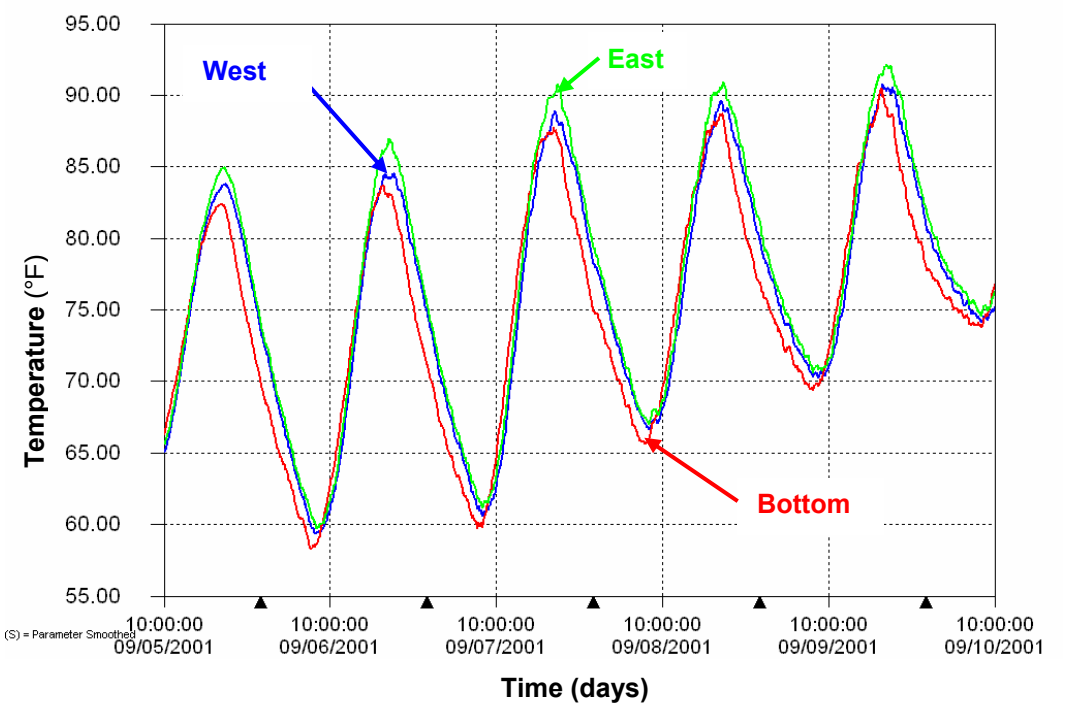

Figure 2.1: Comparison of measured temperature on east upper chord (U16-U18 East) during early September 2001

Figure 2.2 indicates the temperatures of the top and bottom surfaces of the west lower chord (L25-L27 West). Also, the temperatures for the top and bottom surfaces of

stringer 1 are presented. As expected, the temperature of the top surface of the members reaches a much higher temperature than the bottom surface. Temperatures are a minimum between 6 AM and 8 AM in the morning. Overall, the data indicates that temperatures on the east and west face of a member remain relatively uniform throughout the day. However, temperatures on the top and bottom surfaces of a member are quite different due to the exposure of the top surface to the sun.

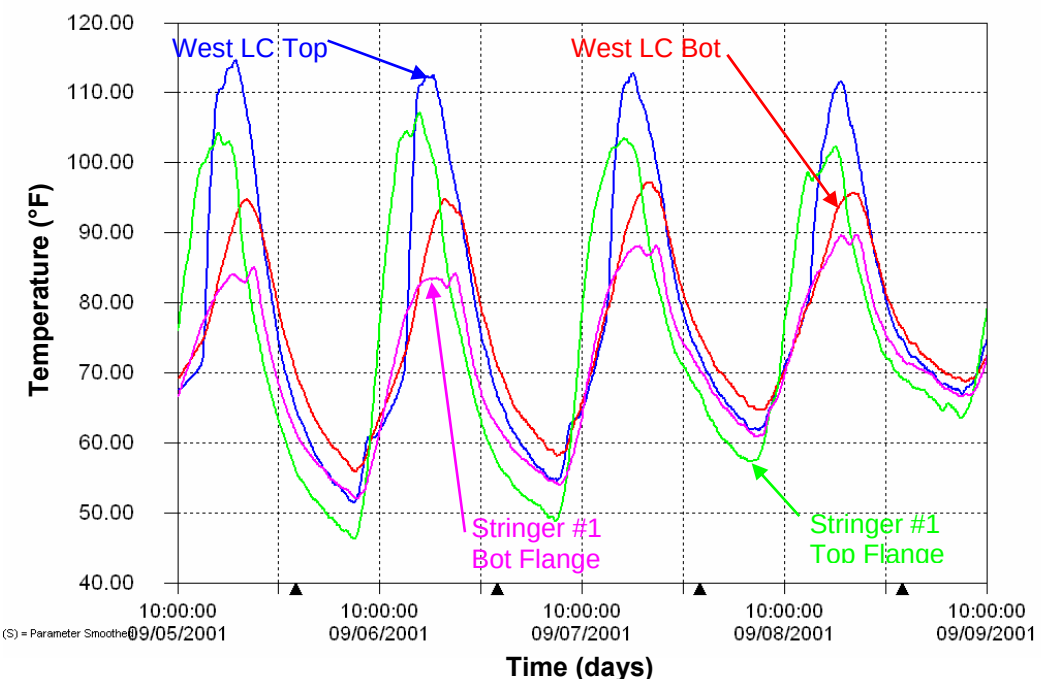

Figure 2.2: Comparison of measured temperature on top and bottom surface of west lower chord L25-L27 and stringer 1 between U16 and U18 during early September

2.1.2 Effect of Temperature Changes After Deck Placement

Placement of the concrete deck was completed on October 23, 2001. A sequence of the pours is shown in Figure 1.2. Members that were directly in contact with the concrete such as the stringers and the upper chords, responded differently to changes in temperature after the concrete deck was placed. Figure 2.3 shows a comparison of temperatures on selected truss members. A vertical line indicates when placement of the concrete was completed. The data are from the period September 28, 2001 through November 23, 2001.

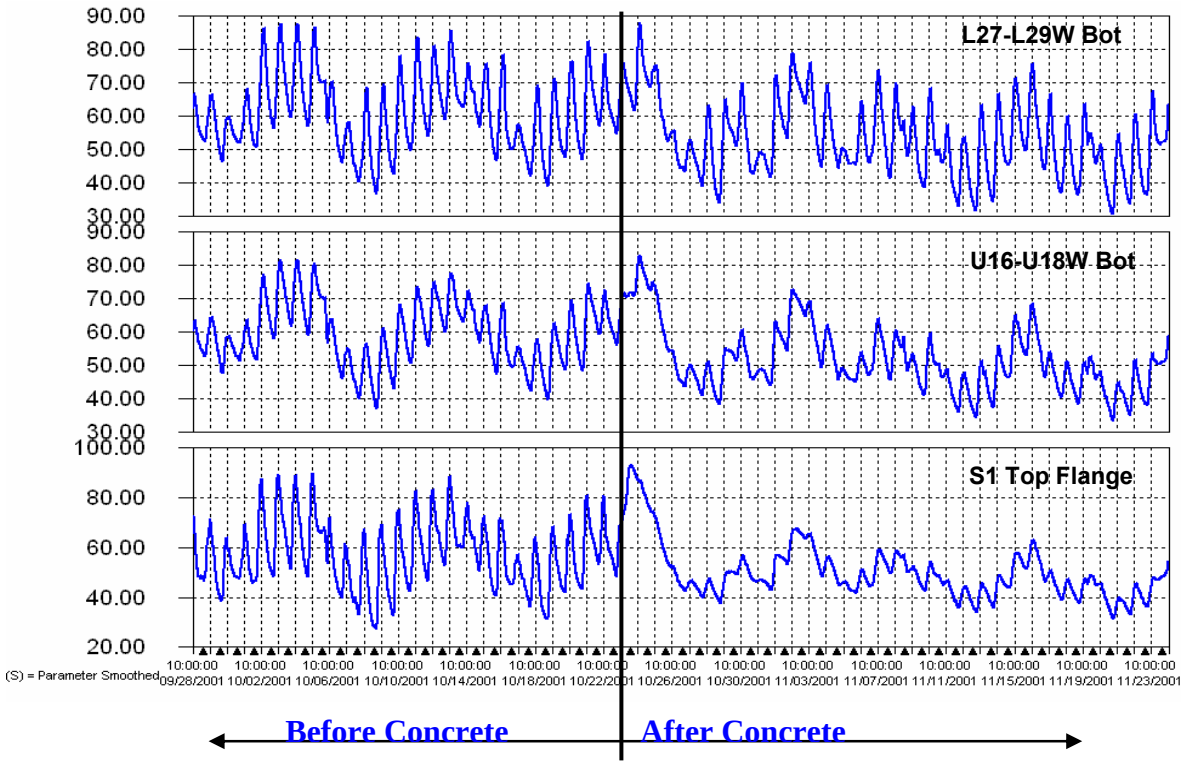

Figure 2.3: Comparison of temperatures of selected truss members

There is an increase in temperature in the upper chord and stringer as a result of the concrete placement. It should be noted that the temperature remains above 70 degrees for about two days and then gradually cools. This is due to the increase in temperature of the concrete from the hydration process. After placement of the deck was completed on October 23, the amplitude of the daily temperature cycles in the upper chord and stringer are greatly reduced. This is due to the fact that the members are shaded by the deck and that the thermal mass of the system was greatly increased by the addition of the concrete. Hence, the upper chords and stringers are not as sensitive to changes in temperature.

2.1.3 Response During Closure of the Main River Span – Span 2

Closure of the main river span took place over a three day period from August 7th through August 9th 2001. Strains were measured during closure of the truss. Figure 2.4 illustrates the truss closure process. The members that could potentially be affected during closure were both of the lower chords at L25-L27 and both of the upper chords at U16-U18. The gages on L27-L29 could not be connected during closure. It should be noted that just prior to closure, the gages were digitally zeroed to measure relative changes in strain. The measurements made during the closure period did not indicate that any significant stresses were induced. Little effort was required to bring the north and south portions of the truss together. Furthermore, the connections were not fully tightened allowing the truss to maintain relative flexibility.

East lower chord in place.
(August 7 – 9:48 AM)

East lower chord, upper chord and diagonal in place. (August 8 – 7:22 AM)

East lower chord, upper chord and diagonal in place. West lower chord being lifted.
(August 8 – 7:43 AM)

East lower chord, upper chord and diagonal in place. West lower chord and diagonal in place, west upper chord being lifted.
(August 8 – 9:40 AM)

Figure 2.4: Stages of closure of the main river span (all photographs looking east)

2.1.4 Response During Placement of Concrete Deck

The concrete deck was placed in thirteen different steps (Figure 1.2) that began on September 11, 2001 and ended on October 23, 2001. The effects from the first five pours had very little effect on the instrumented members of span 2. Also, some pours by themselves had very little effect. Therefore, the effects of pours 6 and 7 were grouped together and pours 10, 11 and 12 were grouped together to see a noticeable change in stress in the members.

Figure 2.5 shows the typical response of the east upper chord to deck pours 6 through 13. The effects from the pours can be seen in the data as the increase in mean strain in the member. The most noticeable increase is seen during pour 13. The upper chord experiences a large increase in strain but then decreases immediately thereafter. This is believed to be the result of multiple factors. The increased temperature of the concrete produced a certain amount of thermal stress in the member. Furthermore, the Bidwell machine and other equipment could have resulted in an increase in stress.

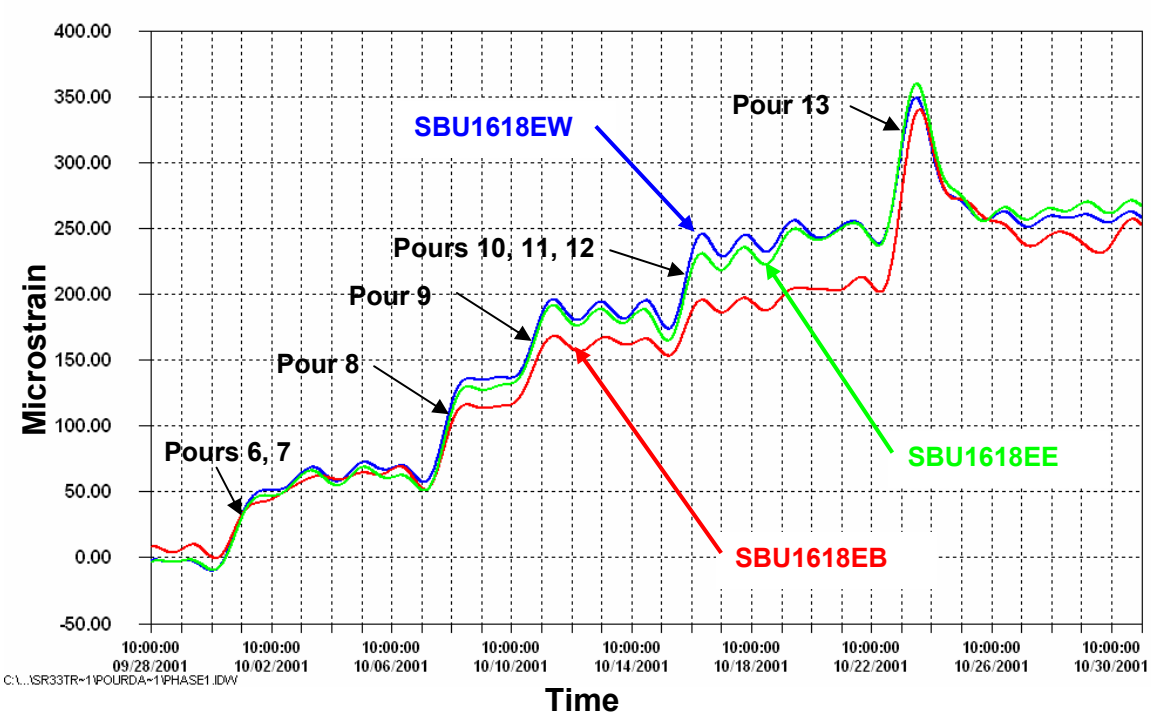

Figure 2.5: Response of east upper chord U16-U18 to placement of concrete during pours 6 through 13

The change in strain for each pour or group of pours is shown in Table 2.1. The data listed was selected at the mean temperature of the day immediately before and after the pour. The total change in strain listed in the last column labeled "Total" is based on the difference in measured strains at the end of pour 5 and the end of pour 13. The upper chord behaved as expected throughout placement of the deck.

Gage	Location	Pour # (micro-strain)					
		6 + 7	8	9	10 + 11 + 12	13	Total
SBU16U18EW	East U.C. West face	70	69	51	55	10	**260**
SBU16U18EB	East U.C. Bottom face	50	56	44	35	36	**240**
SBU16U18EE	East U.C. East face	65	69	51	55	13	**270**
SBU16U18WW	West U.C. West face	62	65	49	62	29	**270**
SBU16U18WB	West U.C. Bottom face	56	69	55	44	58	**290**
SBU16U18WE	West U.C. East face	58	67	51	58	15	**260**

Table 2.1: Measured strains in upper chord U16-U18 due to placement of concrete deck

Vibrating wire gages were installed on the top and bottom faces of the lower chords between panel points L25 and L27 and between panel points L27 and L29. The output from these gages was noisier (i.e. contained more spurious data) than those installed on the upper chords. The length of the wires for these gages most likely caused interference problems. Reliable data were still obtained, although difficult to interpret at times. Questionable data are followed by a "?" in Table 2.2. As noted before, the total

change in strain from the end of pour 5 to the end of pour 13 is noted in the last column labeled "Total". The response of the lower chords between panel points L25 and L27 is shown in Table 2.2. The lower chords between L27 and L29 exhibited similar behavior. All lower chords behaved as expected throughout deck placement.

Gage	Location	Pour # (micro-strain)							
		1 to 5	6 + 7	8	9	10 + 11	12	13	Total
SBL2527EB	East L.C. Bottom face	-50	-50	190	160	-60	10	40	**180**
SBL2527ET	East L.C. Top face	-60	-60	220	200	-30	20	40	**200**
SBL2527WB	West L.C. Bottom face	-60	-60	180	160	-60	*10?*	*90?*	**200**
SBL2527WT	West L.C. Top face	-70	-60	210	190	-90	10	50	**230**

Table 2.2: Measured strains in lower chord L25-L27 due to placement of concrete deck

Vibrating wire strain gages were installed on the east and west flange plates of the diagonal members between L20 and U21. The output from the gages was noisy, however reliable data were obtained. Table 2.3 summarizes the response of the diagonal members to deck placement. The diagonals between U18 and L19 behaved similarly with smaller magnitudes of change in strain. The diagonals behaved as expected throughout deck placement.

Gage	Location	Pour # (micro-strain)							
		1 to 5	6 + 7	8	9	10 + 11	12	13	Total
SDW2021EE	East Diag. East Face	-20	-10	140	240	-70	10	100	**470**
SDW2021EW	East Diag. West Face	-20	-20	120	170	-60	10	100	**350**
SDW2021WE	West Diag. East Face	-20	-20	120	200	-50	10	100	**380**
SDW2021WW	West Diag. West Face	-30	-20	130	230	-60	10	100	**430**

Table 2.3: Measured strains in diagonal U20-L21 due to placement of concrete deck

Vibrating wire strain gages were installed on the top and bottom flange plates of each of the three members making up the sway bracing between panel points L9 and U10. The output from these gages was also noisy, but reliable data were obtained. Table 2.4 summarizes the response of the sway bracing to placement of the concrete deck. The sway bracing between U24 and L25 behaved similarly, however not all of the gages were functioning properly. Overall, the sway bracing members behaved as expected throughout placement of the deck.

Gage	Location	Pour # (micro-strain)							
		1 to 5	6 + 7	8	9	10 + 11	12	13	Total
SSB910ET	East Cross of Sway	-90	30	20	20	-20	0	10	**10**
SSB910EB	East Cross of Sway	-70	30	20	10	-10	0	0	**30**
SSB910WT	West Cross of Sway	-80	80	30	0	-20	-10	10	**50**
SSB910WB	West Cross of Sway	-80	60	30	0	0	-10	10	**20**
SSB910HT	Horiz. Strut of Sway	-40	-150	30	-50	-70	-40	20	**-140**
SSB910HB	Horiz. Strut of Sway	-50	-150	50	-40	-50	-30	20	**-130**

Table 2.4: Measured strains in sway bracing L9-U10 due to placement of concrete deck

Vibrating wire strain gages were installed on the top and bottom flanges of each of the instrumented stringers between panel points U16 and U18 above pier 2. Output from these gages was less noisy and reliable data were obtained. Table 2.5 summarizes the response of the stringers to the pour sequence of the deck. Overall, the stringers behaved as expected throughout placement of the deck.

Gage	Location	Pour # (micro-strain)							
		1 to 5	6 + 7	8	9	10 + 11	12	13	Total
S1TOC	Top Fl. Of S1 18" N of U16	40	0	0	-20	120	0	190	**380**
S1BOC	Bot. Fl. Of S1 18" N of U16	0	10	0	-20	-100	0	-100	**-250**
S2TOC	Top Fl. Of S2 18" N of U16	-10	0	10	0	20	0	-40	**0**
S2BOC	Bot. Fl. Of S2 18" N of U16	-20	10	10	20	0	10	-50	**-70**
S3TOC	Top Fl. Of S3 18" N of U16	30	0	10	-20	20	-30	-40	**0**
S3BOC	Bot. Fl. Of S3 18" N of U16	-20	10	20	0	-20	-10	-30	**-80**
S7TCL	Top Fl. Of S7 27' N of U16	-10	-10	0	0	0	0	-280	**-270**
S7BCL	Bot. Fl. Of S7 27' N of U16	0	20	30	10	0	10	270	**270**
S8TCL	Top Fl. Of S8 27' N of U16	-	-	-	-	-	-	-	**-**
S8BCL	Bot. Fl. Of S8 27' N of U16	0	10	10	10	-10	0	200	**220**

Table 2.5: Measured strains in stringers between U16 and U18 due to placement of concrete deck

2.2 Results of the Controlled Load Tests

Results of the controlled live load monitoring conducted on January 4, 2002, two weeks before the bridge opened are summarized in this section. The effects of vehicle speed and position on the bridge deck are considered. Figure 2.6 illustrates the lane positions used for the controlled live load tests.

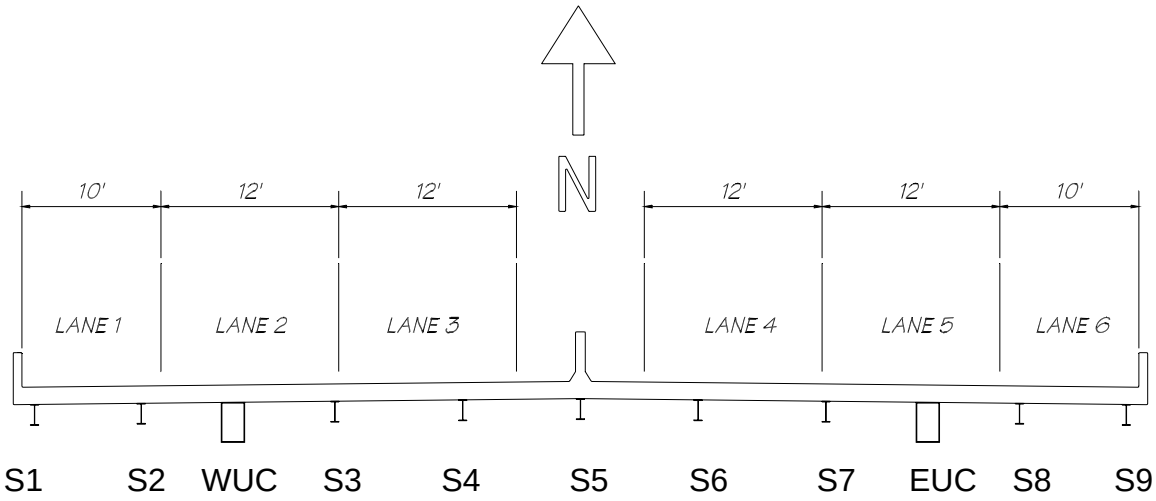

Figure 2.6: Deck cross-section and lane demarcation (Looking North)

Test Trucks

For the controlled load tests, three tri-axle dump trucks were used in order to produce measurable stresses in the main truss members. Trucks #67, #68, and #80 had gross vehicle weights (GVW) of 78.3 kips, 74.1 kips, and 84.8 kips respectively. They were loaded with earth from a nearby site. Individual axle loads were measured by a Penn DOT Weigh Team. Details pertaining to each test truck are included in the Tables 2.5 and 2.6. All test trucks possessed a "floating" third rear axle. This axle can be lowered using air pressure in order to distribute the rear load to three axles. The third axle was in the "up" position for all controlled load tests.

Test Description	Rear Axle Type	Front Axle Load (lb)	First Rear Axle Load (lb)	Second Rear Axle Load (lb)	GVW[1] (lb)	Truck #
Controlled Load Tests	Tandem[2]	15,300	31,800	31,150	78,250	67
	Tandem[2]	15,800	29,330	28,970	74,100	68
	Tandem[2]	17,450	33,250	34,050	84,750	80

Notes
1. GVW=Gross Vehicle Weight
2. Both trucks had a floating third rear axle that was in the "up" position for all tests.

Table 2.6 - Test truck axle load data

Truck	L1 (in)	L2 (in)	Wf (in)	Wr (in)	A[1] (in)	B (in)	C (in)	D[1] (in)	E (in)
Truck # 67[2]	195	52	81.5	72.5	-	9.25	21.5	-	8.5
Truck # 68[2]	193	56	81.5	69.5	-	9.5	22.0	-	8.5
Truck # 80[2]	193	56	81.5	71.5	-	9.0	22.0	-	9.0

Notes
1. This dimension was not measured.
2. All trucks had a floating third rear axle that was in the "up" position for all tests.

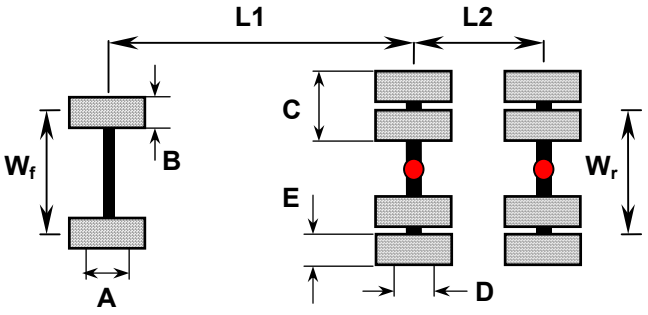

Table 2.6 - Geometry of trucks used for controlled load tests

2.2.1 Upper Chord Response

Uniaxial strain gages were installed on the centerline of the bottom web plate and at mid-depth on both side flange plates of the upper chords at mid-length between U16 and U18. They were positioned to measure any axial force or bending moment at midspan and to determine the neutral axis of the composite upper chord. Park tests were conducted in lanes 2 through 6. The field van, where the laptop was set up during the controlled live load monitoring, was positioned in lane 1 throughout the tests.

A typical upper chord response to a park test in lane 2 is seen in Figure 2.7. The plot shows that a load placed on the west side of the bridge has very little effect on the east side members. The most notable feature is the occurrence of two plateaus. The first plateau represents the static placement of the back axles over the gages located eighteen inches north of the centerline of the floorbeam at U16. The second plateau represents static placement of the back axles of the truck over the strain gages located at midspan of U16-U18. All park tests exhibit these two plateaus.

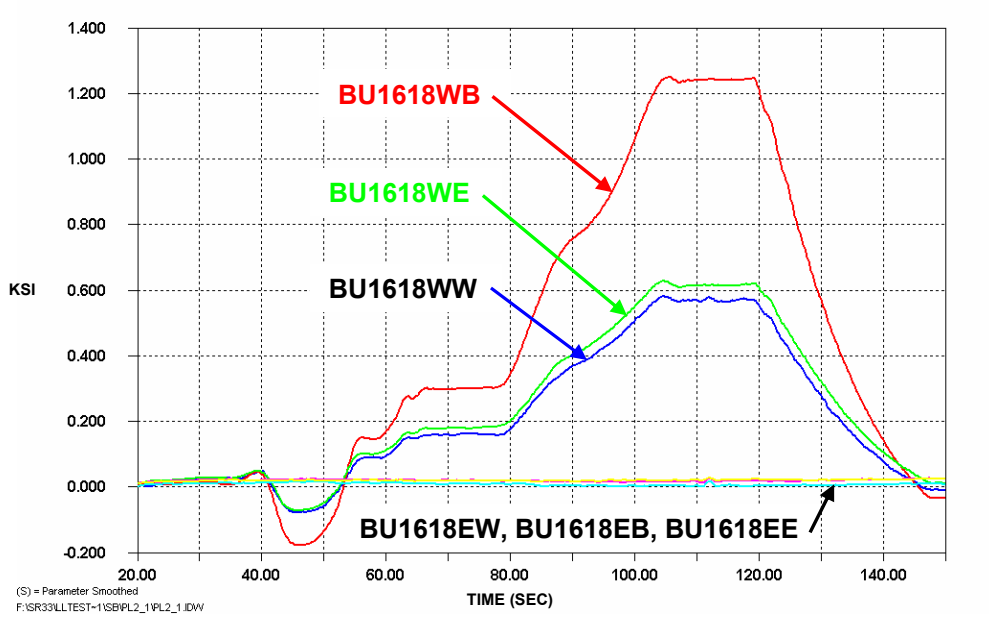

Figure 2.7: Typical upper chord response to a park test in lane 2
(Truck #80 in lane 2 headed north)

It can also be shown that the upper chords behave similarly about the centerline of the bridge. In other words, members that are symmetrical about the bridge centerline exhibit the same output for comparable loads. For example, when lane 2 is loaded the west upper chord gages display the same output as the east upper chord gages when lane 5 is loaded.

Crawl tests (approximately 5 mph) were conducted in each lane of the bridge. Tests were repeated 2 to 3 times to verify the results. Figure 2.8 is the typical response of the west upper chord U16-U18 to a truck traveling in lane 2. It was also shown that superposition is valid for the upper chord members. For example, individual crawl tests run separately for lanes 2 and 3 would produce the same stresses for a test with two trucks running together in lanes 2 and 3.

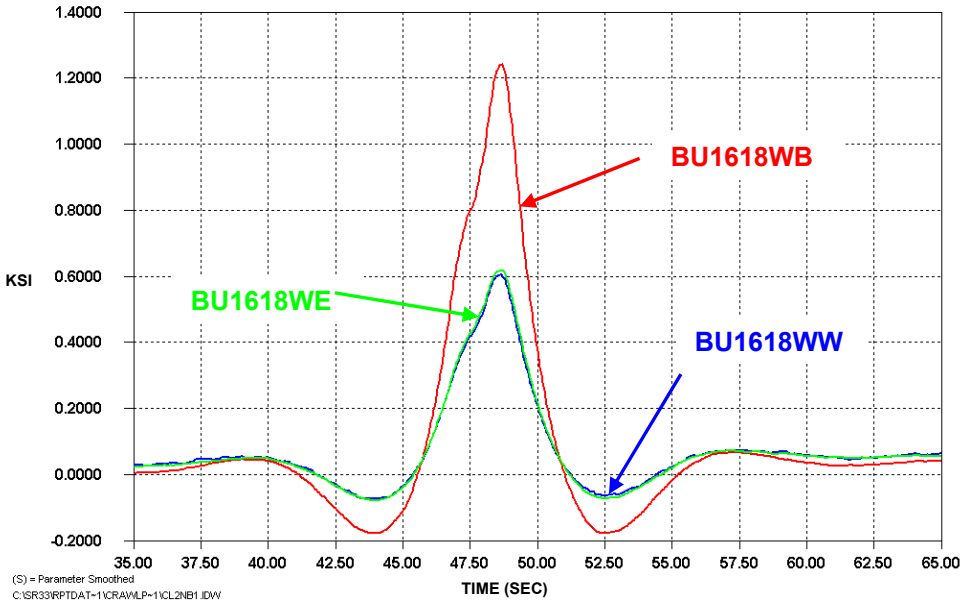

Figure 2.8: Typical west upper chord response during a crawl test in lane 2
(Truck #80 in lane 2 headed north)

Dynamic tests were run in each lane at approximately 45 mph. A comparison of the response of the west upper chord to a dynamic and crawl test run in lane 2 is shown in Figure 2.9. The figure clearly shows that there is little dynamic amplification factor (approximately 3% to 5%). The dynamic amplification factor is the ratio of stress caused by a dynamic test to the stress caused by a crawl test. It should be noted that the relatively low dynamic amplification factor observed is due to the quality of the concrete deck at the time of the testing. Deterioration of the wearing surface would increase the dynamic amplification factor. The primary response of the upper chord to the crawl and dynamic tests was local member bending.

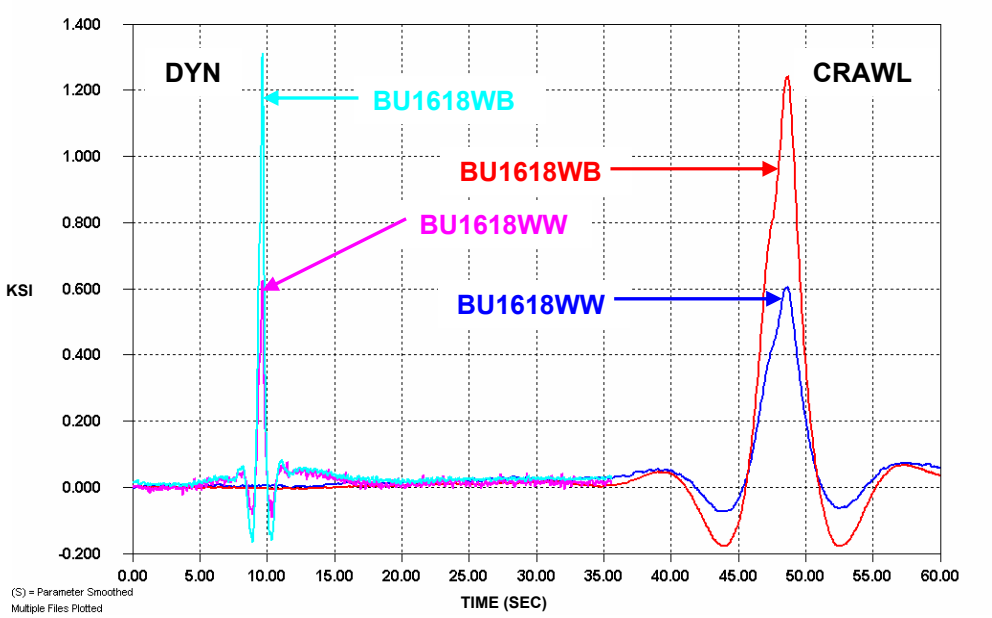

Figure 2.9: Comparison of crawl and dynamic tests in lane 2
(Truck #80 headed north)

2.2.2 Lower Chord Response

The locations of the strain gages installed on the lower chords were between L25 and L27 and between L27 and L29. Because the park tests were conducted over U16-U18, they had little effect on the lower chords. The results of the subsequent crawl and dynamic tests describe the behavior of the lower chord.

Figure 2.10 represents the largest single stress cycle measured in the lower chord L27-L29. This test was performed with all three trucks bumper to bumper forming a train of trucks. This particular arrangement was used to show that the lower chords primarily behave globally and axially. The stress plots from the top and bottom gages are essentially identical. This means there is little bending, if any, in the member. A similar test for the upper chord would have shown three distinct stress cycles compared to one stress cycle observed in the lower chord.

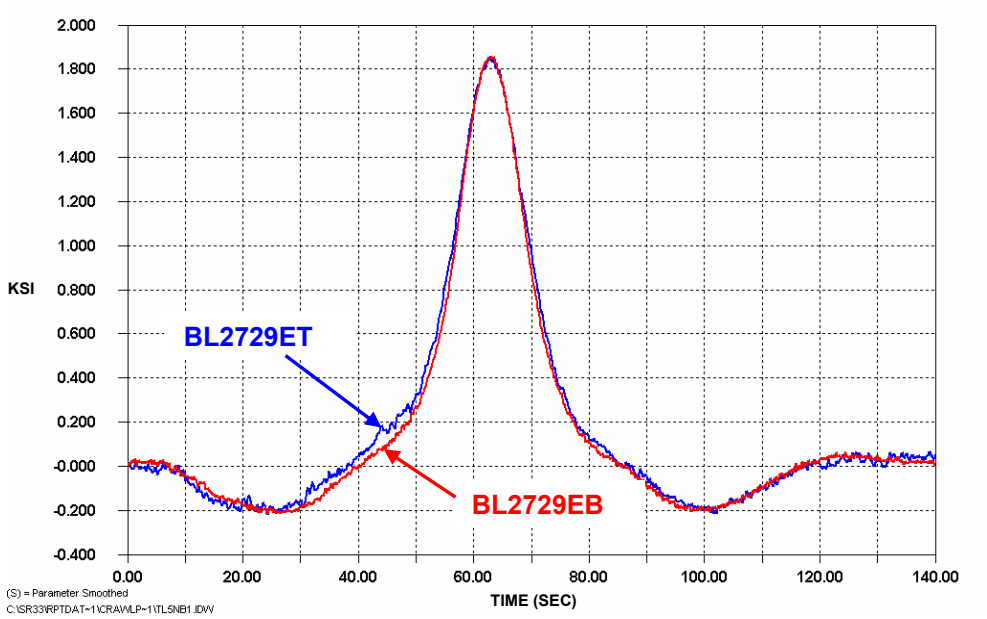

Figure 2.10: Typical lower chord response
(Truck "train" in lane 5)

Figure 2.11 describes the behavior of all four bottom gages on the lower chords with trucks in lanes 4, 5 and 6 traveling northbound. A few important conclusions can be drawn from this plot. The first point to be noted is that the lower chord members experience small stress reversals as the trucks cross the piers. The lower chord inflection point (LCIP) on the left marks where the trucks cross pier 2 and the LCIP on the right marks where they cross pier 3. Simple calculations were shown that the trucks traveling at approximately 6 mph would have crossed the piers where the lower chord inflection points occur. The peak stresses in the members occur when the trucks are directly over the gages. Also, the figure shows that when the load is outside of the span between piers 2 and 3, the lower chords of the two trusses act together more equally. When the main span is loaded however, the chords on that side of the bridge carry most of the load. Overall, the lower chords responded in a global and axial manner.

As expected, the lower chords exhibited very little dynamic amplification factor as seen in Figure 2.12. This was expected since the truss acted in a global manner as described by the crawl test data. The response of the lower chords to dynamic testing was comparable to crawl testing. The lower chords remained as global and axial members.

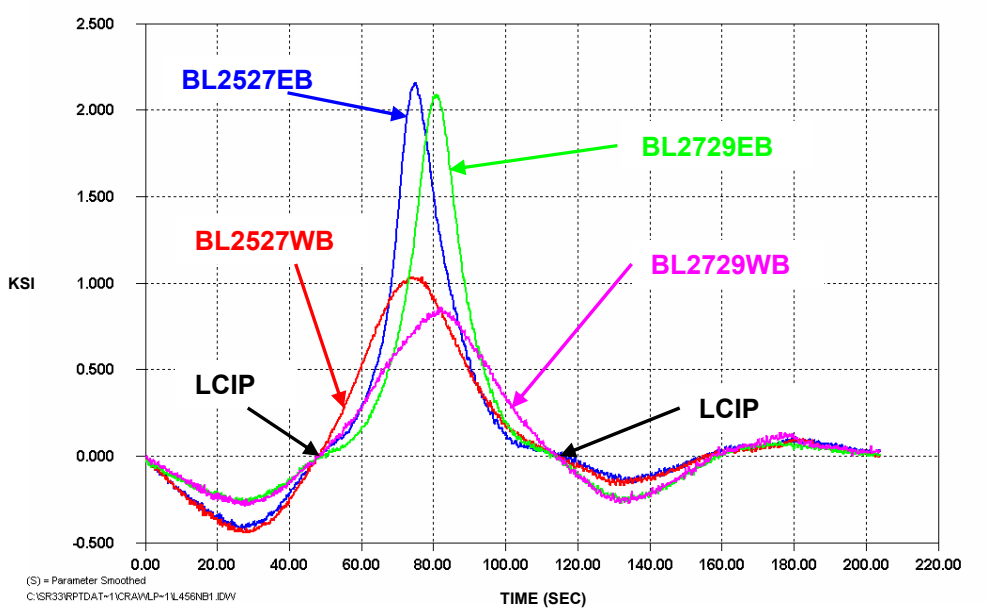

Figure 2.11: Typical lower chord response for adjacent lower chord members

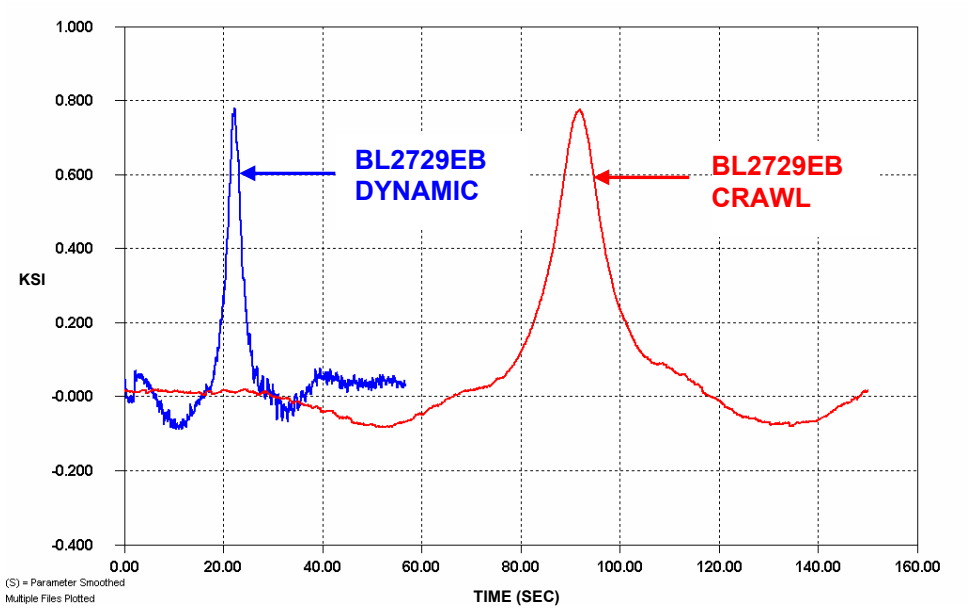

Figure 2.12: Typical dynamic vs. crawl amplitude for the lower chord
(Truck #80 in lane 5)

2.2.3 Diagonal Response

The instrumented diagonal members showed very little response to the park tests conducted at U16-U18 over pier 2. The subsequent crawl and dynamic test results will describe the behavior of the diagonals.

The response of diagonals U18-L19 and U20-L21 on the east truss is shown in Figure 2.13. This figure represents the largest stress cycle caused by a single truck in lane 6. The diagonals primarily exhibit an axially behavior which would be expected.

However, the figure below illustrates a noticeable bending component from the stress reversal on one side of the member and the absence of this reversal on the other side. This out of plane bending was most noticeable when the shoulder (lane 6) was loaded. Nevertheless, this out of plane bending was consistent with expected behavior since lane 6 is cantilevered outside of the truss. Similar behavior would be expected on the west truss diagonals if lane 1 were loaded.

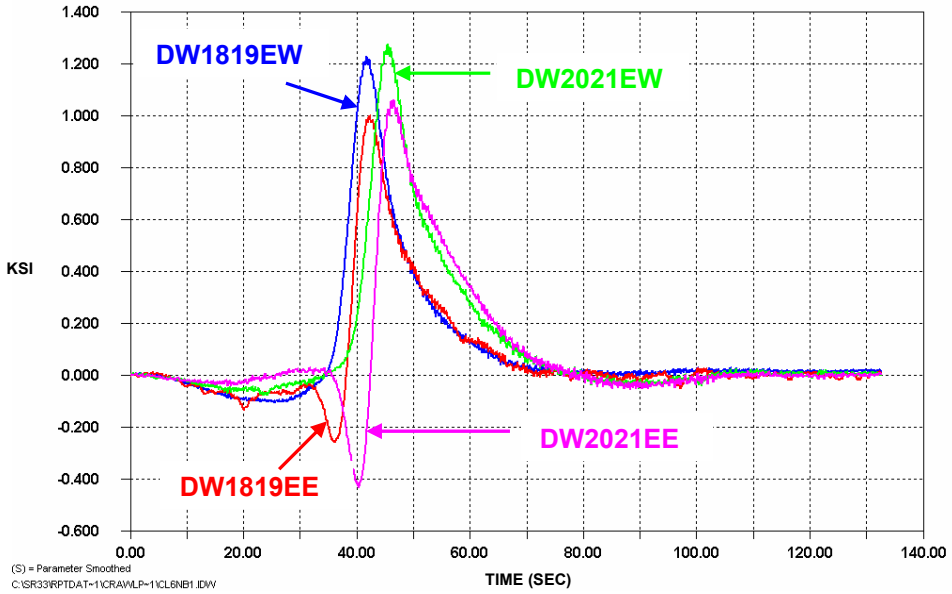

Figure 2.13: Typical east diagonal response to a crawl test in lane 6
(Truck #80 headed north in lane 6)

As with the upper chords, the validity of superposition holds for the diagonal members. Stresses could be added for individual tests in separate lanes to achieve the result from a test conducted in two lanes at once. Little dynamic amplification was expected for the diagonal members since they exhibit a global and axial response much like the response of the lower chords. Figure 2.14 plots the response of the strain gages on the east flange of the west diagonals for crawl and dynamic tests. The figure clearly shows that there is little, if any, dynamic amplification factor for the diagonals. Overall, the response of the diagonals to dynamic testing was comparable to the response due to crawl testing. The diagonals exhibited primarily a global and axial response.

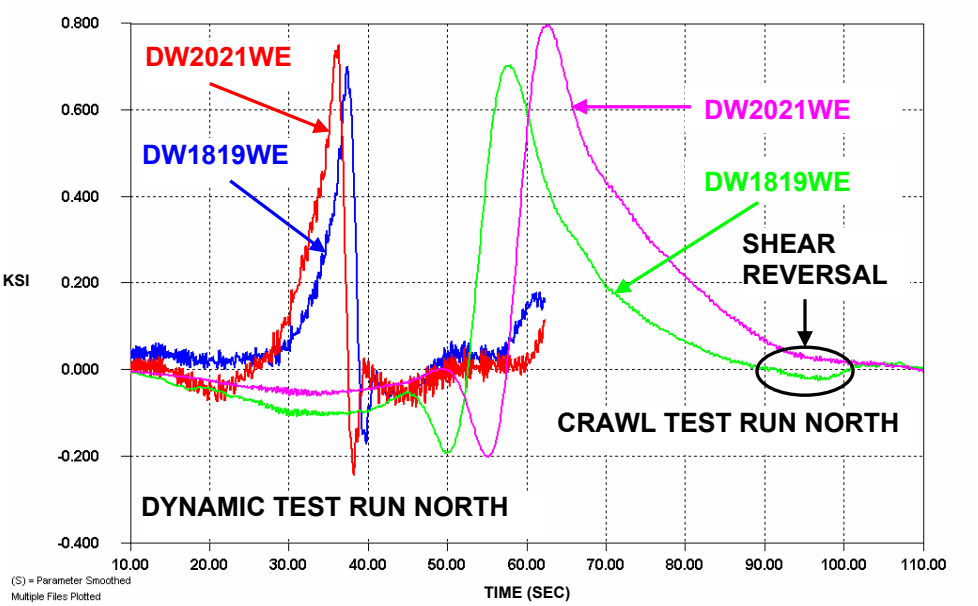

Figure 2.14: Typical dynamic amplification of stress response in west diagonal members (Truck #80 in lane 3)

2.2.4 Stringer Response

Figure 2.15 shows the typical stringer responses to a park test in lane 5. The figure exhibits the two-plateau formation discussed earlier. Also, the neutral axis of the stringers lies close to the steel-concrete interface as seen in the near zero stress read by the top flange gages (S7TCL and S8TCL).

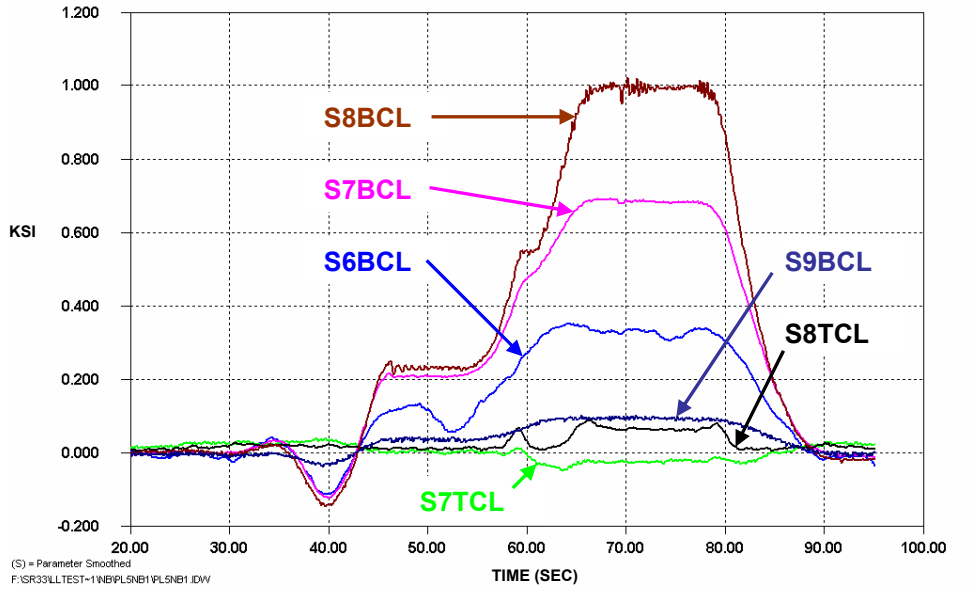

Figure 2.15: U16-U18 centerline of stringer response to a park test in lane 5 (Truck #80 headed north in lane 5)

The difference in behavior between the gages located near the ends of the stringers and near midspan can be seen in the next two figures. Figure 2.16 plots the response of the gages near the floorbeam at U16 to a crawl test in lane 3. It can be seen that the composite action of the deck affected the response of the stringer. Instead of behaving as a beam with a hinged end connection, there is significant compression stress in the bottom flange at the ends of the members. This indicated that the connection is behaving more like a rigid connection due to the addition of the composite deck. Also, the figure reiterates that the neutral axis of the stringers is near the top flange, which is typical behavior of composite beams.

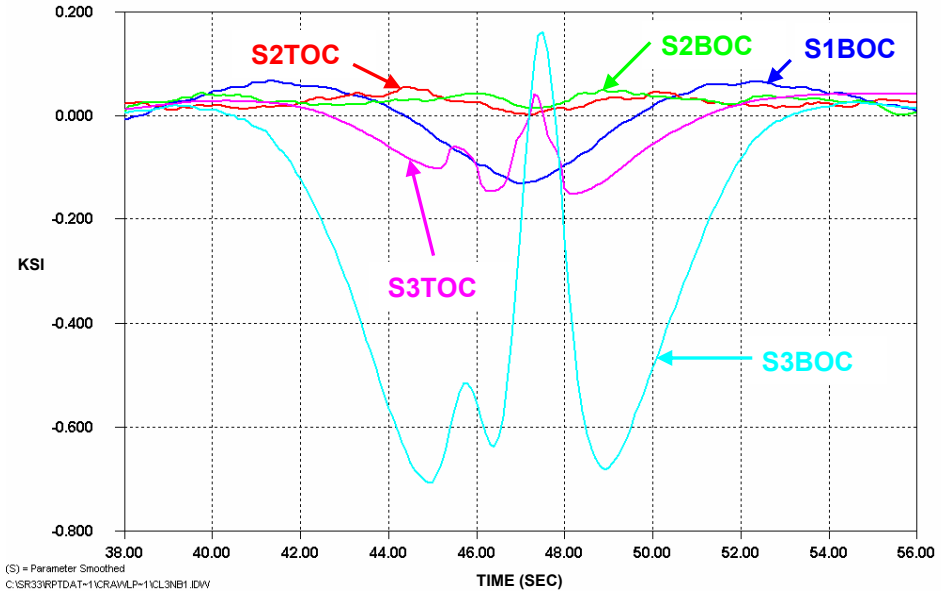

Figure 2.16: Typical crawl response of west stringers (near U16 floorbeam interface) (Truck #80 in lane 3 headed north)

The second figure, Figure 2.17, shows the response of gages at midspan generated by a crawl test in lane 5. The primary action of the stringers is bending and there is considerable lateral load distribution between the members. This behavior was typical of all crawl tests conducted.

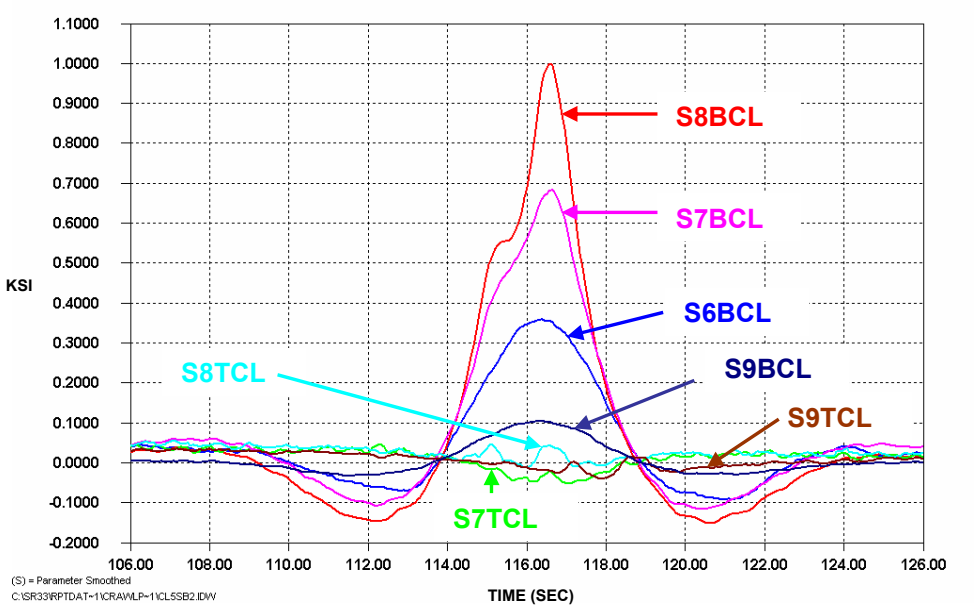

Figure 2.17: Typical crawl response of east stringers (at midspan of stringers)
(Truck #80 in lane 5 headed north)

The dynamic amplification of stress for the stringers at midspan caused by increased truck speed can be seen in Figure 2.18. By comparison, the dynamic stress cycle was between 5% and 12% greater than the stress cycle caused by the crawl test. This is larger than the amount of dynamic amplification observed in the upper chords (3% to 5%). There was little dynamic amplification for the stringers at the ends.

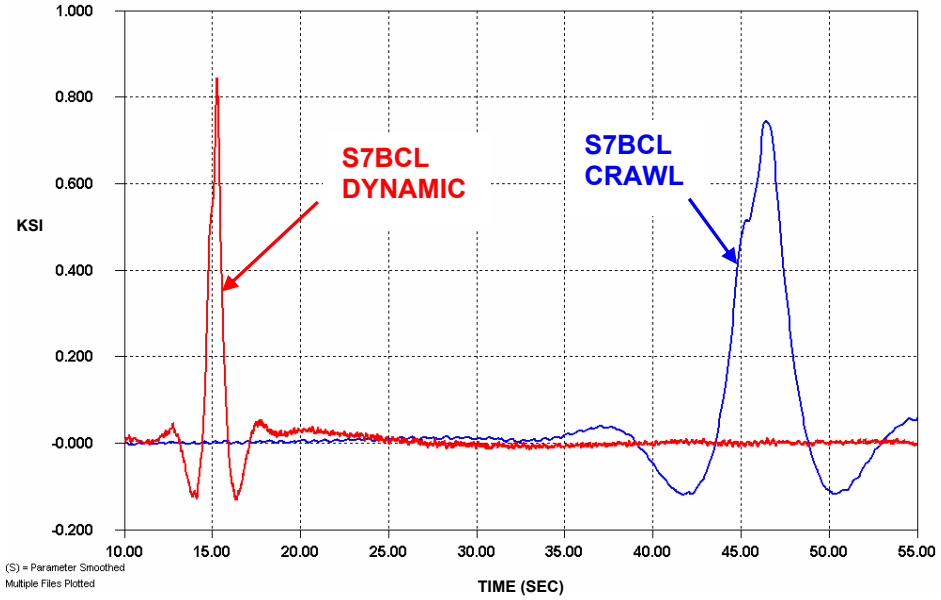

Figure 2.18: Typical dynamic amplification of stress
(Truck #80 in lane 5 headed north)

2.2.5 Deck Reinforcement Response

The response of the gages on the rebar to a park test in lane 5 is shown in Figure 2.19. Only five of the original fourteen embedded gages survived the construction process and consistently produced stable data. These gages were S2WB, EU1618WB, EU1618CB, EU1618EB, and S8WB. The data obtained from these gages was sufficient to characterize the lateral load distribution across the deck. The two-plateau formation is again seen in the plot.

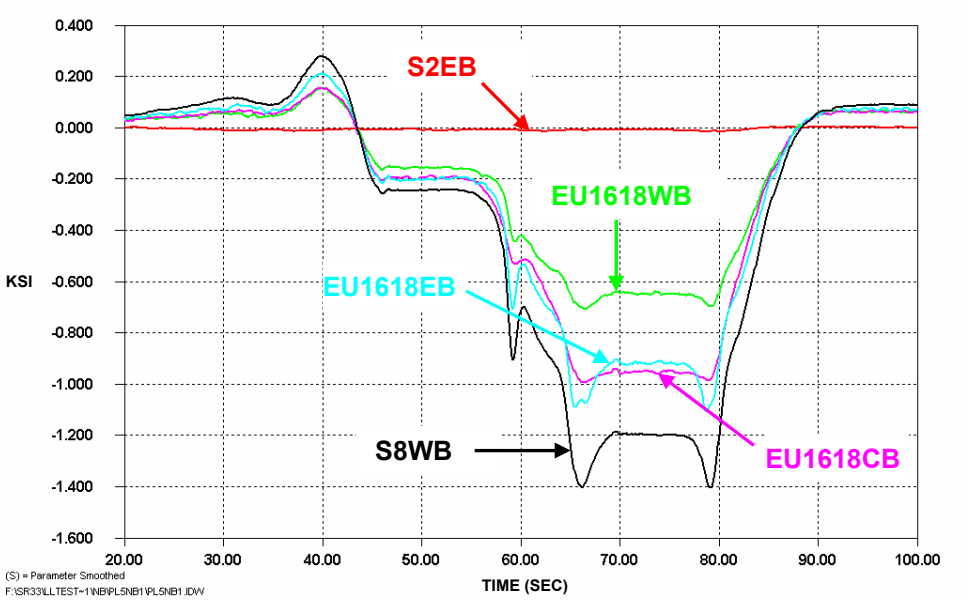

Figure 2.19: Response of instrumented rebar to a park test in lane 5 (Truck #80 headed north)

The response of the deck reinforcement to a crawl test in lane 5 is shown in Figure 2.20. As with previous instrumented members, the validity of superposition holds for the deck reinforcement. Therefore, tests in individual lanes can be added together to form the response of a test in multiple lanes. Figure 2.21 compares the response of the deck reinforcement during a crawl test to its response during a dynamic test. The figure clearly shows the dynamic amplification of stress caused by the increase in vehicle speed. The increase in the dynamic stress cycle was between 20% and 35% greater for the dynamic test.

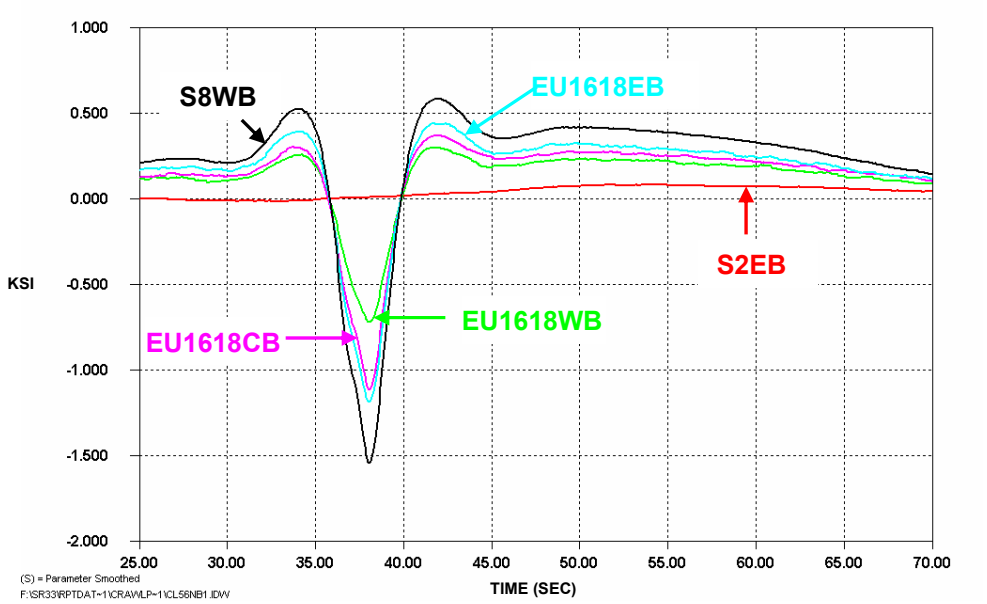

Figure 2.20: Typical response of instrumented reinforcing bars to a crawl test
(Truck #80 in lane 6 and truck #67 in lane 5 headed north)

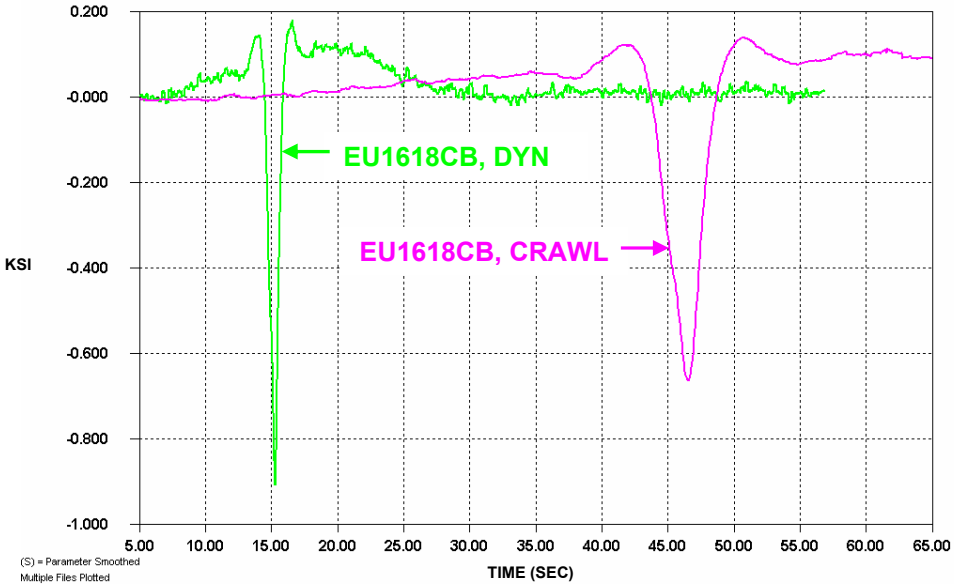

Figure 2.21: Dynamic vs. crawl test response of typical rebar gage
(Truck #80 in lane 5)

2.2.6 Sway Bracing Response

The park tests conducted between panel points U16 and U18 had little effect on the instrumented sway bracing members L9-U10 and U24-L25. The following crawl and dynamic test results will be used to characterize response of the sway bracing.

The typical response of the sway bracing L9-U10 to a crawl test in lane 4 is shown in Figure 2.22. The top and bottom gages do not show the same amount of stress

meaning there is a small bending component present. However, the responses are very similar in magnitude and axial compression or tension is the dominant behavior. The comparison between a crawl and a dynamic test in lane 5 is shown in Figure 2.23. In general, the dynamic stress cycle amplification was between 10% and 20% greater than the crawl test. All conclusions regarding the sway bracing between L9 and U10 are valid for the sway bracing between U24 and L25.

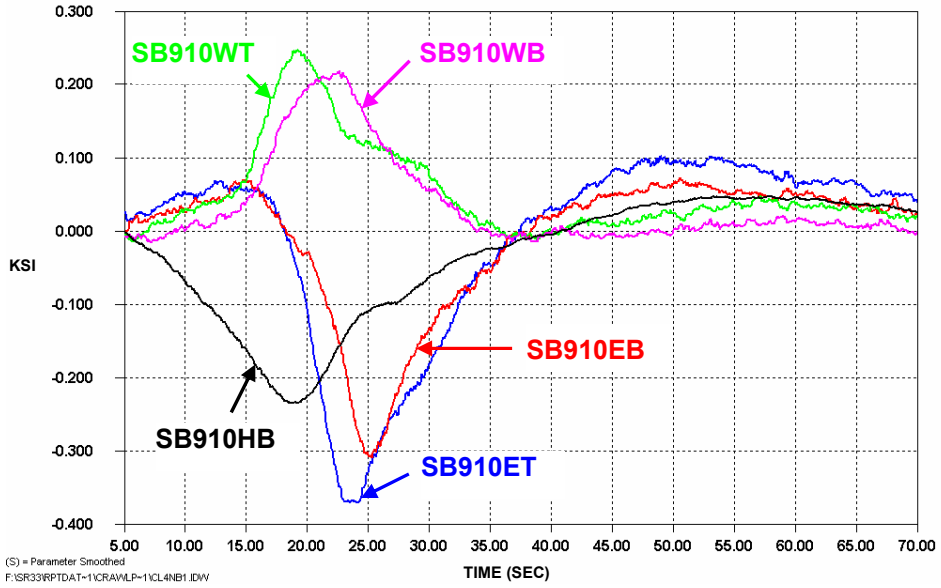

Figure 2.22: Typical sway bracing response to a crawl test
(Truck #80 in lane 4 headed north)

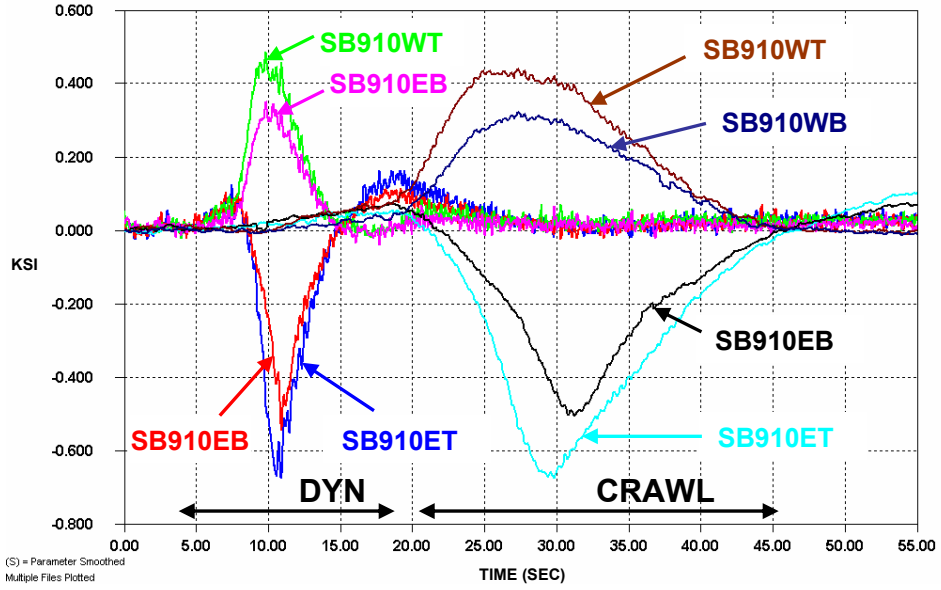

Figure 2.23: Typical dynamic vs. crawl data for sway bracing
(Truck #80 headed north in lane 5 for both tests)

3.0 Instrumentation and Data Acquisition

Instrumentation was located in order to measure both global and local effects from temperature, creep, shrinkage, and live load. Sensors were installed on the upper chords, lower chords, diagonals, sway bracing, stringers, and deck reinforcement at selected locations. The majority of instrumentation from Phase I was concentrated above and around pier 2. The instrumentation for Phase II was concentrated at midspan of the main river span between panel points U26 and U28.

3.1 Review of Previous Instrumentation and Data Acquisition

Uniaxial, spot weldable resistance strain gages were installed at various locations on truss members and in the reinforced concrete deck. Vibrating wire gages were also installed at various locations. Figure 3.1 shows gages installed at a typical location on the truss. Figure 3.2 is a photograph of strain gages installed at a typical location in the concrete deck.

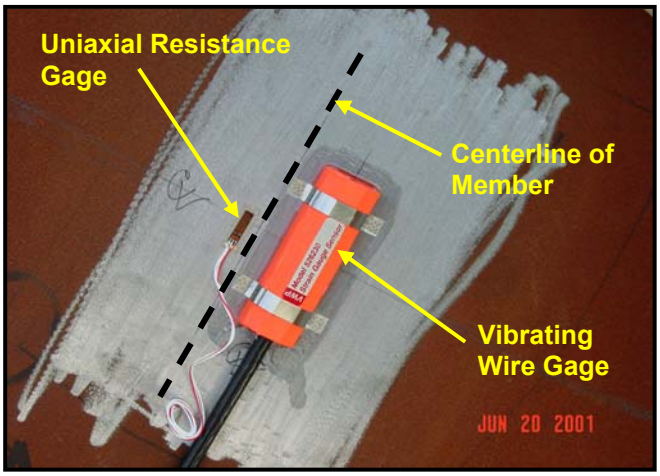

Figure 3.1: Typical strain gage at each location on the structural steel (DW2021WW)

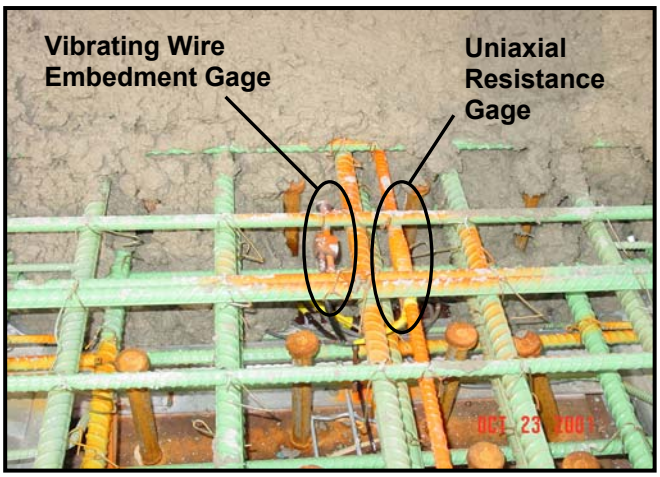

Figure 3.2: Typical strain gage placed at each location within the concrete deck

The locations of all strain gages instrumented during the summer of 2001 are presented in Figure 3.3 through Figure 3.11 and summarized in Table 3.1. Each gage location is named according to the location in reference to the nodes of the truss and the type of structural member to which it is mounted. For example, the gage location BU1618EW indicates it is on a box member (B) located on the upper chord (U) between nodes 16 and 18 (1618) on the east truss of the bridge (E) and on the west side of the member (W). All other gages are named in a similar fashion.

The spot weldable vibrating wire gages were installed at fifty-nine (59) locations and were broken into two categories: midrange gages and tension gages. The midrange gages were Slope Indicator type 52602100 and the tension gages were Slope Indicator type 52602102. This separation is necessary because vibrating wire gages come with a pretension in the internal steel wire. The pretension level must be selected based on the anticipated behavior of each member (i.e., predominantly tension or compression). The vibrating wire embedment gages were Slope Indicator type 5240126. The initial pretension can be set by the user for this type of gage.

The spot weldable uniaxial resistance strain gages were Measurements Group type LWK-06-W250B-350. These gages are fully temperature compensated. The vibrating wire gages described above were fully temperature compensated by applying the recommended thermal expansion coefficients for structural steel. Two vibrating wire gages were mounted on pieces of structural steel at the ATLSS laboratory to determine if any more adjustment was required for the gages. The results showed that only slight adjustments to the manufacturer's published calibration data were necessary to obtain more accurate temperature compensation.

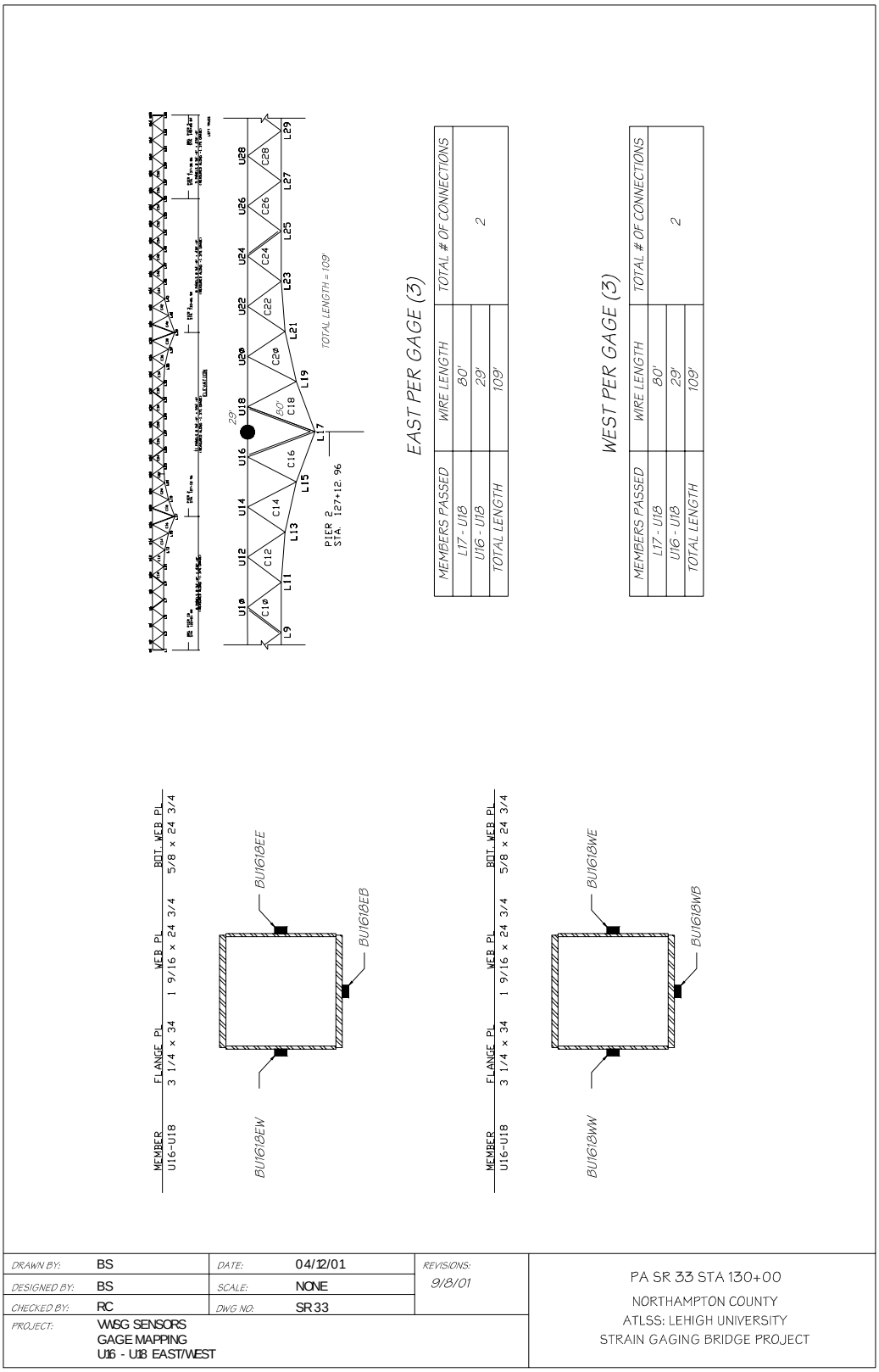

Figure 3.3: Strain gage layout on the upper chord between U16 and U18

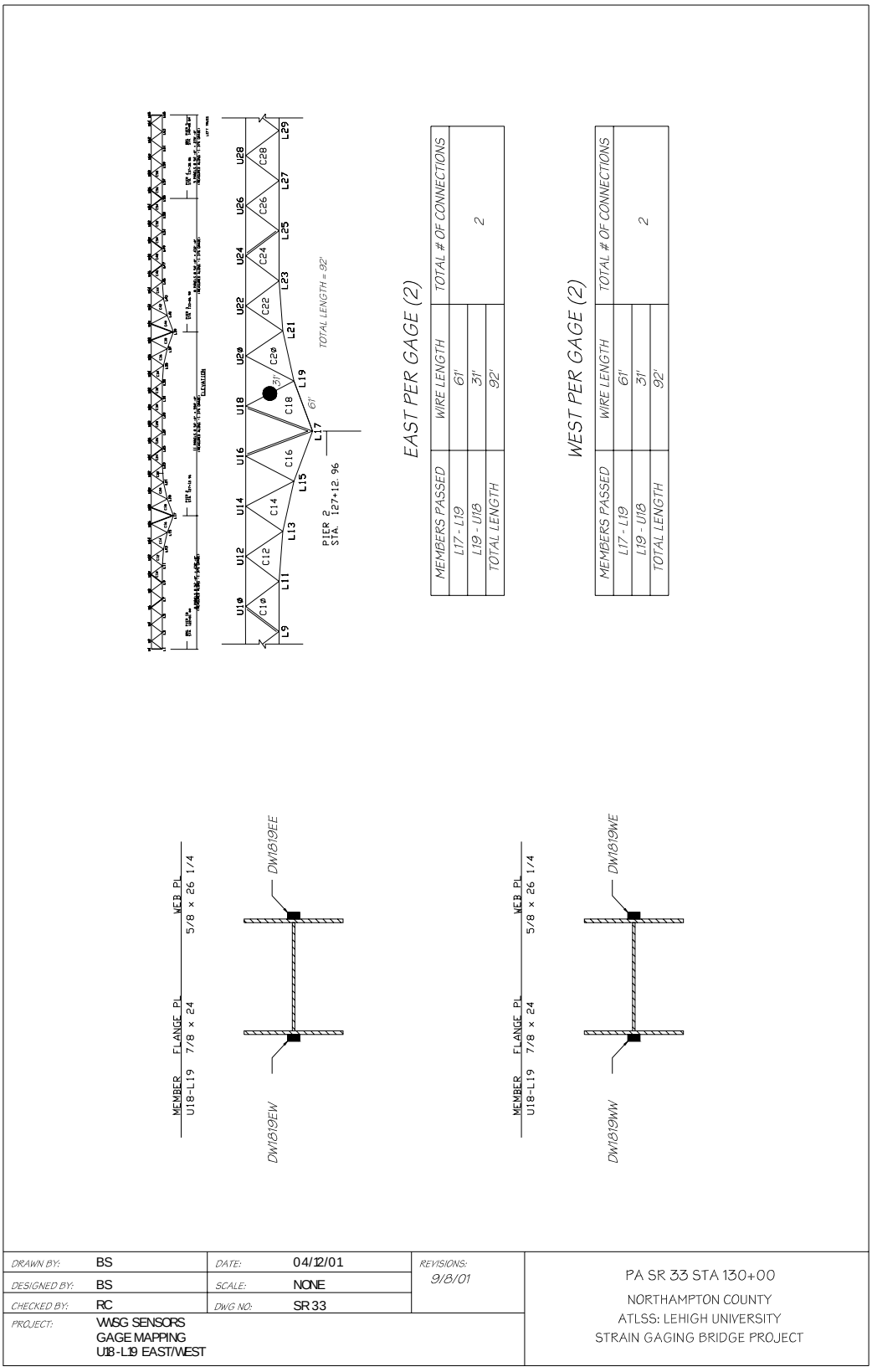

Figure 3.4: Strain gage layout on the diagonal between U18 and L19

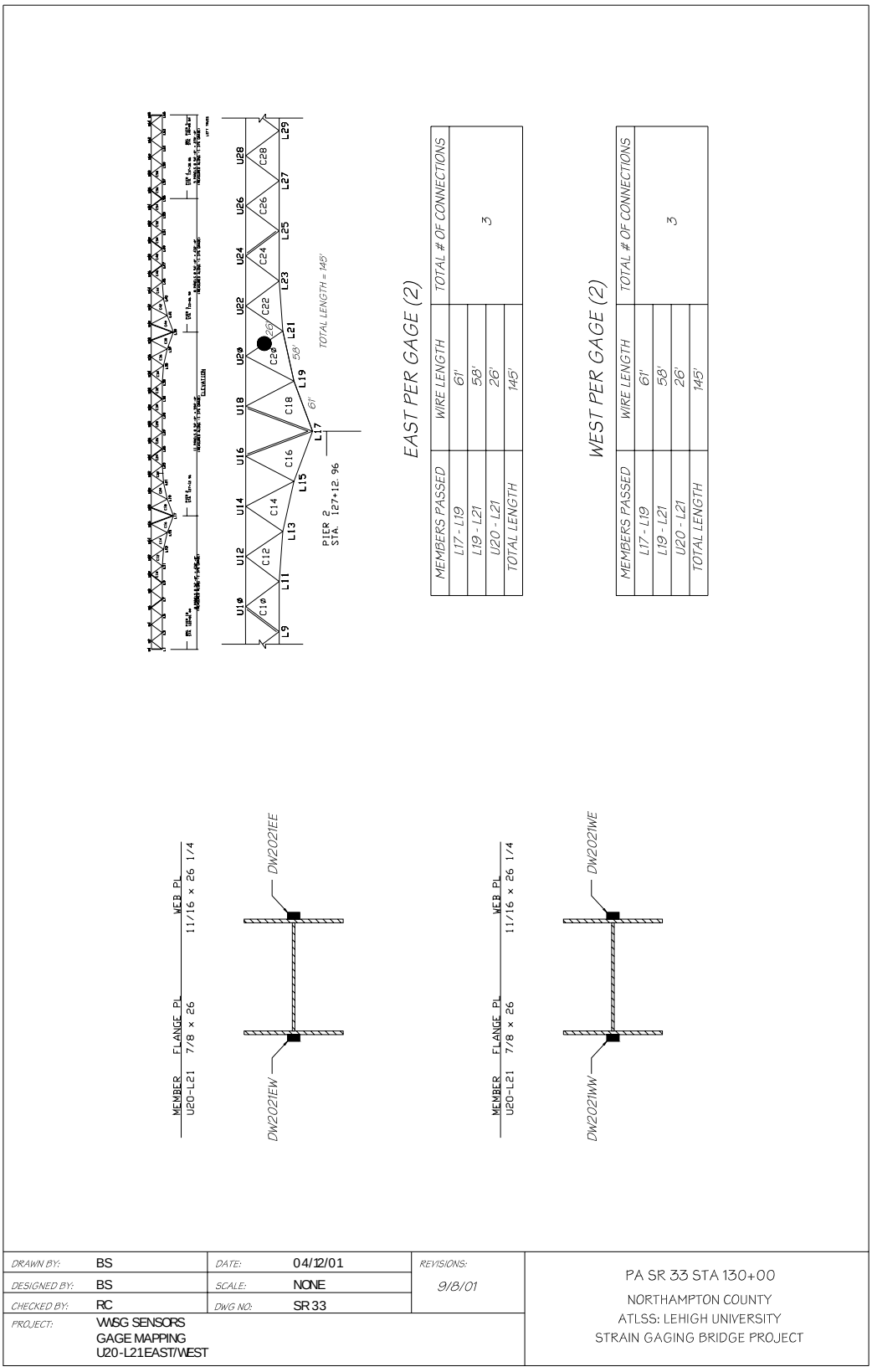

Figure 3.5: Strain gage layout on the diagonal between U20 and L21

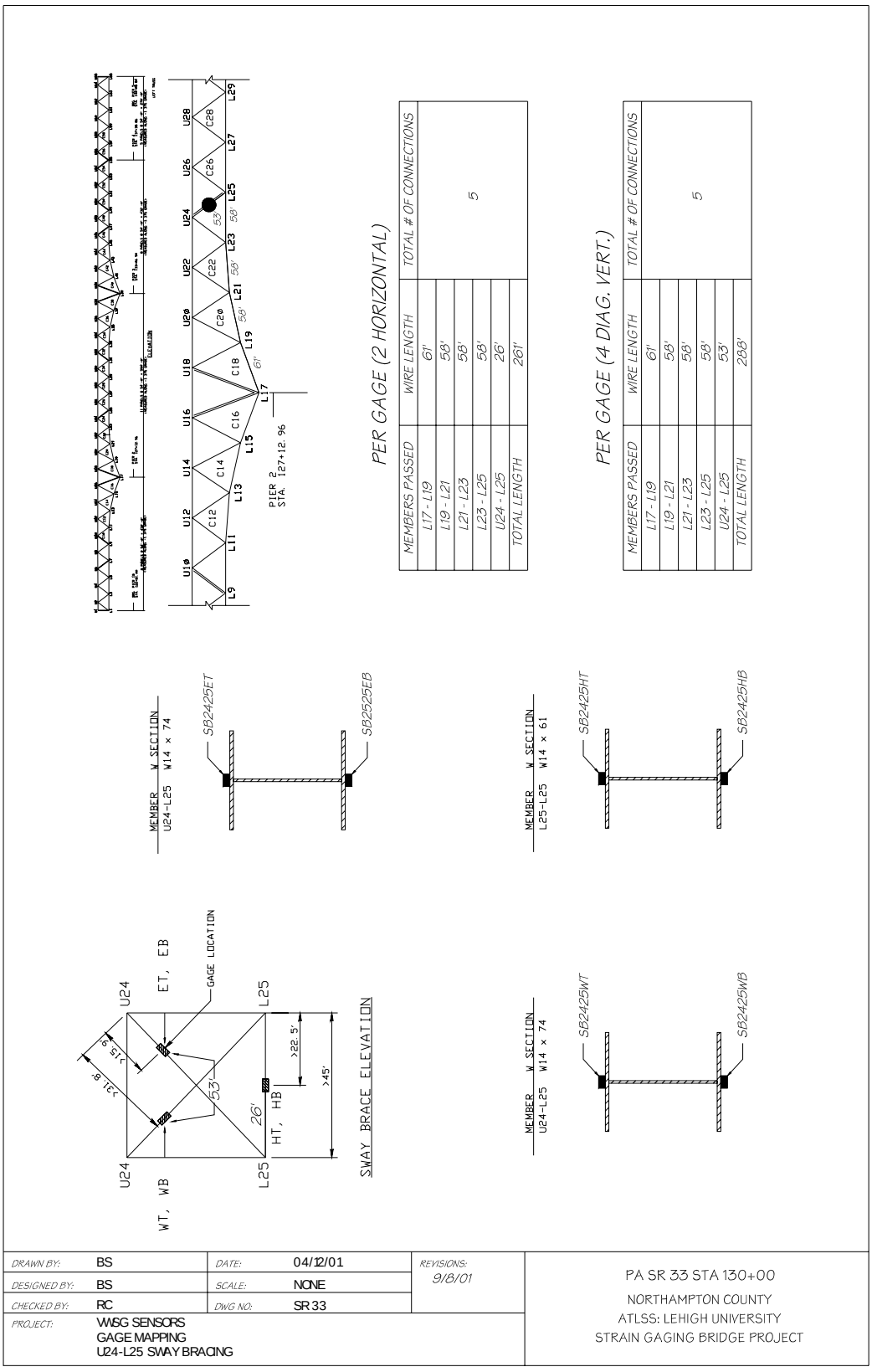

Figure 3.6: Strain gage layout on the sway bracing between U24 and L25

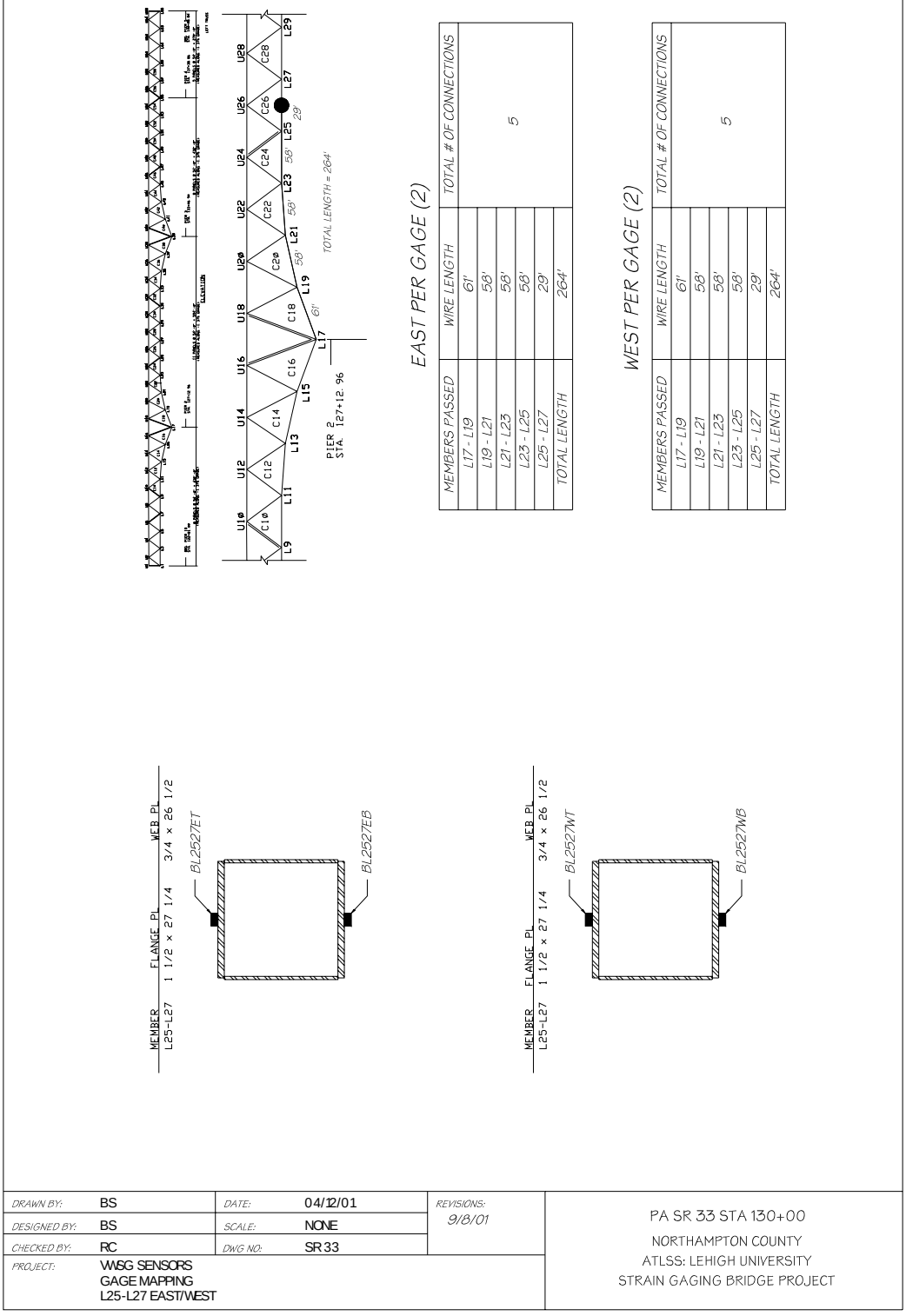

Figure 3.7: Strain gage layout on the lower chord between L25 and L27

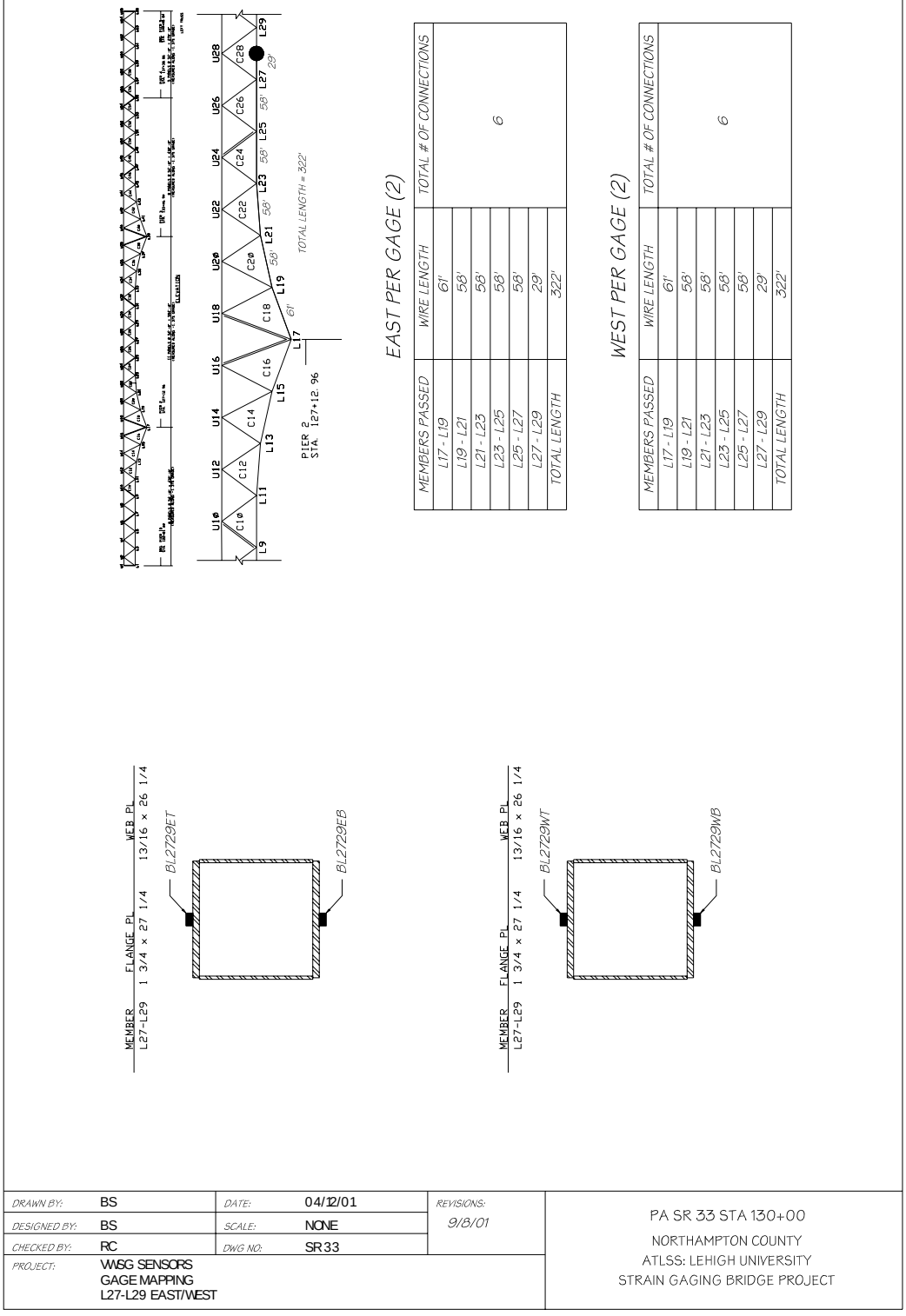

Figure 3.8: Strain gage layout on the lower chord between L27 and L29

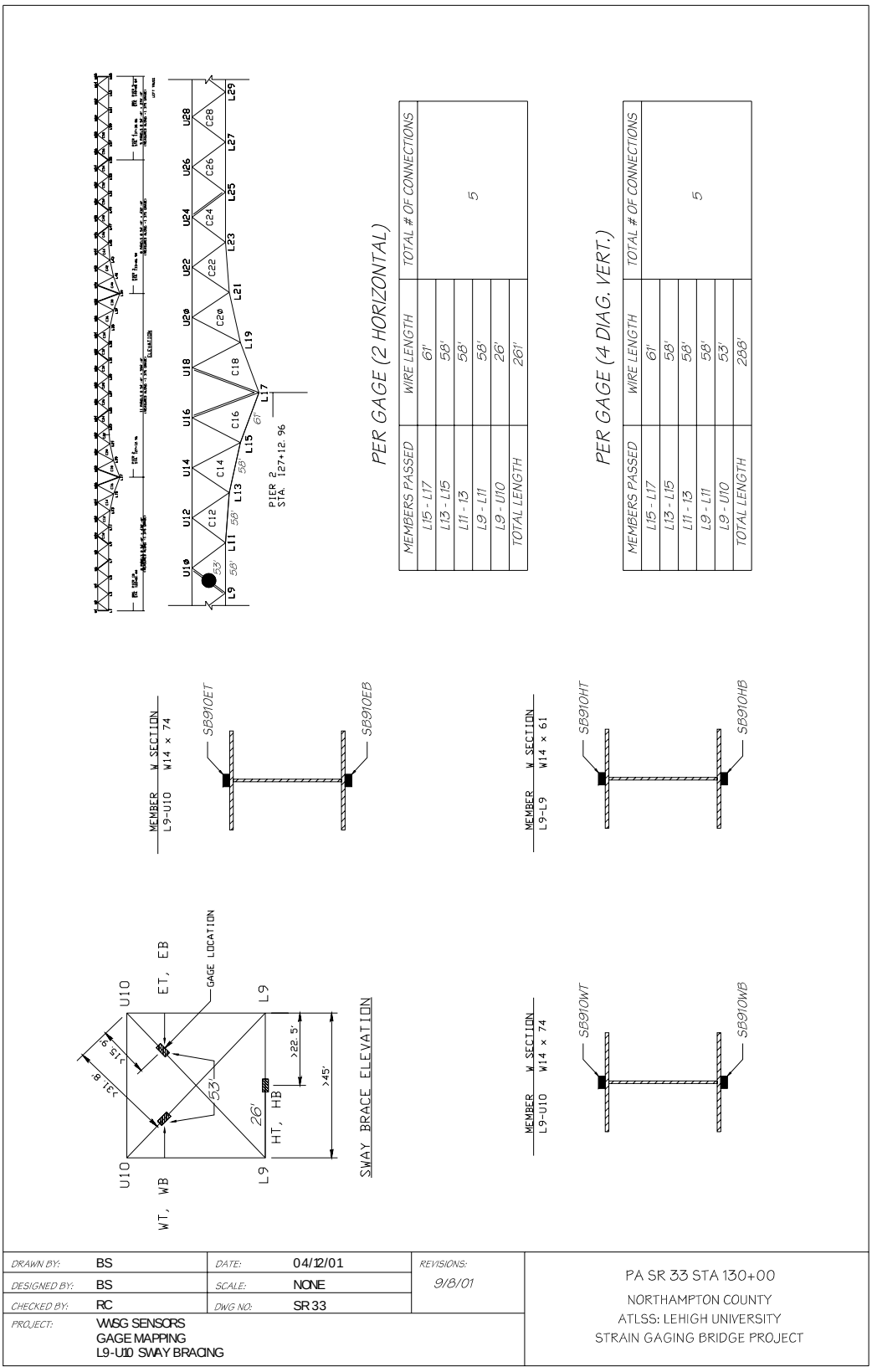

Figure 3.9: Strain gage layout on the sway bracing between L9 and U10

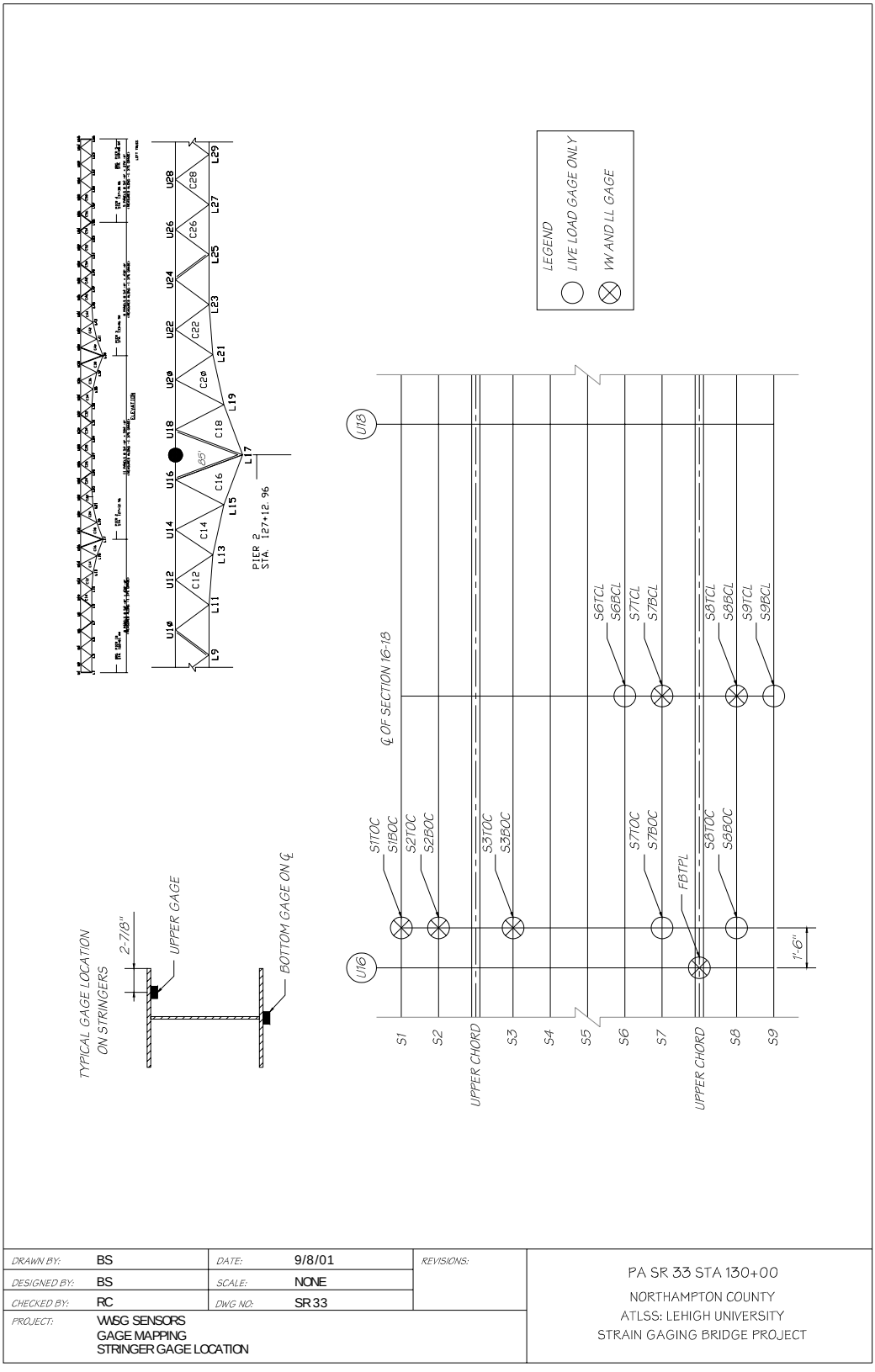

Figure 3.10: Strain gage layout on the steel stringers between U16 and U18

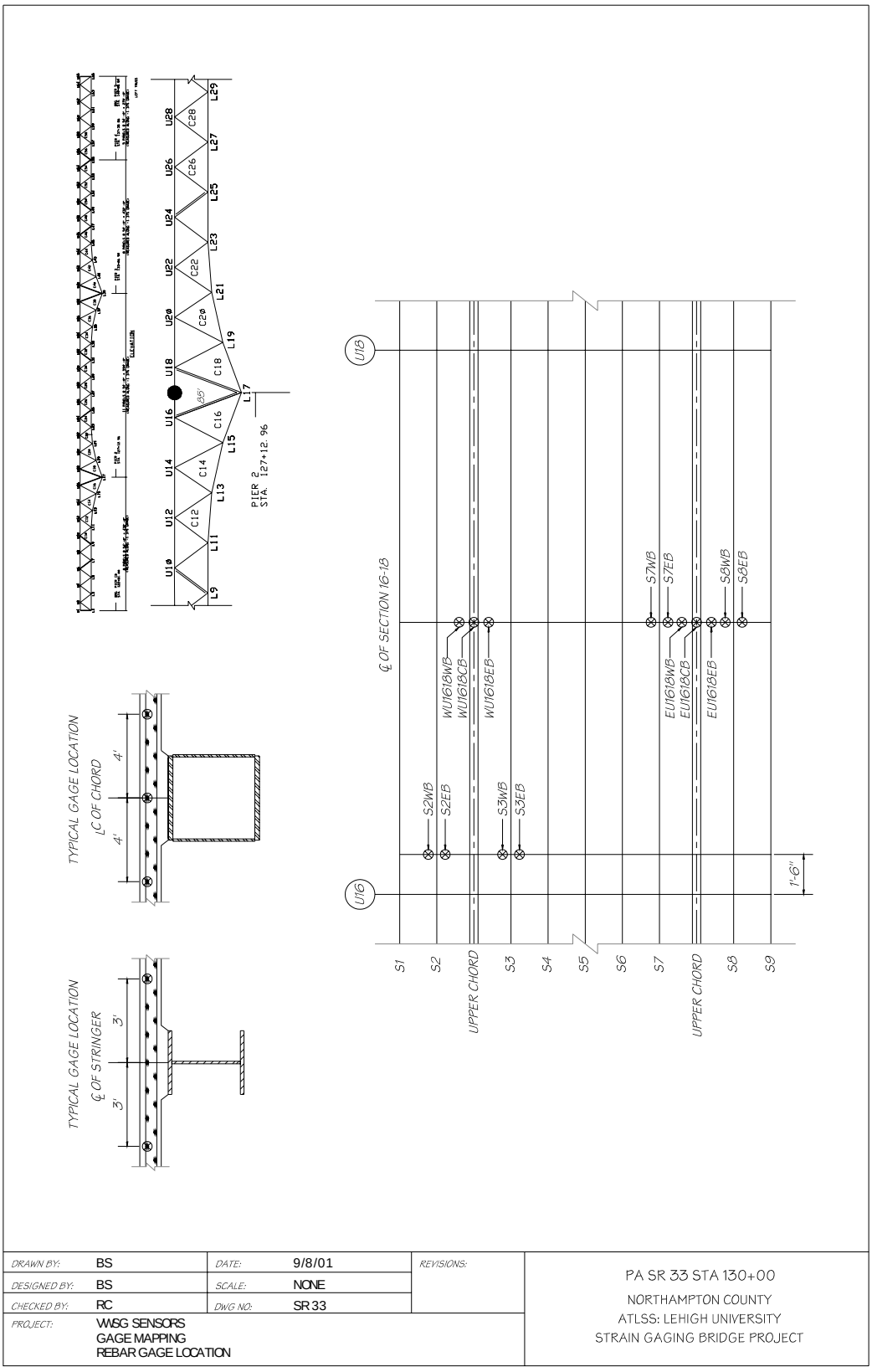

Figure 3.11: Strain gage layout on the rebar embedded in the deck between U16 and U18

Wire #	Gage Name	VW Gage Type	Fig #	Comments
1	BU1618EW	T	3.3	1 SWVW Gage, 1 Thermister, 1 SWUR Gage
2	BU1618EB	T	3.3	1 SWVW Gage, 1 Thermister, 1 SWUR Gage
3	BU1618EE	T	3.3	1 SWVW Gage, 1 Thermister, 1 SWUR Gage
4	BU1618WW	T	3.3	1 SWVW Gage, 1 Thermister, 1 SWUR Gage
5	BU1618WB	T	3.3	1 SWVW Gage, 1 Thermister, 1 SWUR Gage
6	BU1618WE	T	3.3	1 SWVW Gage, 1 Thermister, 1 SWUR Gage
7	DW1819EW	T	3.4	1 SWVW Gage, 1 Thermister, 1 SWUR Gage
8	DW1819EE	T	3.4	1 SWVW Gage, 1 Thermister, 1 SWUR Gage
9	DW1819WW	T	3.4	1 SWVW Gage, 1 Thermister, 1 SWUR Gage
10	DW1819WE	T	3.4	1 SWVW Gage, 1 Thermister, 1 SWUR Gage
11	DW2021EW	T	3.5	1 SWVW Gage, 1 Thermister, 1 SWUR Gage
12	DW2021EE	T	3.5	1 SWVW Gage, 1 Thermister, 1 SWUR Gage
13	DW2021WW	T	3.5	1 SWVW Gage, 1 Thermister, 1 SWUR Gage
14	DW2021WE	T	3.5	1 SWVW Gage, 1 Thermister, 1 SWUR Gage
15	SB2425ET	M	3.6	1 SWVW Gage, 1 Thermister, 1 SWUR Gage
16	SB2425EB	M	3.6	1 SWVW Gage, 1 Thermister, 1 SWUR Gage
17	SB2425WT	M	3.6	1 SWVW Gage, 1 Thermister, 1 SWUR Gage
18	SB2425WB	M	3.6	1 SWVW Gage, 1 Thermister, 1 SWUR Gage
19	SB2425HT	M	3.6	1 SWVW Gage, 1 Thermister, 1 SWUR Gage
20	SB2425HB	M	3.6	1 SWVW Gage, 1 Thermister, 1 SWUR Gage
21	BL2527ET	T	3.7	1 SWVW Gage, 1 Thermister, 1 SWUR Gage
22	BL2527EB	T	3.7	1 SWVW Gage, 1 Thermister, 1 SWUR Gage
23	BL2527WT	T	3.7	1 SWVW Gage, 1 Thermister, 1 SWUR Gage
24	BL2527WB	T	3.7	1 SWVW Gage, 1 Thermister, 1 SWUR Gage
25	BL2729ET	T	3.8	1 SWVW Gage, 1 Thermister, 1 SWUR Gage
26	BL2729EB	T	3.8	1 SWVW Gage, 1 Thermister, 1 SWUR Gage
27	BL2729WT	T	3.8	1 SWVW Gage, 1 Thermister, 1 SWUR Gage
28	BL2729WB	T	3.8	1 SWVW Gage, 1 Thermister, 1 SWUR Gage
29	SB910ET	M	3.9	1 SWVW Gage, 1 Thermister, 1 SWUR Gage
30	SB910EB	M	3.9	1 SWVW Gage, 1 Thermister, 1 SWUR Gage
31	SB910WT	M	3.9	1 SWVW Gage, 1 Thermister, 1 SWUR Gage
32	SB910WB	M	3.9	1 SWVW Gage, 1 Thermister, 1 SWUR Gage
33	SB910HT	M	3.9	1 SWVW Gage, 1 Thermister, 1 SWUR Gage
34	SB910HB	M	3.9	1 SWVW Gage, 1 Thermister, 1 SWUR Gage

VW Gage Type Key:

"M" = Midrange Gage

"T" = Tension Gage

Comment Key:

"SWVW" = Spot Weldable Vibrating Wire

"SWUR" = Spot Weldable Uniaxial Resistance

Table 3.1: Summary of strain gage locations on steel truss members

Wire #	Gage Name	VW Gage Type	Fig #	Comments
35	S1TOC	T	3.10	1 SWVW Gage, 1 Thermister, 1 SWUR Gage
36	S1BOC	T	3.10	1 SWVW Gage, 1 Thermister, 1 SWUR Gage
37	S2TOC	T	3.10	1 SWVW Gage, 1 Thermister, 1 SWUR Gage
38	S2BOC	T	3.10	1 SWVW Gage, 1 Thermister, 1 SWUR Gage
39	S3TOC	M	3.10	1 SWVW Gage, 1 Thermister, 1 SWUR Gage
40	S3BOC	T	3.10	1 SWVW Gage, 1 Thermister, 1 SWUR Gage
41	S7TCL	T	3.10	1 SWVW Gage, 1 Thermister, 1 SWUR Gage
42	S7BCL	T	3.10	1 SWVW Gage, 1 Thermister, 1 SWUR Gage
43	S8TCL	T	3.10	1 SWVW Gage, 1 Thermister, 1 SWUR Gage
44	S8BCL	T	3.10	1 SWVW Gage, 1 Thermister, 1 SWUR Gage
45	FBTPL	T	3.10	1 SWVW Gage, 1 Thermister, 1 SWUR Gage
46	S2WB	-	3.11	1 EVW Gage, 1 Thermister, 1 SWUR Gage
47	S2EB	-	3.11	1 EVW Gage, 1 Thermister, 1 SWUR Gage
48	WU1618WB	-	3.11	1 EVW Gage, 1 Thermister, 1 SWUR Gage
49	WU1618CB	-	3.11	1 EVW Gage, 1 Thermister, 1 SWUR Gage
50	WU1618EB	-	3.11	1 EVW Gage, 1 Thermister, 1 SWUR Gage
51	S3WB	-	3.11	1 EVW Gage, 1 Thermister, 1 SWUR Gage
52	S3EB	-	3.11	1 EVW Gage, 1 Thermister, 1 SWUR Gage
53	S7WB	-	3.11	1 EVW Gage, 1 Thermister, 1 SWUR Gage
54	S7EB	-	3.11	1 EVW Gage, 1 Thermister, 1 SWUR Gage
55	EU1618WB	-	3.11	1 EVW Gage, 1 Thermister, 1 SWUR Gage
56	EU1618CB	-	3.11	1 EVW Gage, 1 Thermister, 1 SWUR Gage
57	EU1618EB	-	3.11	1 EVW Gage, 1 Thermister, 1 SWUR Gage
58	S8WB	-	3.11	1 EVW Gage, 1 Thermister, 1 SWUR Gage
59	S8EB	-	3.11	1 EVW Gage, 1 Thermister, 1 SWUR Gage
60	S6TCL	-	3.10	1 SWUR Gage
60	S6BCL	-	3.10	1 SWUR Gage
61	S7TOC	-	3.10	1 SWUR Gage
61	S7BOC	-	3.10	1 SWUR Gage
62	S8TOC	-	3.10	1 SWUR Gage
62	S8BOC	-	3.10	1 SWUR Gage
63	S9TCL	-	3.10	1 SWUR Gage
63	S9BCL	-	3.10	1 SWUR Gage

VW Gage Type Key:

"M" = Midrange Gage

"T" = Tension Gage

Comment Key:

"SWVW" = Spot Weldable Vibrating Wire

"EVW" = Embedded Vibrating Wire

"SWUR" = Spot Weldable Uniaxial Resistance

Table 3.1 (cont.): Summary of strain gage locations on stringers and in concrete deck

The current long-term monitoring system is installed on pier 2 and consists of a Campbell Scientific CR5000 data logger, Campbell Scientific AVW100 Vibrating Wire Interfaces, and a series of four Campbell Scientific AM416 analog mutiplexers. The multiplexers made it possible to collect data from up to 64 vibrating wire sensors while utilizing only eight of the forty single-ended inputs available on the data logger. Each vibrating wire sensor provides both temperature and strain data for a total of 128 data. The AVW100 Vibrating Wire Interfaces excite the wires and condition the output signal. A photograph of the long-term monitoring system is shown in Figure 3.12.

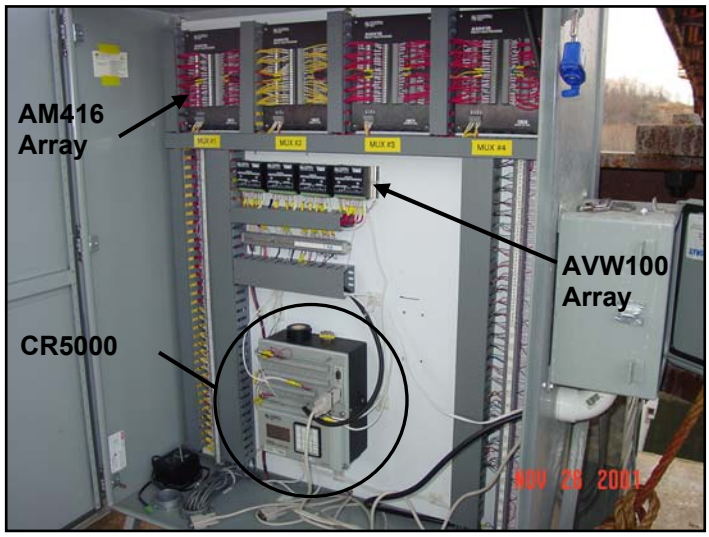

Figure 3.12: Photograph of long-term monitoring system and housing on pier 2

Data were recorded at two intervals during the construction stage of the bridge. Data were sampled at once every two minutes until three weeks after the main span of the truss was "closed". Since that time, data has been recorded at five-minute intervals up until June of 2004 and three-hour intervals since that time. The modification in June 2004 was made to accommodate long-term live load monitoring and will be discussed in more detail in a later section of the report. The long-term monitoring system is powered by nine 12-volt marine batteries which are charged by two solar panels. The solar panels constantly charge the batteries during the day, providing a maximum of 14 amps (7 amps from each solar panel). The draw from the system varies between 0.2 and 1.0 amps for the CR5000 data logger only. Figure 3.13 shows a view of the battery box installed on pier 2.

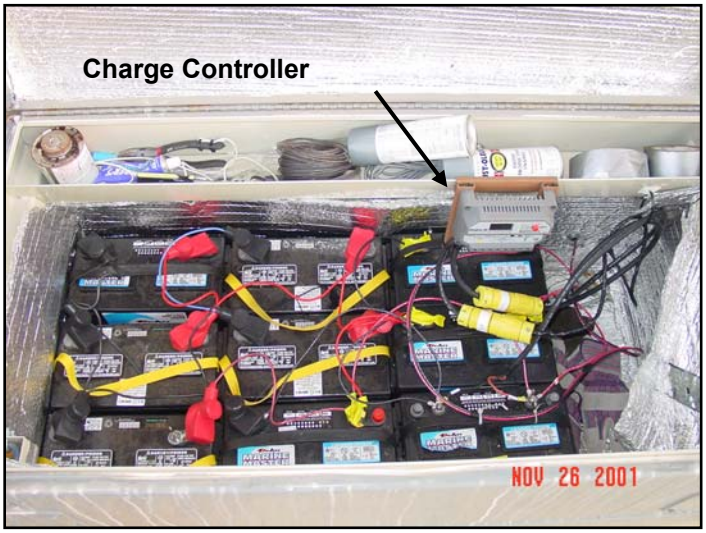

Figure 3.13: Photograph of battery box and charge controller

The Campbell Scientific CR9000 data logger is used to monitor the uncontrolled vehicular live load. It offers 16-bit resolution and up to 100,000 samples per second system throughput. Data has been collected at a variety of sampling rates varying from 5 Hz to 250 Hz. The logger is mounted on pier 2 in a box as seen in Figure 3.21. While on site, a laptop is connected to the logger as seen in Figure 3.14 and data can be reviewed in real time.

Figure 3.14: Photograph of laptop during uncontrolled live load monitoring

3.2 Description of New Instrumentation and Data Acquisition

A total of sixteen (16) live load gages were installed between panel points U26 and U28 of the truss on three separate days during the month of July, 2003. These locations consisted of the two upper chords of the truss and five stringers under the southbound lanes of the bridge.

An Aspen Aerial UB50 snooper with a 50' boom was used to install the additional sixteen gages. A photograph of the snooper is shown in Figure 3.15.

Figure 3.15: Aspen Aerial UB50 snooper used for instrumentation of bridge

The same spot weldable uniaxial resistance strain gages used during Phase I were selected. These were Measurements Group type LWK-06-W250B-350. As previously stated, these gages are fully temperature compensated. All gages installed on the two upper chords and five stringers between panel points U26 and U28 of the truss were instrumented in the same fashion as during Phase I for members of the same type. A total of three gages were placed on each upper chord, one on each side flange plate and one on the bottom web plate. A photograph of typical instrumentation installed on an upper chord location with gages circled in yellow is shown in Figure 3.16.

Each stringer contained two gages. One gage was placed on the bottom side of the top flange at a 2-7/8" offset from the outside edge and a second gage was placed on the bottom side of the bottom flange along the web centerline. It should be noted that all gages were placed 8" south of midspan of U26-U28. Diaphragm connection plates were encountered at the midspan of these members making installation of the gage on the stringer top flange difficult. The small offset from midspan should have a negligible effect on maximum bending moment measured in the members. A photograph of a typical stringer location is seen in Figure 3.17. The instrumentation of all gages installed during July, 2003 is shown in Figure 3.18 and Figure 3.19.

Figure 3.16: Instrumentation of the east upper chord (U26-U28 East)

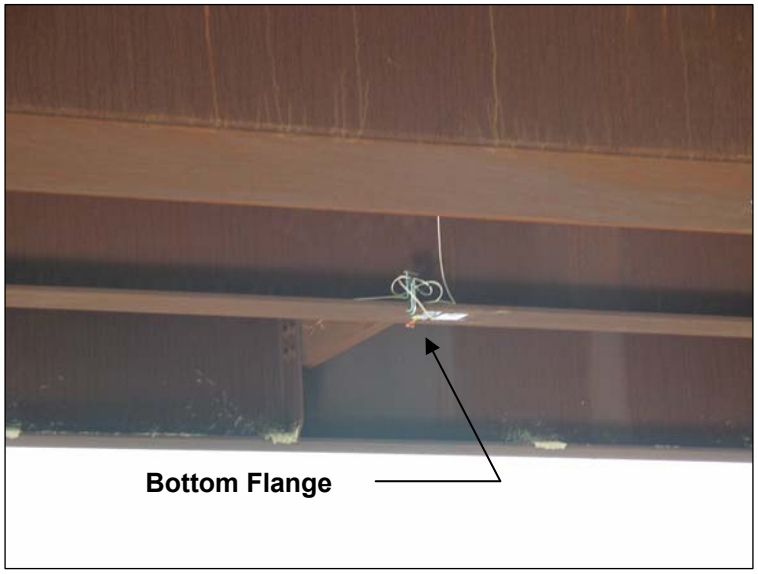

Figure 3.17: Typical instrumentation of stringer location

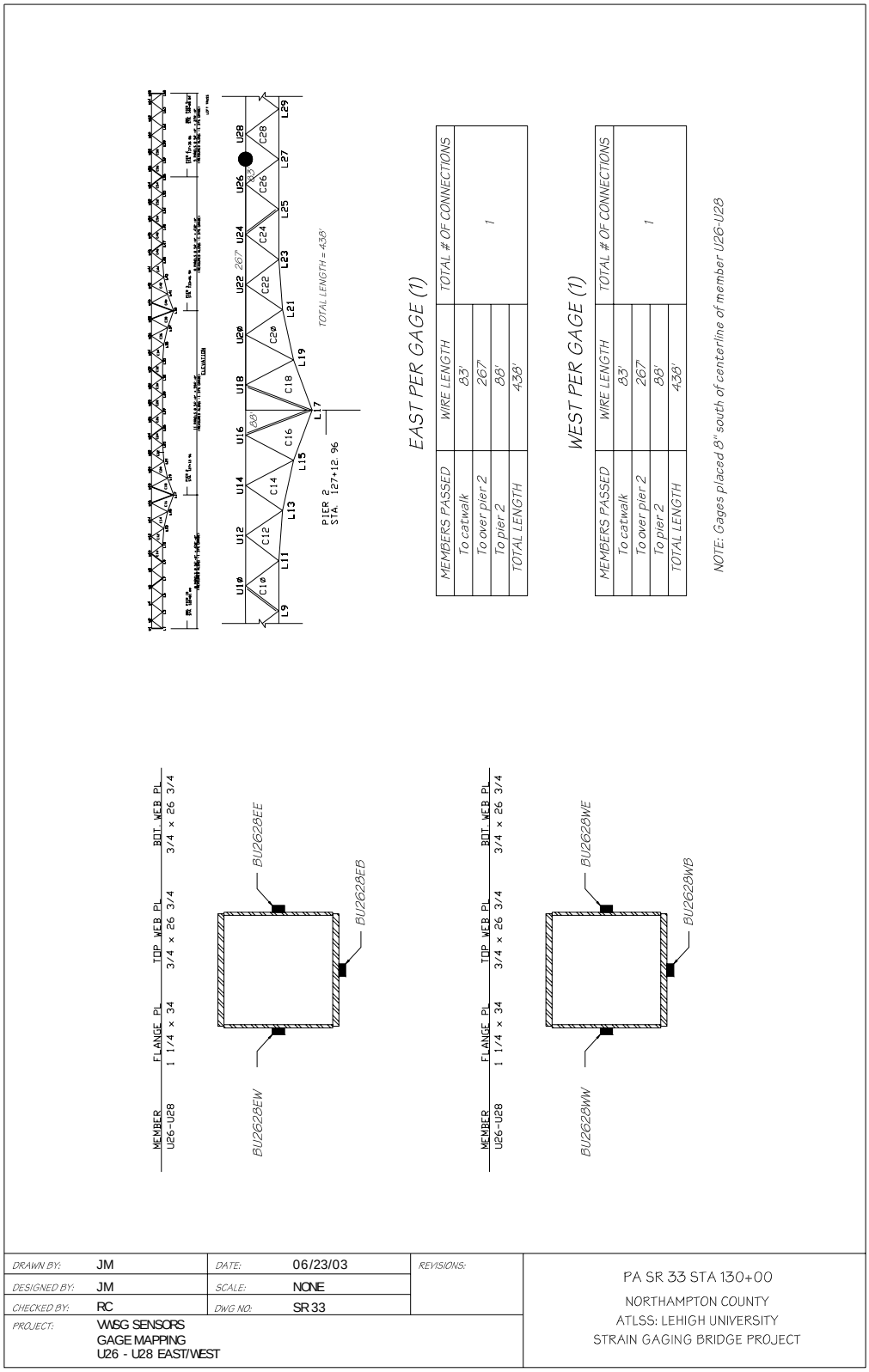

Figure 3.18: Strain gage layout on the upper chord between U26 and U28

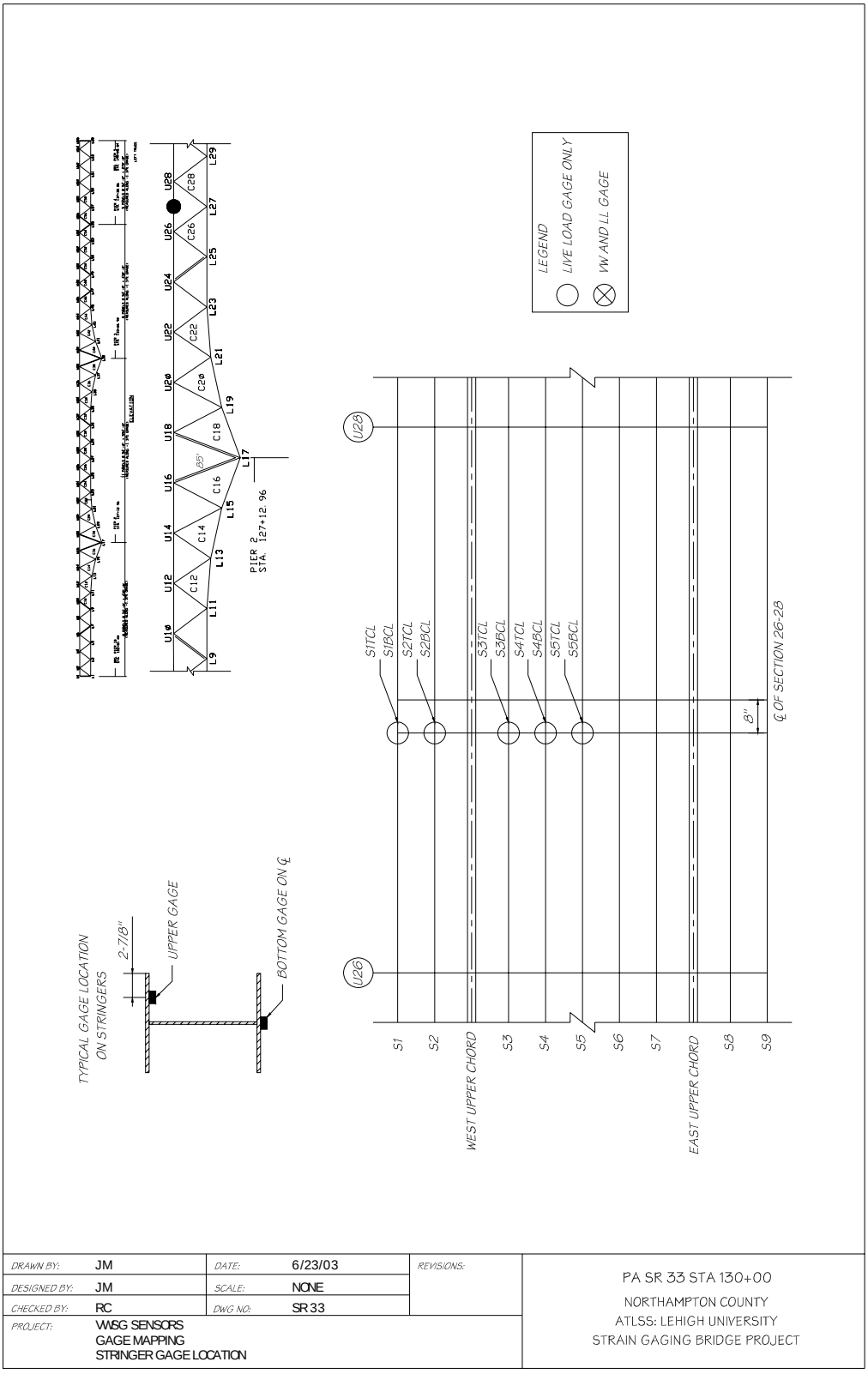

Figure 3.19: Strain gage layout on steel stringers between U26 and U28

A second solar panel was installed on pier cap 2 in order to supply additional power during the daylight hours for uncontrolled live load testing. A picture of the solar panels is shown in Figure 3.20. In addition, a second weather-tight box was installed to house the CR9000 data logger for uncontrolled live load monitoring of traffic on the bridge. This unit is independent of the box housing the CR5000 long-term monitoring unit described in the previous section. A picture of the box and the CR9000 data logger is shown in Figure 3.21.

Figure 3.20: View of solar panels on pier 2 looking west

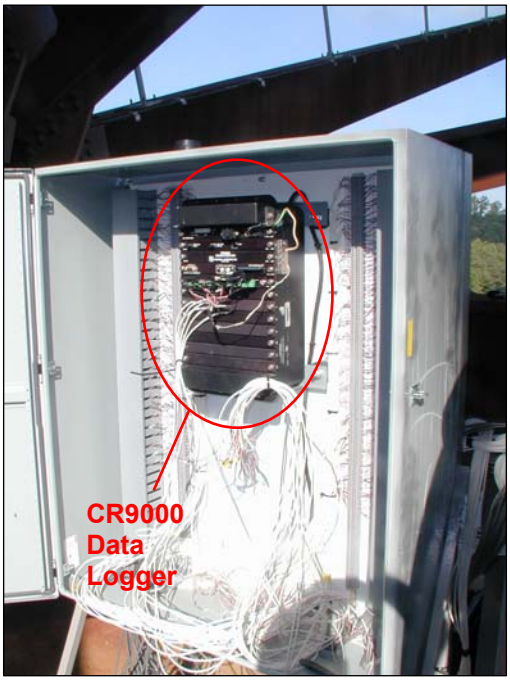

Figure 3.21: CR9000 data logger and housing structure

In order to enable the long-term monitoring system (CR9000) to run for extended periods of time, an additional power source was required to charge the batteries during the night (The approximate power draw of the CR9000 and all of the high-speed wireless communication devices is approximately 8.5 amps DC). The source of this power comes from a light pole mounted on the abutment wing wall near the southwest end of the bridge and was fully operational in early February, 2004. Power lines were run to the catwalk, through existing conduit above the catwalk, and down to the pier cap. A step-down transformer (240V/120V) was mounted on the east face of the box housing the 12-volt marine batteries. A picture of the step-down transformer is shown in Figure 3.22.

A panel with two circuit breakers, a 4-outlet box, and an additional charge controller were added to the battery box. These items are shown in Figure 3.23. The charge controller was required to guarantee that the batteries would not be overcharged by this new power source. To ensure that the CR5000 and CR9000 data loggers operate properly, the input battery voltage is required to not drop below a specified level. Six (6) additional 12-volt marine batteries were added to the existing battery box to ensure battery voltage would not drop below the requirement of these data loggers and to ensure that the loggers would continue to operate for a few days if the external power source failed.

Figure 3.22: Step-down transformer mounted on east face of battery box

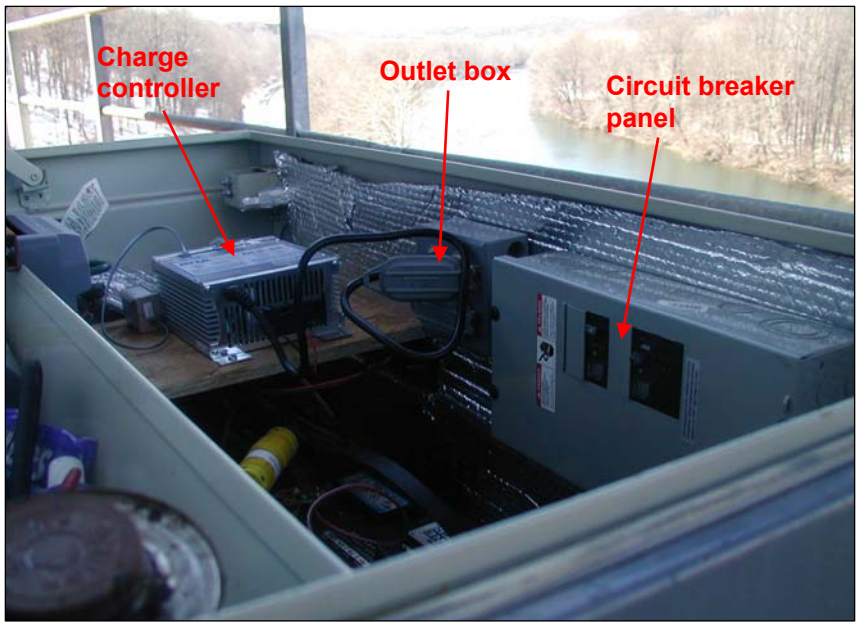

Figure 3.23: Charge controller, outlets, and circuit breaker panel in battery box

A high-speed internet connection was initiated between the ATLSS Laboratory on Lehigh University's Mountaintop Campus and the Lehigh River Bridge. This internet connection was made possible through the use of high-speed wireless bridges and directional antennas. The horizontal distance from ATLSS to Martin Tower is approximately 2.75 miles as shown in Figure 3.24. Two (2) Cisco Aironet 350 Series wireless bridges were used to establish the connection from ATLSS to Martin Tower. A view of one of the Cisco wireless bridges installed on Martin Tower is shown in Figure 3.25. A 24 dBi directional parabolic grid antenna was mounted on the roof of ATLSS and directed towards a 14 dBi yagi directional antenna located on Martin Tower (see Figure 3.26). The distance between Martin Tower and the Lehigh River Bridge is approximately 6.07 miles (see Figure 3.24). It was difficult to establish a strong and robust connection between these two locations using the Cisco wireless bridges. Therefore, two (2) Locus OS2400-HSE High Speed Ethernet radios were utilized. One radio was installed on a catwalk landing leading down to pier 2 of the bridge and the other was located on top of Martin Tower (see Figure 3.25). Two (2) 24 dBi directional parabolic antennas were used to communicate between the bridge and Martin Tower. A photograph of the antenna installed on the roof top is shown in Figure 3.26. This connection made it possible to view the data in real time, retrieve data files wirelessly, and make any changes to the programs running the data loggers from the ATLSS Laboratory.

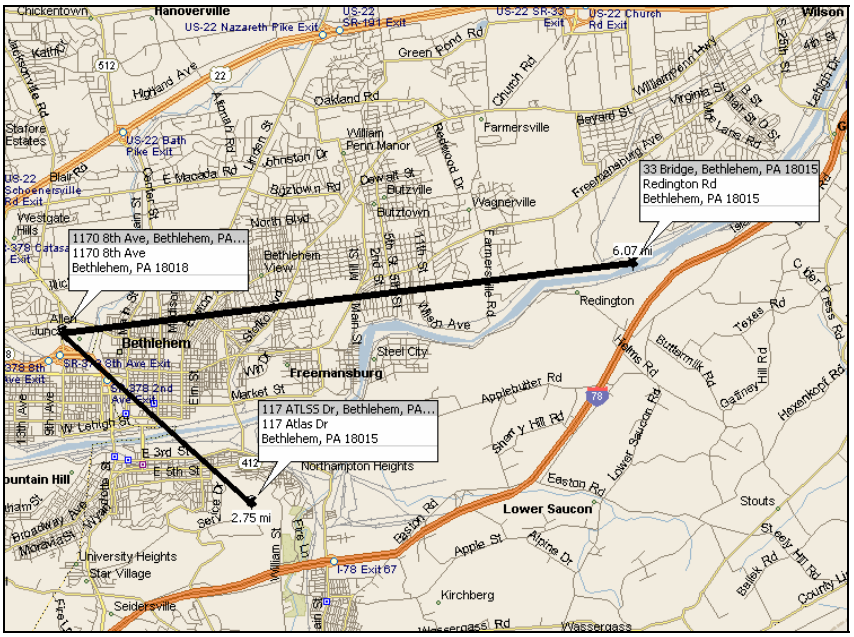

Figure 3.24: Map of SR-33 high-speed wireless internet connection

Figure 3.25: Wireless bridge and radio installed on roof of Martin Tower

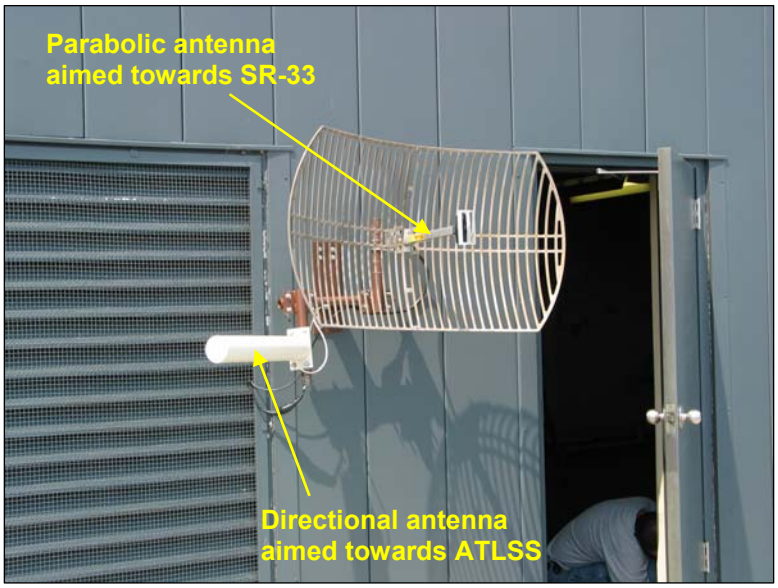

Figure 3.26: Antennas installed on roof of Martin Tower

3.3 Instrumentation and Equipment Not Installed

Unfortunately, efforts to install a high-speed network camera were not successful. The use of power for this camera from the luminaires on the sign structure or the light pole on the abutment wing wall and other concerns from Penn DOT prevented the camera from being installed. This camera would have given researchers the ability to view traffic on the bridge in real time. It also would have provided images and video of heavy truck traffic that caused a certain level of stress in a specified member. The response of instrumented members could be associated with a particular vehicle, namely the number of axles and axle spacing. The camera also would have verified the assumptions of transverse vehicle position (i.e., lane of travel).

4.0 Long-Term Data

The long-term data were collected over the past 38 months beginning in January 2002, from the vibrating wire gages installed on selected truss members and in the reinforced concrete deck. The findings presented in this Final Report reflect data collected up until late February, 2005. The fluctuations in temperature and strain from the inherent daily cycles were measured. However, the daily cycles made it difficult to distinguish patterns and draw conclusions about the long-term time dependent behavior directly for the 38-month period. Therefore, a program employing a Chebyshev filter was developed to remove the unwanted effects of daily cycles from the data.

A Chebyshev filter is used to separate one band of frequencies from another (Smith, 1999). Essentially, it removes unwanted frequencies above or below a specified frequency. In this case, a low-pass filter was used to remove the unwanted high frequency inherent in the daily cycles (over the 38-month period, the daily cycles can be thought of as high frequency cycles). A comparison of the unfiltered raw temperature data to the filtered temperature data for the west gage of U18-L19 West can be seen in Figure 4.1 for a portion of the data collection period. A closer view of the filter eliminating the inherent daily cycles in the data can be seen in Figure 4.2 for the same gage. Filtering was performed on all of the long-term temperature and strain gages.

In addition to filtering, the strain gage data were numerically zeroed. This is reflected in all long-term microstrain figures in this report. Figures in the previous Interim Report were not numerically zeroed. Each strain gage had a unique starting value, and numerical changes in strain over the long run were less apparent. Numerical increases (or decreases) in microstrain are much more visible in this Final Report since the scale of microstrain has been numerically zeroed for each strain gage. Also, there are periods of time where long-term data were not collected for various reasons. These "gaps" appear in the long-term figures of this section as horizontal lines in the plots.

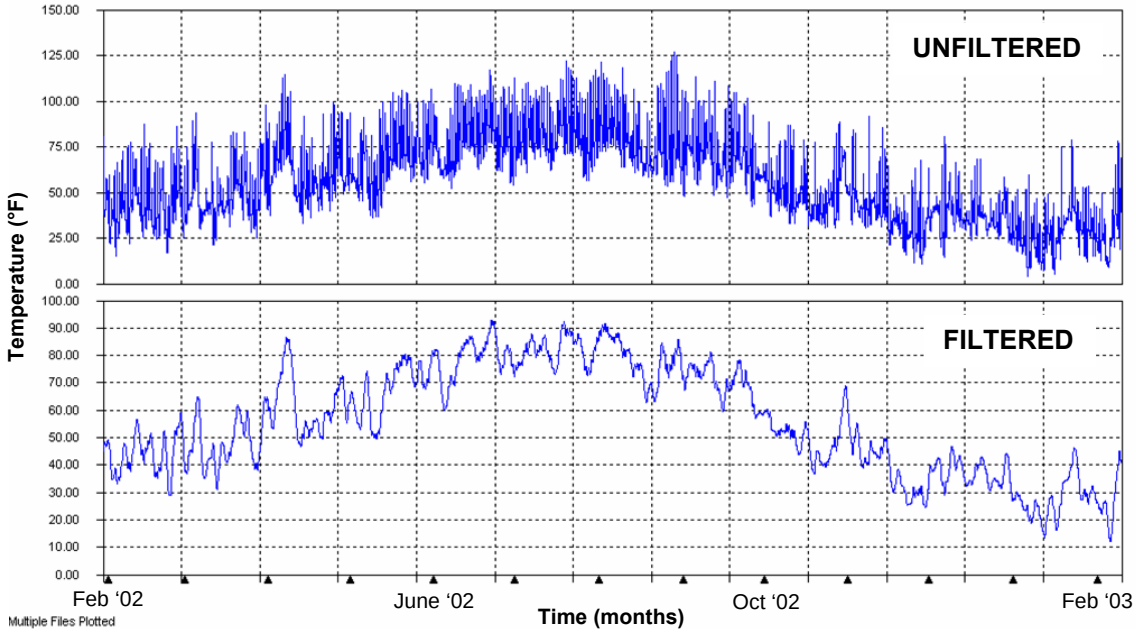

Figure 4.1: Comparison of unfiltered to filtered temperature data for west gage of U18-L19 West (TDW1819WW) for a portion of the collection period

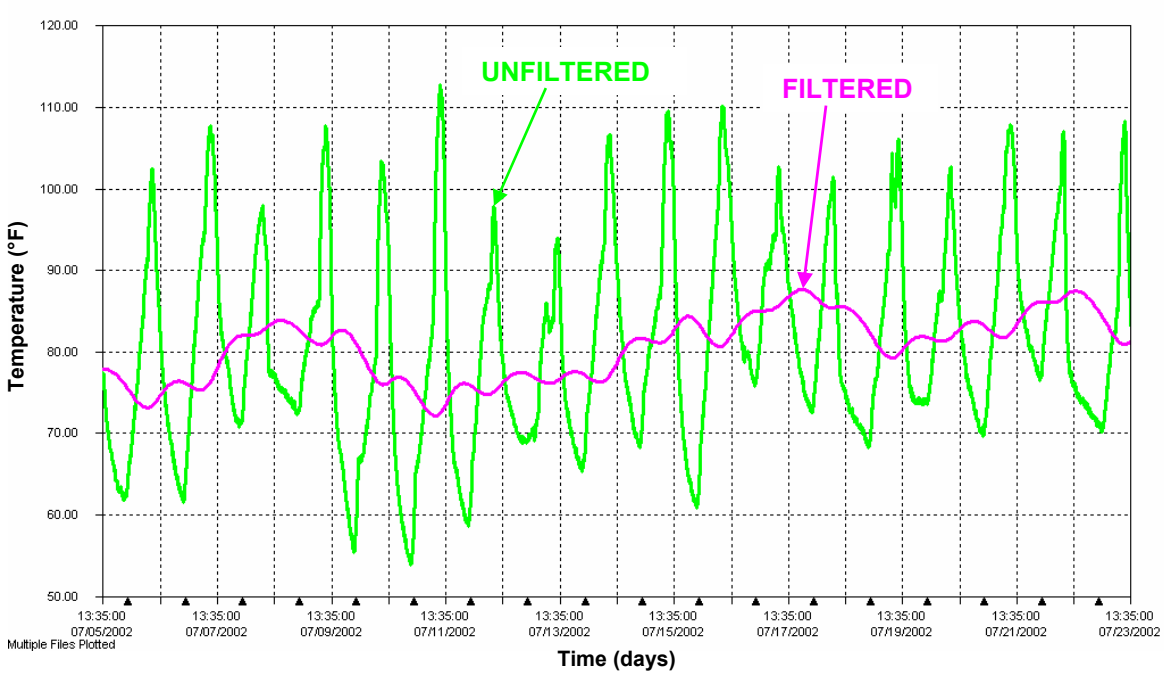

Figure 4.2: Close up view of a portion of unfiltered and filtered temperature data for west gage of U18-L19 West (TDW1819WW)

When examining the response of the long-term strain gages to a change in temperature, the upper chords above pier 2 experienced an increase in strain with an increase in temperature and a decrease in strain with a decrease in temperature. On the other hand, the lower chords at midspan of span 2 behaved in the opposite manner. The lower chords experienced an increase in strain with a decrease in temperature and decrease in strain with an increase in temperature. Although this was the expected behavior for these members at their particular locations of the truss, the behavior required verification.

Therefore, a simplified two-dimensional finite element model of the truss was created using SAP2000 to verify the response of the upper and lower chord members. The model consisted of frame elements. The cross-section of the bridge near midspan of span 2 over the river was used to simulate the geometry of the bridge. Thus, most individual truss members were not assigned a property corresponding to its true cross-section and geometry. Upper chord frame elements were assigned the area and moment of inertia equivalent for the composite deck, upper chord and stringers. A typical diagonal was chosen from the design drawings to represent all diagonals in the model for simplicity. The lower chord geometry was chosen in the similar manner. The restraints were chosen to simulate those called out in the drawings prepared by URS Corporation and the two large river piers were included in the model. A picture of the model is shown in Figure 4.3.

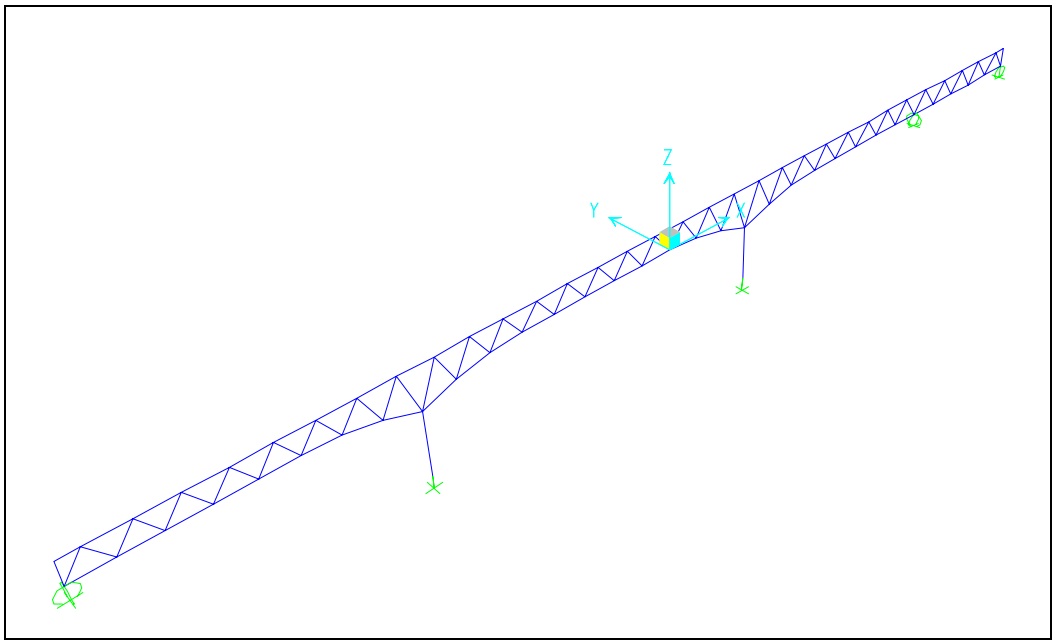

Figure 4.3: Two-dimensional SAP2000 model of SR-33 truss bridge

It should be noted that the model created only verifies the behavior of the upper chords and lower chords. A more detailed three-dimensional model would be required to analyze the response of other members such as the stringers, deck reinforcement, and sway bracing. However, it is reasonable to assume that the measured response for all other instrumented members is accurate from the behavior of the upper and lower chords.

4.1 Upper Chord Response

4.1.1 Temperature Behavior

A review of all temperature gages installed on upper chord members is summarized in Table 4.1 with their respective locations. An "X" in the column labeled "Functionality" denotes that the gage is not functioning properly. This was determined by examining the data over the collection period from January, 2002 to February, 2005.

Gage Name	Location	Functionality
TBU1618EW	East U16-U18 West face	OK
TBU1618EB	East U16-U18 Bottom face	X
TBU1618EE	East U16-U18 East face	OK
TBU1618WW	West U16-U18 West face	OK
TBU1618WB	West U16-U18 Bottom face	OK
TBU1618WE	West U16-U18 East face	OK

Table 4.1: Upper chord temperature gages and their functionality

The long-term temperature response of a typical upper chord gage is shown in Figure 4.4. The bottom gage temperature response of U16-U18 West is plotted versus time. Overall, the gage behaves as expected. The temperature rises during the summer months and declines during the winter. The figure appears to indicate slightly warmer

temperatures during the summer of 2002 than the following two summers. The lowest temperatures observed during the winter months remained fairly consistent throughout the data collection period. The red arrow in the figure indicates a high temperature during the middle of the month of April, 2002. This was consistent with measured data from a weather station located on Lehigh University's campus. This temperature response in April, 2002 is typical for other instrumented members and will be seen in subsequent long-term temperature figures. The other upper chord gages exhibited similar behavior as the gage shown in Figure 4.4. All figures illustrating long-term response (i.e., temperature or strain) will have a time scale in months as shown in Figure 4.4. The letter "F" is an abbreviation for the month of February as is the letter "A" for the month of August.

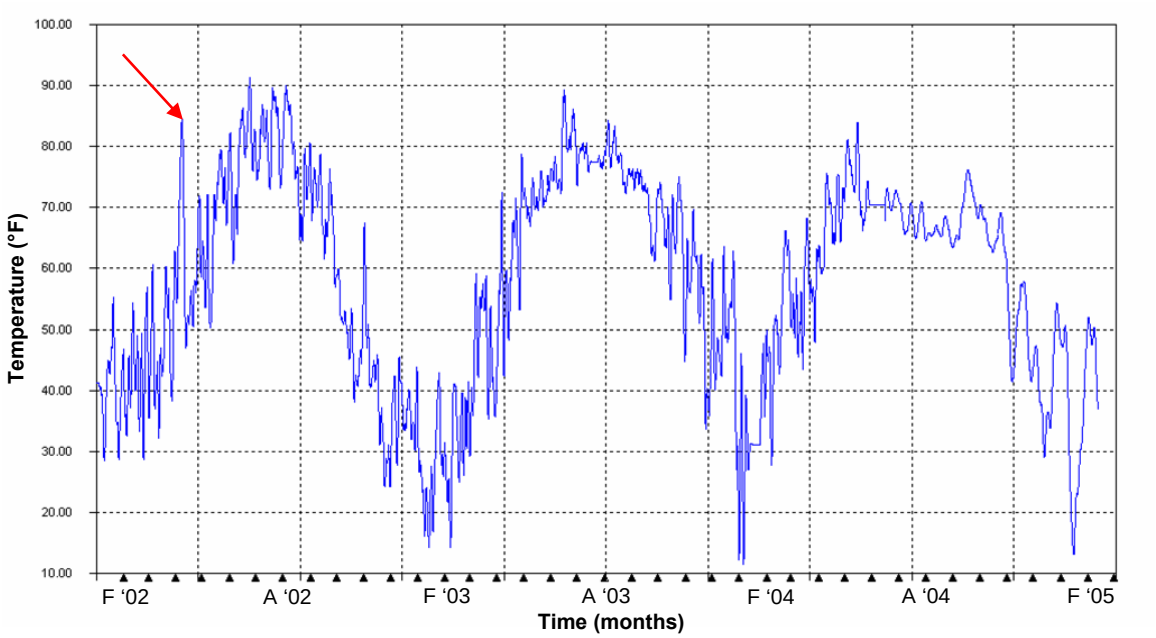

Figure 4.4: Temperature response of bottom gage of U16-U18 West (TBU1618WB)

The temperature distribution of the upper chords remained fairly uniform throughout the period of data retrieval. Figure 4.5 shows the plot of all three gages of the west upper chord. Both side gages and the bottom gage exhibit very similar temperature responses. Variations of only a few degrees Fahrenheit occur throughout the time period. The proximity of the gages to the thermal mass of the concrete deck and the shielding the deck provides to the composite upper chords are the main factors influencing the uniform temperature distribution. This behavior could not be verified over the entire 20 month period for the east upper chord. The bottom temperature gage (TBU1618EB) experienced an offset in August, 2002 which caused the gage to read temperature values approximately 10 °F below its side temperature gages. However, the east upper chord exhibited a uniform temperature distribution up until August, 2002 similar to the distribution for the west upper chord in Figure 4.5.

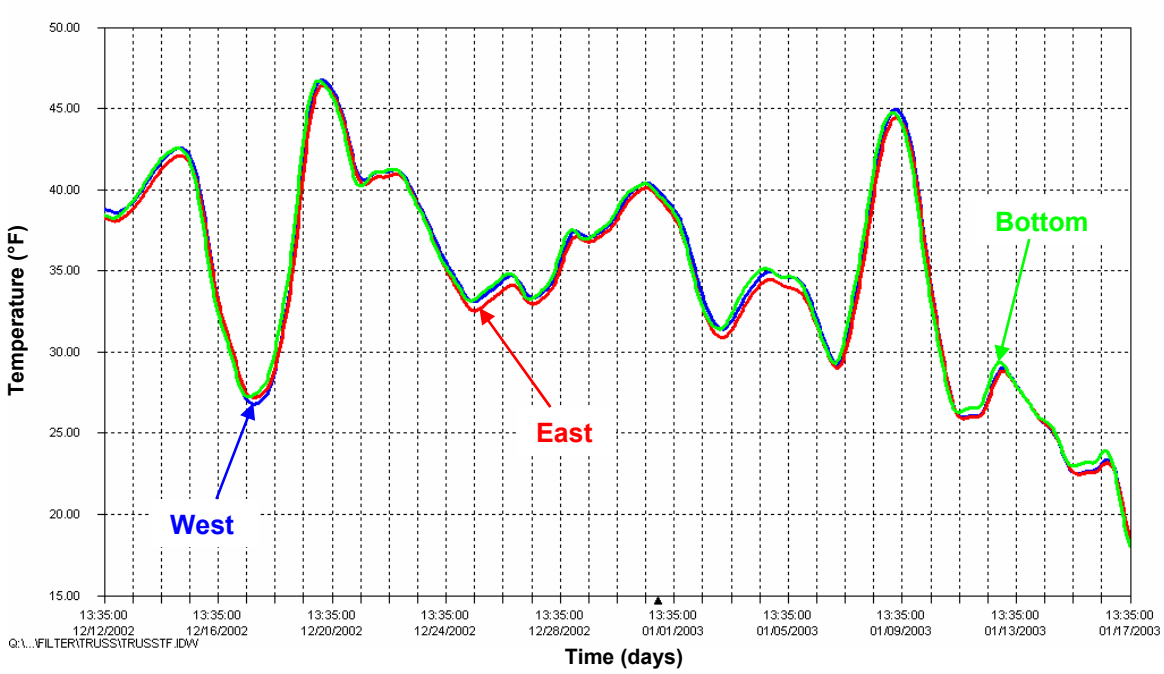

Figure 4.5: Portion of temperature response of all gages on U16-U18 West

4.1.2 Strain Behavior

Vibrating wire strain gages were installed on the upper chords at the following locations listed in Table 4.2. An "X" indicates that the gage is not functioning properly.

Gage Name	Location	Functionality
SBU1618EW	East U16-U18 West face	OK
SBU1618EB	East U16-U18 Bottom face	X
SBU1618EE	East U16-U18 East face	OK
SBU1618WW	West U16-U18 West face	OK
SBU1618WB	West U16-U18 Bottom face	OK
SBU1618WE	West U16-U18 East face	OK

Table 4.2: Upper chord vibrating wire strain gages and their functionality

The unfiltered temperature response of an upper chord, diagonal, and lower chord to the daily temperature cycles is seen in Figure 4.6 for a period of about four days. It is clear from the figure that the upper chord lags behind the diagonal and lower chord when the truss heats up. The diagonal and lower chord both reach higher peaks in temperature than the upper chord. Also, it is apparent that the upper chord cools more slowly than the diagonal and lower chord. Typically, this results in differential heating of the truss because there is a point in time when the diagonal and lower chord are warmer than the upper chord and a point when the diagonal and lower chord are cooler than the upper chord.

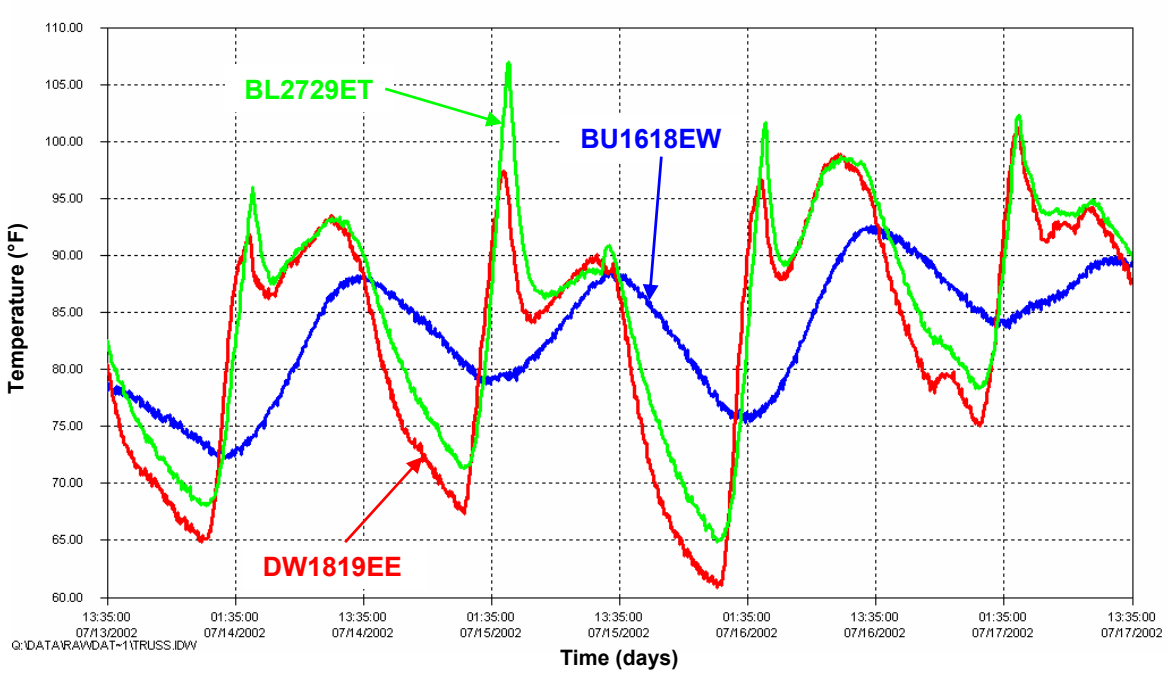

Figure 4.6: Temperature response of typical upper chord, lower chord and diagonal

These two temperature load cases were applied to the model to further verify the measured strain response of members to differential heating. The first load case applied a higher temperature to all of the diagonals and lower chords in the model. The second load case applied a higher temperature to all of the upper chords. Table 4.3 indicates these two load cases and the specific temperatures applied to the members. These temperature values were taken from data at specific points in time when either the upper chord was cooler than or warmer than both the diagonal and lower chord. These load cases will be referred to as Load Case 1 and Load Case 2 for the remainder of the discussion.

Load Case	Temperature (°F)		
	Upper Chords	Diagonals	Lower Chords
1	75	90	95
2	80	65	65

Table 4.3: Temperature load cases applied to SAP2000 model

Figure 4.7 illustrates the response of the east gage of U16-U18 East. The temperature and strain response are both plotted with respect to time. It can be seen that the trend for this upper chord gage is an increase in strain with increasing temperature and a decrease in strain with decreasing temperature.

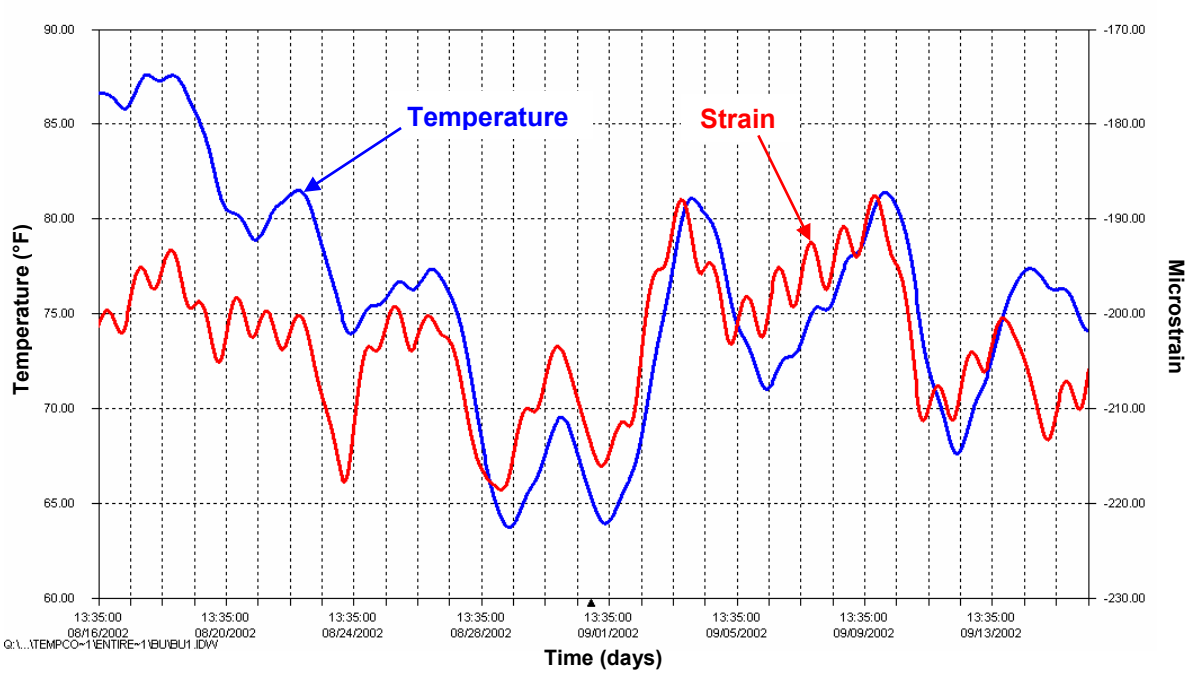

Figure 4.7: Portion of temperature and strain response of east gage of U16-U18 East (BU1618EE)

The bottom gage temperature and strain behavior of U16-U18 West is seen in Figure 4.8. The same trend in the east upper chord prevails in the west upper chord. Strain increases with increasing temperature and decreases with decreasing temperature. As noted before, the lower chords behave in the opposite sense. Strain decreases with increasing temperature and increases with decreasing temperature. This behavior will be discussed in Section 4.2.2.

It would be expected that from this behavior, the upper chord would be in compression whenever the lower chord is in tension due to the differential heating. The model created using SAP2000 also demonstrated this same behavior. When the lower chords and diagonals were heated to a temperature warmer than the upper chord (Load Case 1), the upper chord above pier 2 experienced tension while the lower chord at midspan of span 2 experienced compression. Applying Load Case 2, the upper chord experienced compression while the lower chord experienced tension.

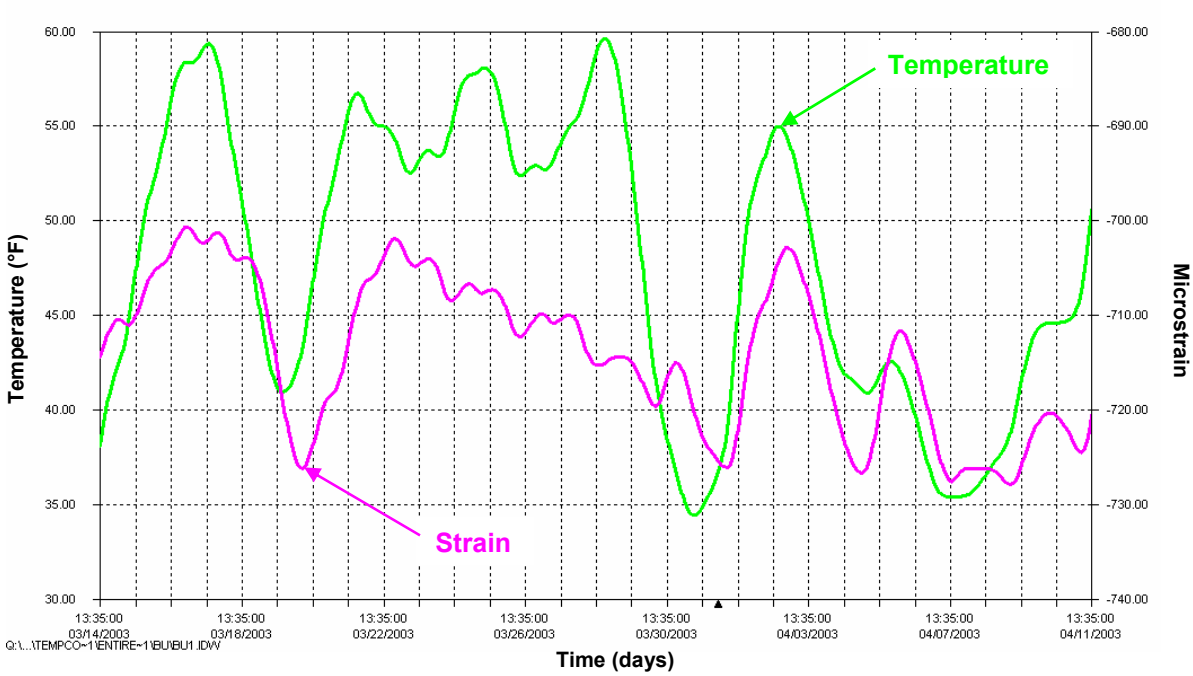

Figure 4.8: Portion of temperature and strain response of bottom gage of U16-U18 West (BU1618WB)

The long-term variation in temperature and strain for the east gage of U16-U18 West can be seen in Figure 4.9. It is apparent from the plot that the upper chord is experiencing a gradual and slight increase in strain over time. From a structural analysis viewpoint, it is expected that the upper chords over pier 2 would experience increasing tension over time due to creep in the concrete. As the concrete creeps at midspan of span 2, the truss would begin to sag similar to the structure under its own self-weight. Since the upper chords at U16-U18 are located in the negative moment region of the bridge, downward vertical deflection of the structure causes tensile stress in the chords.

The microstrain curve also appears to be "leveling off" suggesting most of the shrinkage and creep effects have stabilized. The rate of increase in microstrain due to creep seems to be diminishing over time. This is consistent with the expected long-term characteristics of creep in concrete. This very gradual increase in strain is typical for all other functioning upper chord gages.

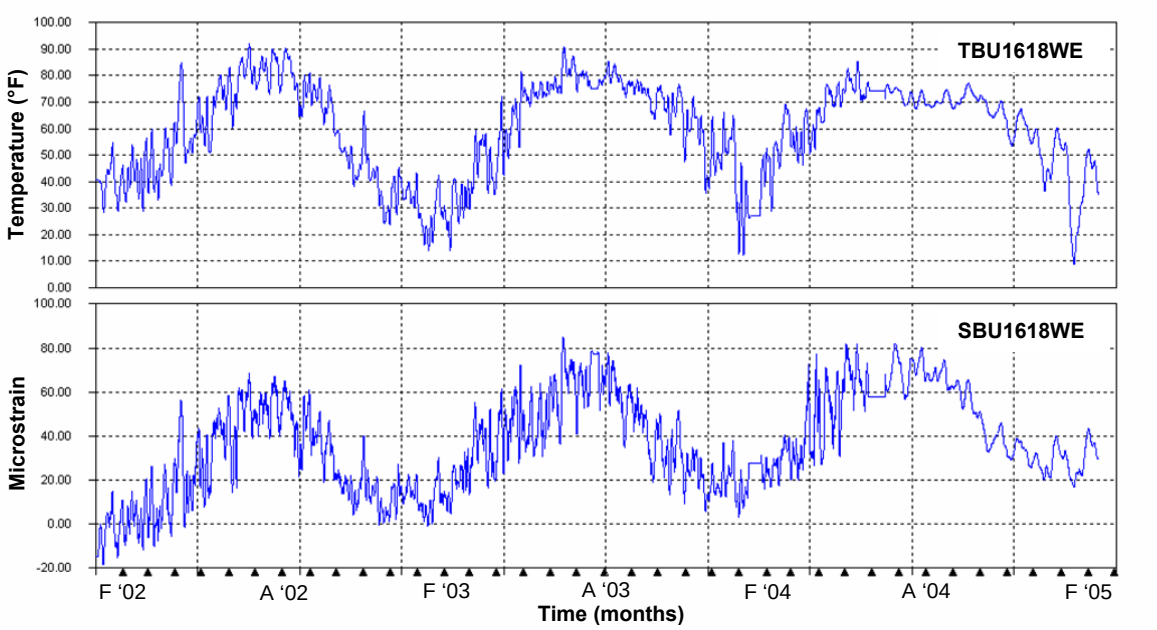

Figure 4.9: Long-term temperature and strain response of east gage of U16-U18 West

The strain response of all three vibrating wire gages on U16-U18 West is illustrated in Figure 4.10. It is evident from the figure that the gages on the east and west flange plates (SBU1618WE and SBU1618WW) of the box have very similar responses. The bottom gage (SBU1618WB) readings are of larger magnitude than the side gages. Therefore, the overall response of the member to creep is not purely axial. However, the difference in magnitude of microstrain between the gages is so little that the response of the upper chord to creep over time is predominantly axial. The responses of the side flange plate gages on U16-U18 East are also very similar. As noted earlier, the bottom gage of U16-U18 East (SBU1618EB) was not functioning properly.

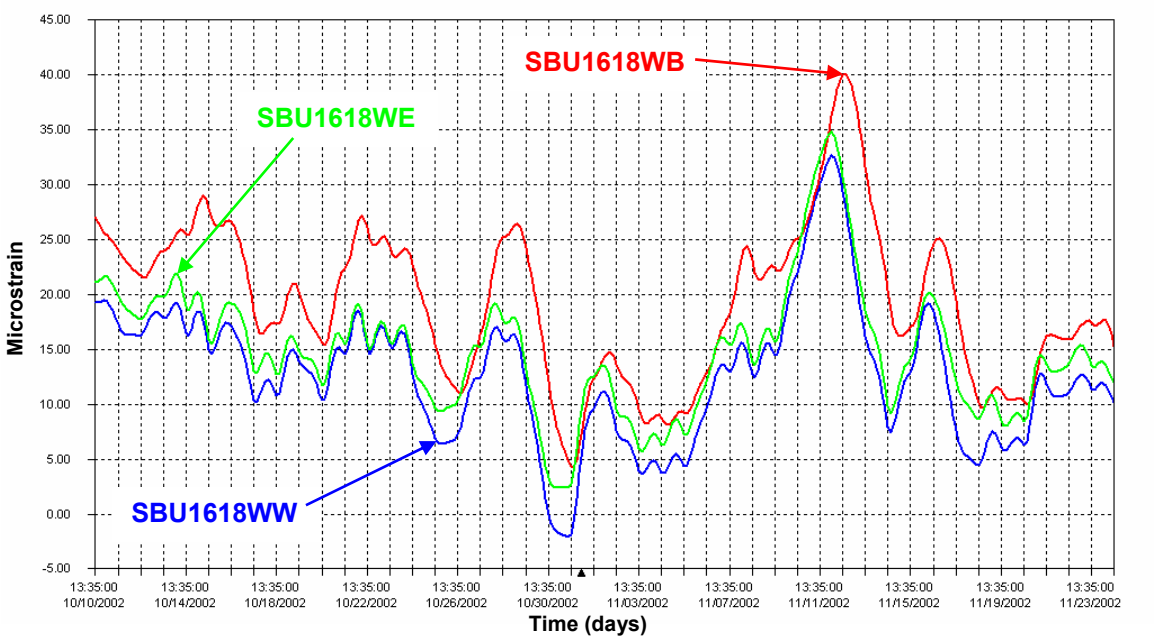

Figure 4.10: Portion of strain response of all gages on U16-U18 West

The changes in stress over time were calculated for each of the functioning upper chord gages. This was achieved by averaging the temperature and strain data over ten (10) days for each time interval. Periods of time that had similar average temperature values were compared to each other in order to eliminate any thermal effects. The change in microstrain was converted to change in stress using a modulus of elasticity E = 29000 ksi. A summary of these changes is presented in Table 4.4. From the table it is clear that the upper chords are experienced very small changes in stress. It is apparent that all gages experienced a decrease in stress from March, 2003 to February, 2004. The largest increases in stress occurred early in the data. Overall, the upper chords encountered a gradual increase in stress over time, consistent with the behavior shown in Figure 4.9.

Gage Name	Change in Stress (ksi)		
	Mar '02 to Mar '03	Mar '03 to Feb '04	Feb '04 to Feb '05
SBU1618EW	0.83	-0.25	0.32
SBU1618EE	0.85	-0.29	0.36
SBU1618WW	0.70	-0.25	0.42
SBU1618WB	0.92	-0.24	0.48
SBU1618WE	0.78	-0.27	0.36

Table 4.4: Summary of changes in stress for upper chord gages

4.2 Lower Chord Response

4.2.1 Temperature Behavior

Table 4.5 lists the temperature gages installed on the lower chords and their functionality. An "X" denotes that the gage is not functioning properly.

Gage Name	Location	Functionality
TBL2527ET	East L25-L27 Top face	OK
TBL2527EB	East L25-L27 Bottom face	X
TBL2527WT	West L25-L27 Top face	OK
TBL2527WB	West L25-L27 Bottom face	OK
TBL2729ET	East L27-L29 Top face	OK
TBL2729EB	East L27-L29 Bottom face	X
TBL2729WT	West L27-L29 Top face	OK
TBL2729WB	West L27-L29 Bottom face	OK

Table 4.5: Lower chord temperature gages and their functionality

A lower chord temperature gage response is seen in Figure 4.11. The top gage response of L25-L27 East is plotted versus time. As expected, the temperature rises during the summer months and declines during the winter. There are minor differences in temperature from summer to summer and winter to winter. It could be argued that the summer of 2004 experienced slightly cooler temperatures than the previous two years. Overall, the winter months reach similar lows in temperature. There was a rapid increase in temperature discussed in the Interim Report that occurred around June 20, 2003 for all other functioning lower chord gages. After reducing the latest data, it was determined that this rapid increase in temperature was questionable as it led to extremely high temperatures during the winter of 2004 for these lower chord gages and is believed to be the result of electrical noise. Therefore, the long-term temperature response of BL2527ET is shown since it provides a response that is in better agreement with anticipated behavior.

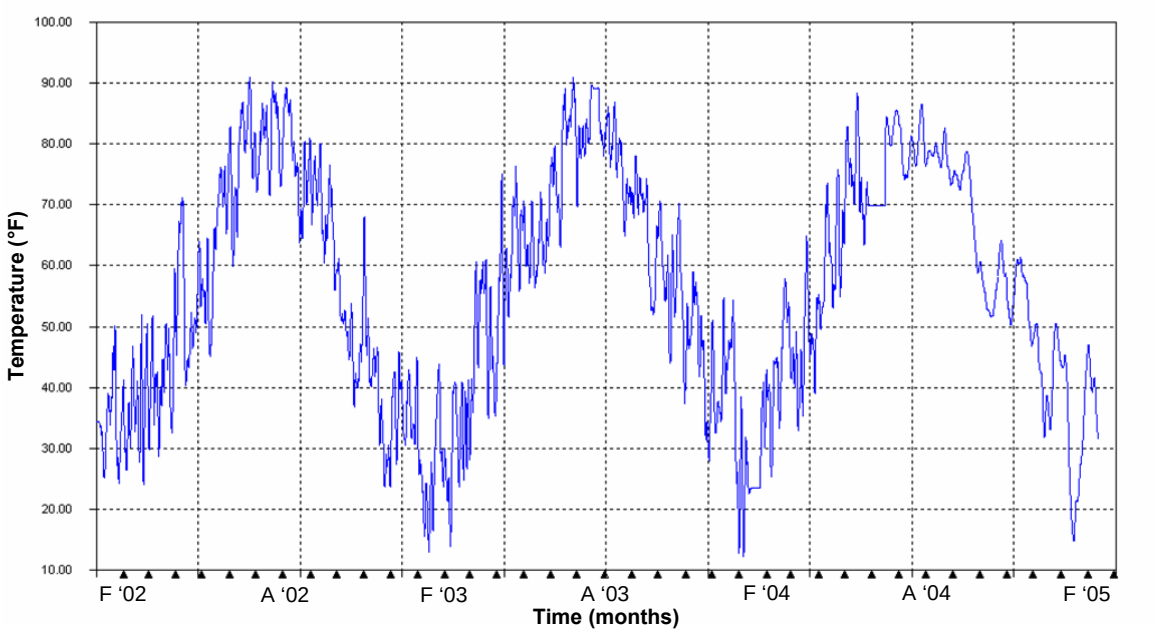

Figure 4.11: Temperature response of top gage of L25-L27 East (TBL2527ET)

The temperature response of top and bottom gages on the same lower chord behaved as expected. The top gage usually measured a higher temperature than the bottom gage. The top face is directly exposed to the sun and therefore would have a higher temperature response than the bottom face of the member. For the most part, this difference was minimal. However, the lower chords consistently displayed this behavior. Figure 4.12 shows the response of both top and bottom gages of L27-L29 West. This behavior could not be verified for all lower chord members since some temperature gages were not functioning properly. However, it is reasonable to assume this response is typical for other lower chord members because the top face of the member is more directly exposed to sunlight.

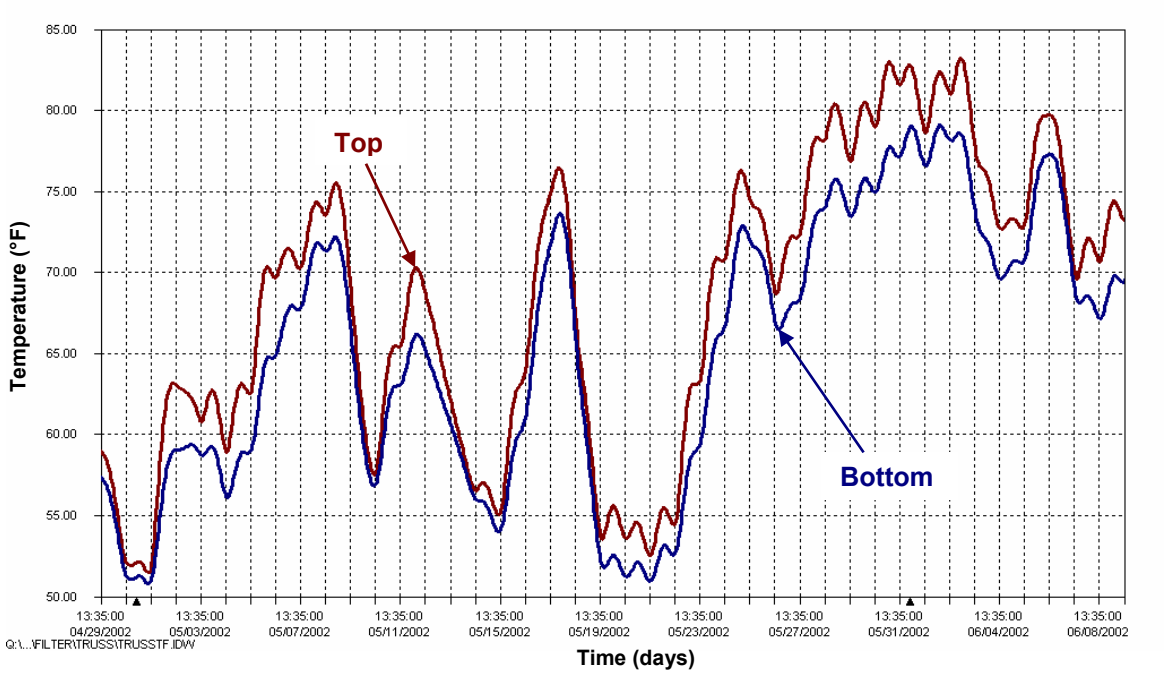

Figure 4.12: Portion of temperature response of both gages on L27-L29 West

4.2.2 Strain Behavior

The vibrating wire strain gages installed on the lower chords are listed in Table 4.6. Gages that are not functioning properly are designated by an "X" in the column labeled "Functionality".

Gage Name	Location	Functionality
SBL2527ET	East L25-L27 Top face	OK
SBL2527EB	East L25-L27 Bottom face	OK
SBL2527WT	West L25-L27 Top face	OK
SBL2527WB	West L25-L27 Bottom face	OK
SBL2729ET	East L27-L29 Top face	X
SBL2729EB	East L27-L29 Bottom face	X
SBL2729WT	West L27-L29 Top face	OK
SBL2729WB	West L27-L29 Bottom face	X

Table 4.6: Lower chord vibrating wire strain gages and their functionality

As described earlier, the lower chords behave in the opposite sense to that of the upper chords. Figure 4.13 shows the temperature and strain response of the top gage of L25-L27 East. It is clear from the figure that this lower chord experiences decreases in strain with increasing temperature and increases in strain with decreasing temperature. Thus, the upper and lower chords have opposite strain responses to corresponding changes in temperature.

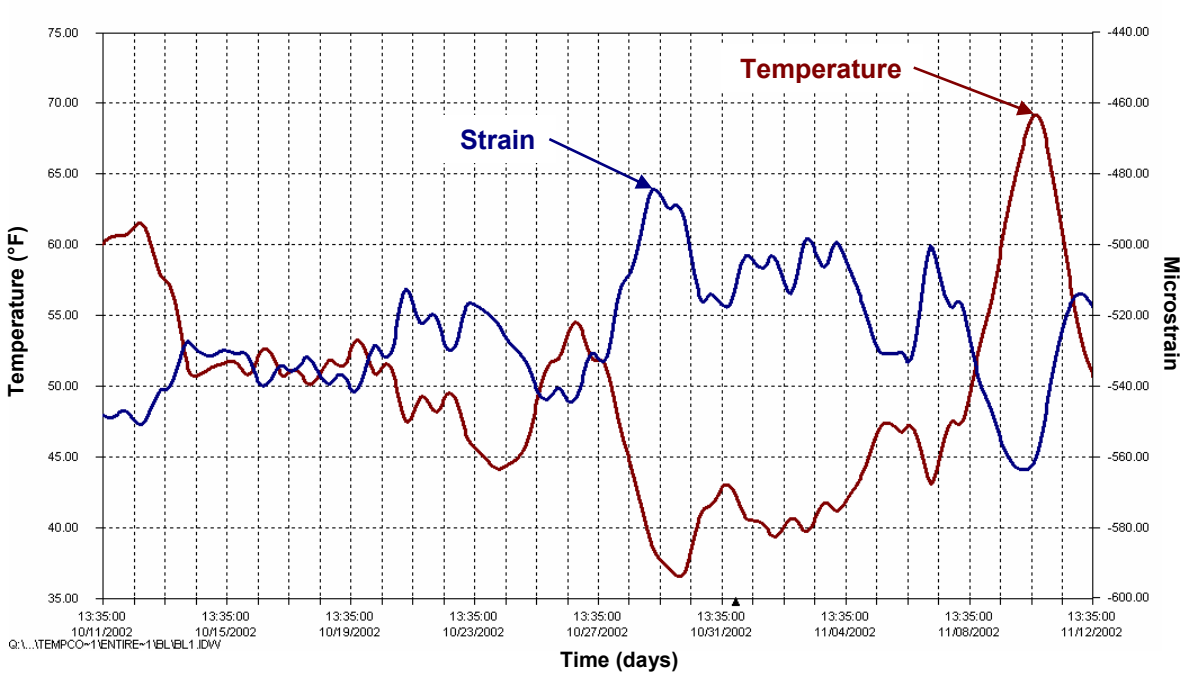

Figure 4.13: Portion of temperature and strain response of top gage of L25-L27 East (BL2527ET)

The behavior seen for L25-L27 East can also be seen for L27-L29 West. The response of the bottom gage of L27-L29 West is shown in Figure 4.14. This lower chord experiences decreases in strain with increasing temperature and increases in strain with decreasing temperature. Other functioning lower chord gages exhibit this behavior.

It would be expected from this behavior that the lower chords would act in the opposite sense of the upper chords due to the differential heating between these members. The two-dimensional SAP2000 model is also consistent with this behavior when Load Case 1 and Load Case 2 are applied to the simplified finite element model.

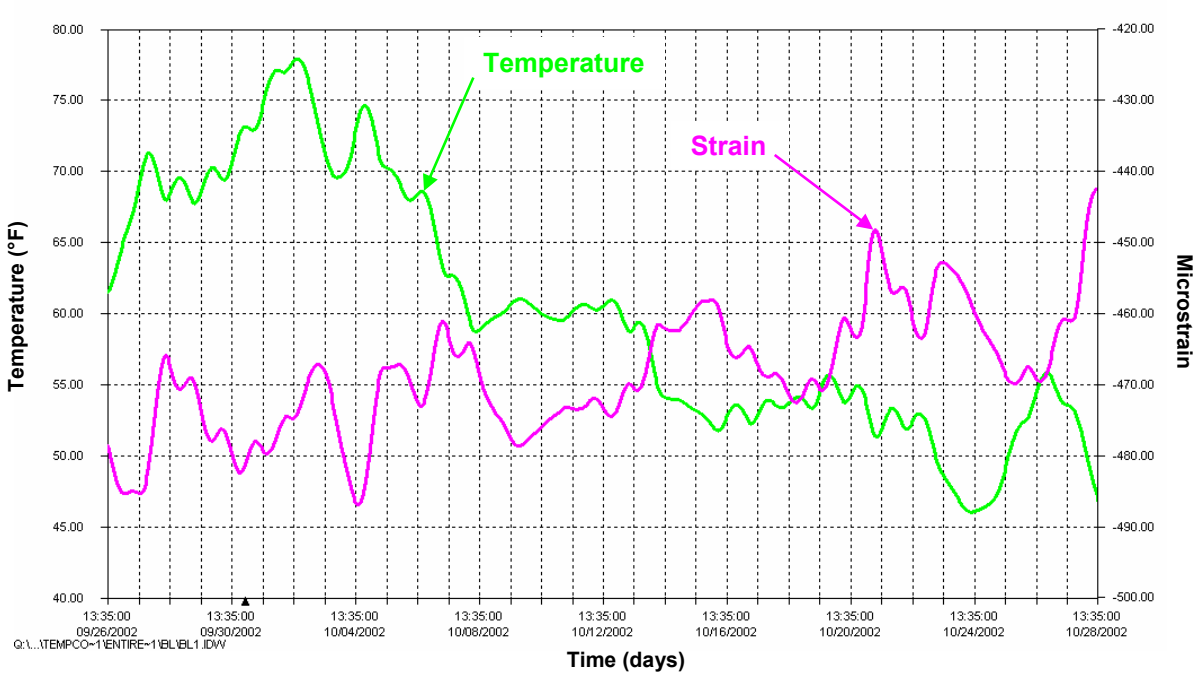

Figure 4.14: Portion of temperature and strain response of bottom gage of L27-L29 West (BL2729WB)

The long-term strain response of the top gage of L25-L27 West from the Interim Report is shown in Figure 4.15. The long-term strain data for the lower chords was much noisier than the data for the upper chords. However, the filtering techniques employed were successful in removing most of the noise. It is apparent from the plot that the lower chord is experiencing an increase in strain over time. However, a rapid increase in microstrain occurs near May 2003 as indicated in the figure. This rapid increase in strain was also observed for all other gages on the lower chords. Additional data were reduced and it was determined that this was a fictitious numerical offset in the data. It is felt that an event occurred which caused the vibrating wire strain gages on the lower chords to appear to abruptly offset to a higher level of microstrain due to electrical noise.

The long-term temperature and strain behavior for the top gage of L25-L27 East is shown in Figure 4.16. This plot contains data up until February, 2005 and has removed the numerical offset that occurred due to noise in May, 2003. The figure illustrates that there is little change in strain over time for this gage location. If any, there is a slight increase in strain over time for the data collected up to this point. This slight increase in tension over time is consistent with expected behavior from structural analysis. As discussed for the upper chords over pier 2, concrete creep in the structure causes downward vertical deflection of span 2. The lower chords near midspan (L25-L27 and L27-L29) experience tensile stress.

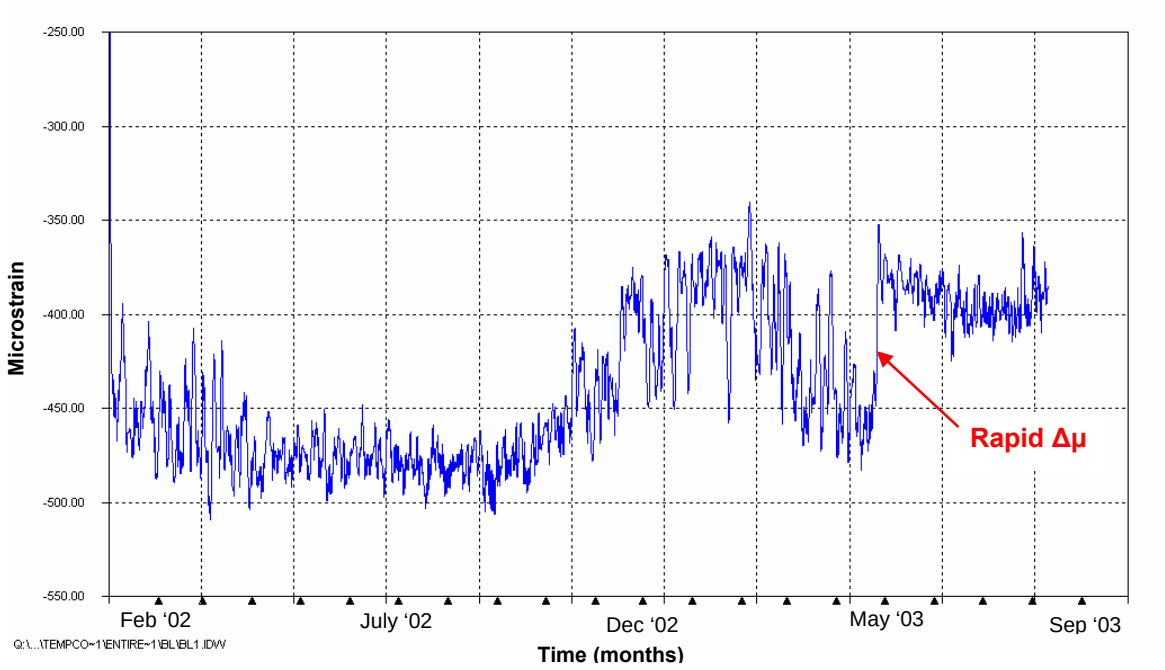

Figure 4.15: Long-term strain response of top gage of L25-L27 West from Interim Report (SBL2527WT)

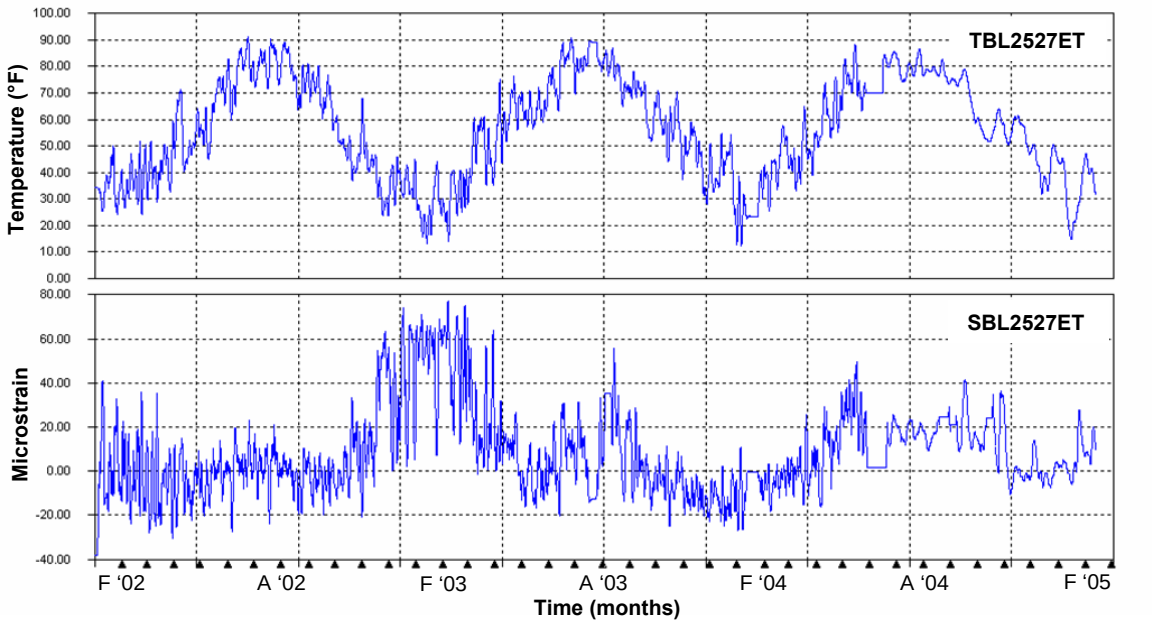

Figure 4.16: Long-term temperature and strain response of top gage of L25-L27 East (offset in May 2003 removed)

Changes in stress were calculated for the lower chord gages that produced accurate data. These variations are presented in Table 4.7. Overall, the largest increase in stress occurred early in the data. A decrease in stress then occurred from March, 2003 to March, 2004. This was followed by a slight increase in stress from March, 2004 to February, 2005. The increase for SBL2527EB is identified with a "?" since there were

numerous noise spikes near the end of the data in February, 2005 for this gage. It appears that the stress is "leveling off" over time, consistent with the response shown in Figure 4.16.

Gage Name	Change in Stress (ksi)		
	Mar '02 to Mar '03	Mar '03 to Mar '04	Mar '04 to Feb '05
SBL2527ET	1.26	-1.10	0.32
SBL2527EB	1.45	-0.95	*1.51?*
SBL2527WB	1.44	-0.57	0.48
SBL2729WT	1.22	-1.12	0.17

Table 4.7: Summary of changes is stress for lower chord gages

4.3 Diagonal Response

4.3.1 Temperature Behavior

A list of the temperature gages installed on the diagonal members is presented in Table 4.8. Gages that are not functioning properly are marked with an "X".

Gage Name	Location	Functionality
TDW1819EW	East U18-L19 West face	OK
TDW1819EE	East U18-L19 East face	OK
TDW1819WW	West U18-L19 West face	OK
TDW1819WE	West U18-L19 East face	OK
TDW2021EW	East U20-L21 West face	X
TDW2021EE	East U20-L21 East face	OK
TDW2021WW	West U20-L21 West face	X
TDW2021WE	West U20-L21 East face	OK

Table 4.8: Diagonal temperature gages and their functionality

A typical diagonal temperature response is shown by the west gage of U18-L19 West in Figure 4.17. The temperature increases during the summer and decreases during the winter as expected. The summers of 2003 and 2004 appear to have experienced slightly cooler temperatures than 2002. The low temperatures during the winters are comparable in value. Also, the maximum temperature of the diagonal did not reach the same peak as the gages on the top surface of the lower chord (see Figure 4.6). This is because the vertical face of the diagonal does not receive the same intensity of sunlight as the top face of the lower chord.

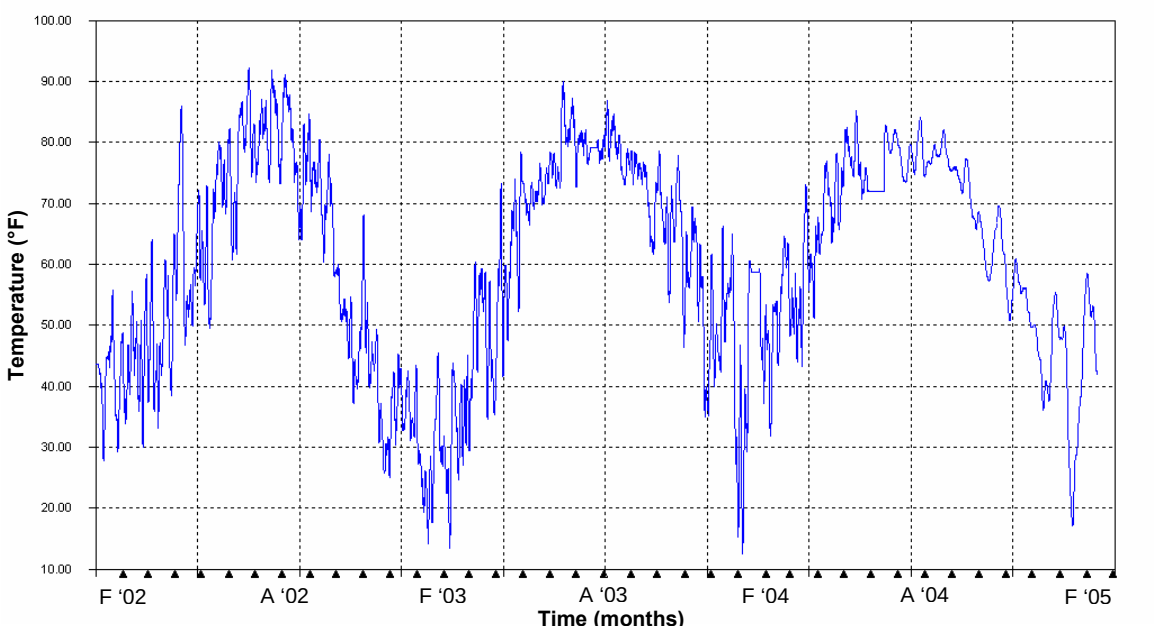

Figure 4.17: Temperature response of west gage of U18-L19 West (TDW1819WW)

The temperature response of both east and west gages on U18-L19 West is shown in Figure 4.18. The two gages on this member exhibit the same temperature response. Differences in temperature are minimal and the temperature distribution for this member remains fairly uniform as shown previously with the upper chords. This response could not be verified for all instrumented diagonals since all temperature gages were not functioning correctly. However, this behavior was verified for both U18-L19 West and U18-L19 East. It is reasonable to assume this behavior prevails in the diagonals at U20-L21 as well.

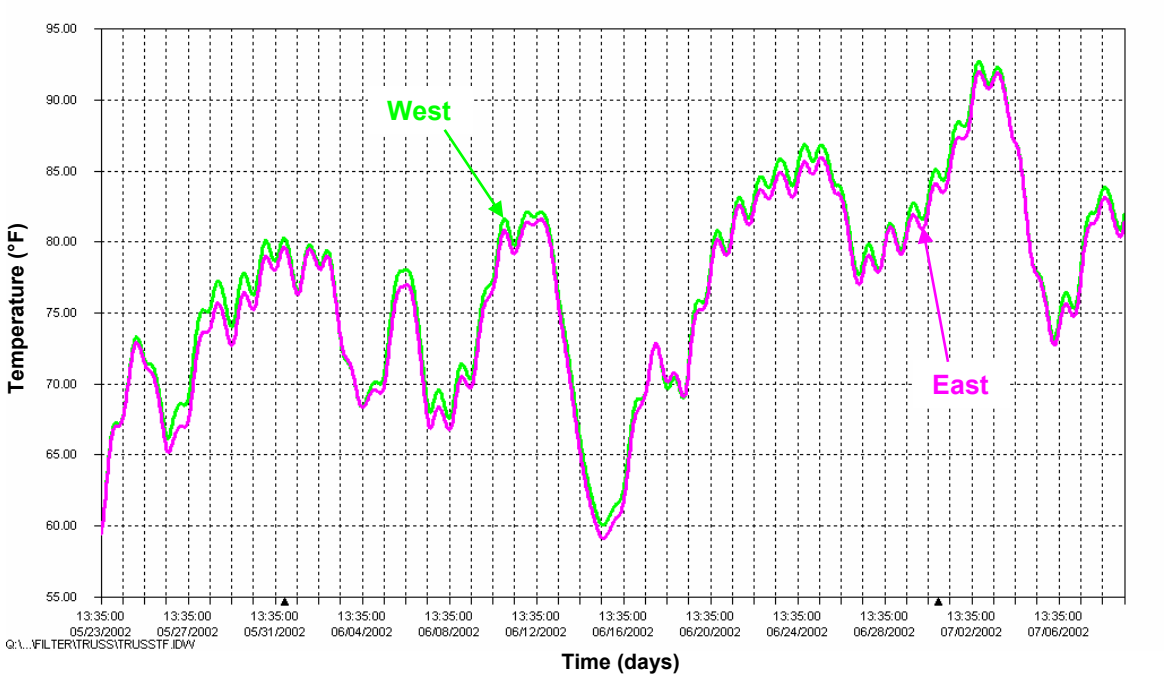

Figure 4.18: Portion of temperature response of both gages on U18-L19 West

The response of diagonal gages on opposite sides of the truss is shown in Figure 4.19. Specifically, U20-L21 East and U20-L21 West are compared. The plot shows that both diagonals exhibit similar temperature responses. In some cases, the diagonal on the west truss is slightly warmer than the diagonal on the east truss. The sun is usually positioned on the west side of the bridge during the warmest part of the day. However, the response shown in Figure 4.19 is the predominant behavior for the instrumented diagonals.

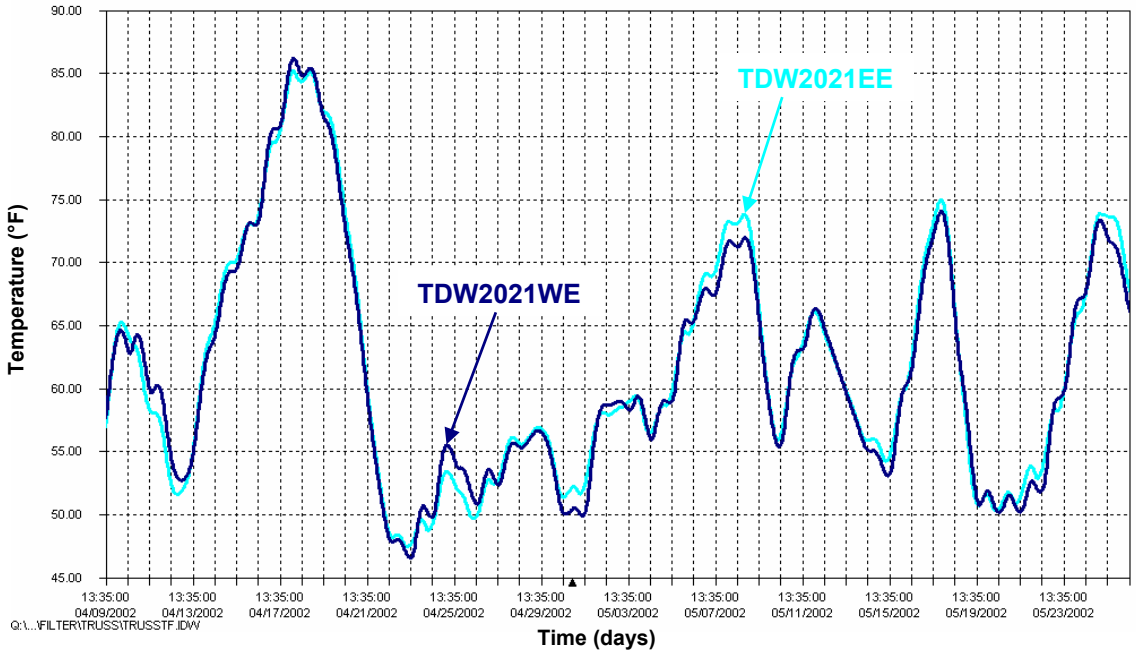

Figure 4.19: Portion of temperature response of U20-L21 East and U20-L21 West

4.3.2 Strain Behavior

Table 4.9 displays the locations of all vibrating wire strain gages installed on the diagonal members. An "?" denotes that there were periods of questionable data but reliable data were obtained for most of the data collection period.

Gage Name	Location	Functionality
SDW1819EW	East U18-L19 West face	OK
SDW1819EE	East U18-L19 East face	OK
SDW1819WW	West U18-L19 West face	?
SDW1819WE	West U18-L19 East face	OK
SDW2021EW	East U20-L21 West face	OK
SDW2021EE	East U20-L21 East face	OK
SDW2021WW	West U20-L21 West face	OK
SDW2021WE	West U20-L21 East face	OK

Table 4.9: Diagonal vibrating wire strain gages and their functionality

The filtered temperature and strain response of the east gage of U18-L19 West is shown in Figure 4.20. In general, this diagonal experiences increases in strain with increasing temperature and decreases in strain with decreasing temperature. This is similar to the upper chord response. The relationship between temperature and strain for the diagonals throughout the collected data was not as consistent as the upper and lower chords previously discussed.

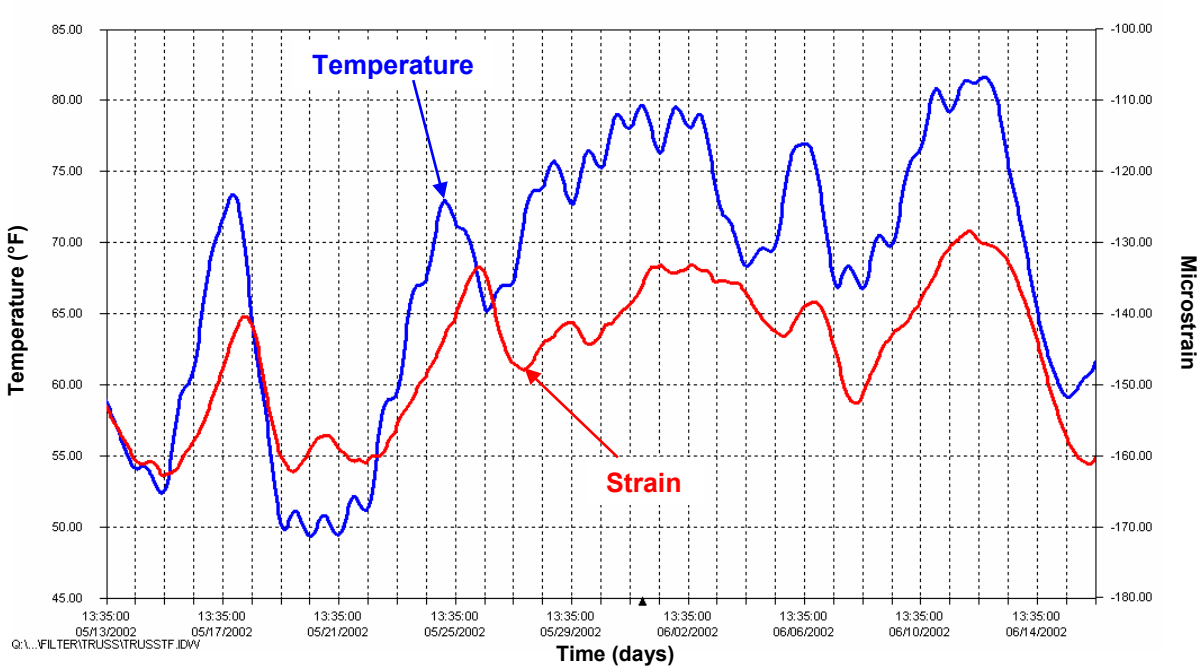

Figure 4.20: Portion of temperature and strain response of east gage of U18-L19 West (DW1819WE)

The response of the east gage of U20-L21 East is shown in Figure 4.21. Generally, this diagonal experiences increases in strain with increasing temperature and decreases in strain with decreasing temperature. This behavior is typical of all the gages installed on the diagonals although the consistency of the trend between temperature and strain is less apparent than in the upper and lower chords. Since the relationship between temperature and strain was not as consistent as the upper and lower chords, a direct comparison to results from the model was not made.

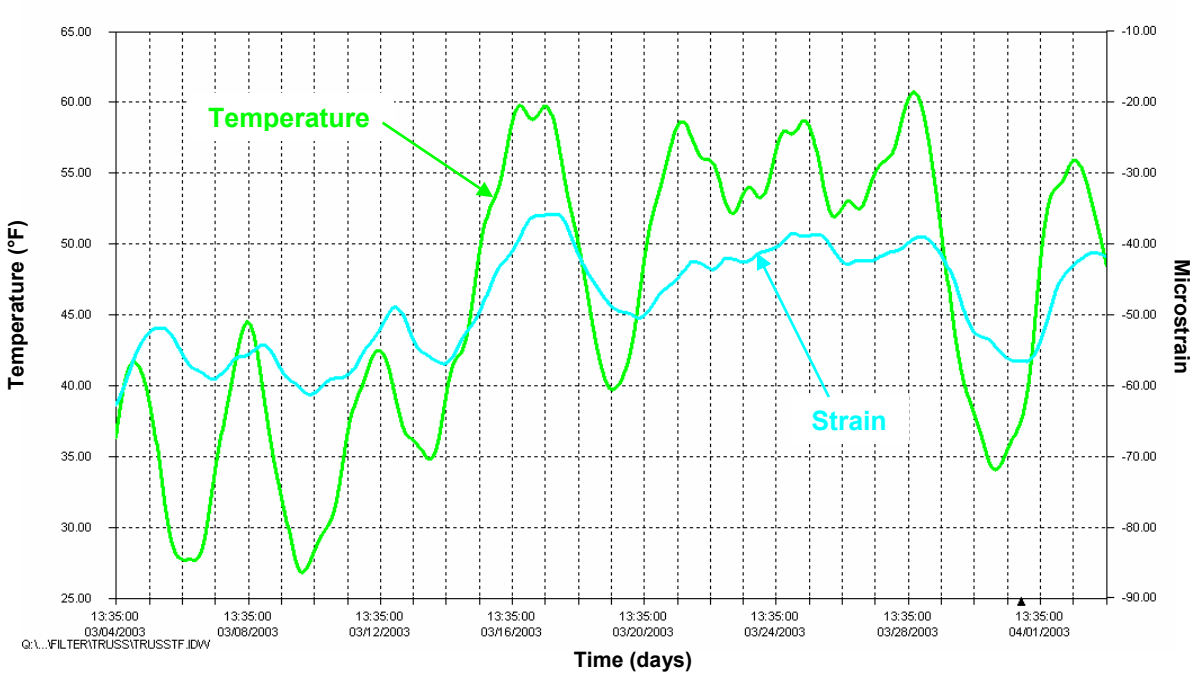

Figure 4.21: Portion of temperature and strain response of east gage of U20-L21 East (DW2021EE)

The long-term variation in temperature and strain for the east gage of U18-L19 West can be seen in Figure 4.22. It is apparent from the plot that the diagonal is experiencing a slight increase in strain over time based on the data collected to date. A similar gradual increase in strain over time prevails in all other functioning diagonal strain gages. Similar to the upper chords, it appears that the increase in microstrain for the diagonals is "leveling off" over time. This is consistent with the expected long-term response of concrete due to creep. As discussed for the upper and lower chords, creep of the concrete near midspan initiates downward vertical deflection of the truss. From structural analysis of the bridge under its own self-weight, the instrumented diagonals (U18-L19 and U20-L21) are primarily tension members. This is comparable to the long-term response of the diagonals due to creep in the concrete.

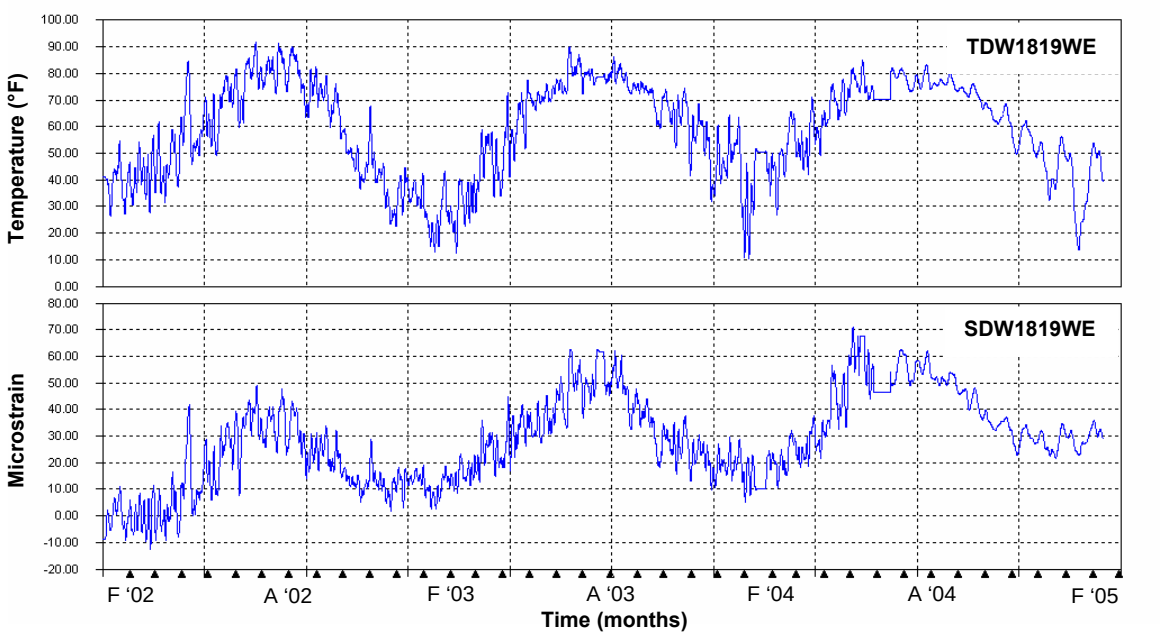

Figure 4.22: Long-term temperature and strain response of east gage of U18-L19 West

Changes in stress over time were calculated for the diagonal members. These changes are presented in Table 4.10. Similar to the upper chords, the stress due to creep in the concrete has increased over the data collection period. For almost all of the gages, this magnitude of increase in stress decreased over time. This is comparable to the plot illustrated in Figure 4.22. The long-term response of the diagonals is consistent with expected behavior due to concrete creep.

Gage Name	Change in Stress (ksi)		
	Feb '02 to Dec '02	Dec '02 to Dec '03	Dec '03 to Dec '04
SDW1819EW	0.33	0.23	0.14
SDW1819EE	0.13	0.32	0.12
SDW1819WE	0.39	0.25	0.25
SDW2021EW	0.35	0.37	0.27
SDW2021EE	0.17	0.39	0.12
SDW2021WW	0.34	0.29	0.17
SDW2021WE	0.39	0.18	0.22

Table 4.10: Summary of changes in stress for diagonal gages

4.4 Sway Bracing Response

4.4.1 Temperature Behavior

The temperature gages installed on the sway bracing members and their functionality are portrayed in Table 4.11. Gages marked with "?" signify that there were periods of questionable data. However, accurate data were recovered for most of the data collection interval.

Gage Name	Location	Functionality
TSB910ET	East cross of sway brace Top face	X
TSB910EB	East cross of sway brace Bottom face	OK
TSB910WT	West cross of sway brace Top face	OK
TSB910WB	West cross of sway brace Bottom face	?
TSB910HT	Horiz. strut of sway brace Top face	OK
TSB910HB	Horiz. strut of sway brace Bottom face	?
TSB2425ET	East cross of sway brace Top face	OK
TSB2425EB	East cross of sway brace Bottom face	X
TSB2425WT	West cross of sway brace Top face	X
TSB2425WB	West cross of sway brace Bottom face	?
TSB2425HT	Horiz. strut of sway brace Top face	X
TSB2425HB	Horiz. strut of sway brace Bottom face	X

Table 4.11: Sway bracing temperature gages and their functionality

The filtered temperature response of the bottom gage of the east cross of sway brace L9-U10 is shown in Figure 4.23. Temperatures increase during the summer and decrease in the winter. It appeared that the sway bracing are exposed to warmer temperatures during the summer of 2003 and 2004. However, this response required verification. A closer view of unfiltered temperature data for all functioning gages on sway brace L9-U10 is shown in Figure 4.24. Note the rapid increase in temperature of approximately 60 °F near June 20, 2003. From this point on the data experiences much larger daily cycles in temperature change. This response was confirmed from temperature data at a Lehigh University weather station. The majority of temperature gages on sway bracing members U24-L25 were not functioning properly as noted in Table 4.11 and accurate data could not be obtained.

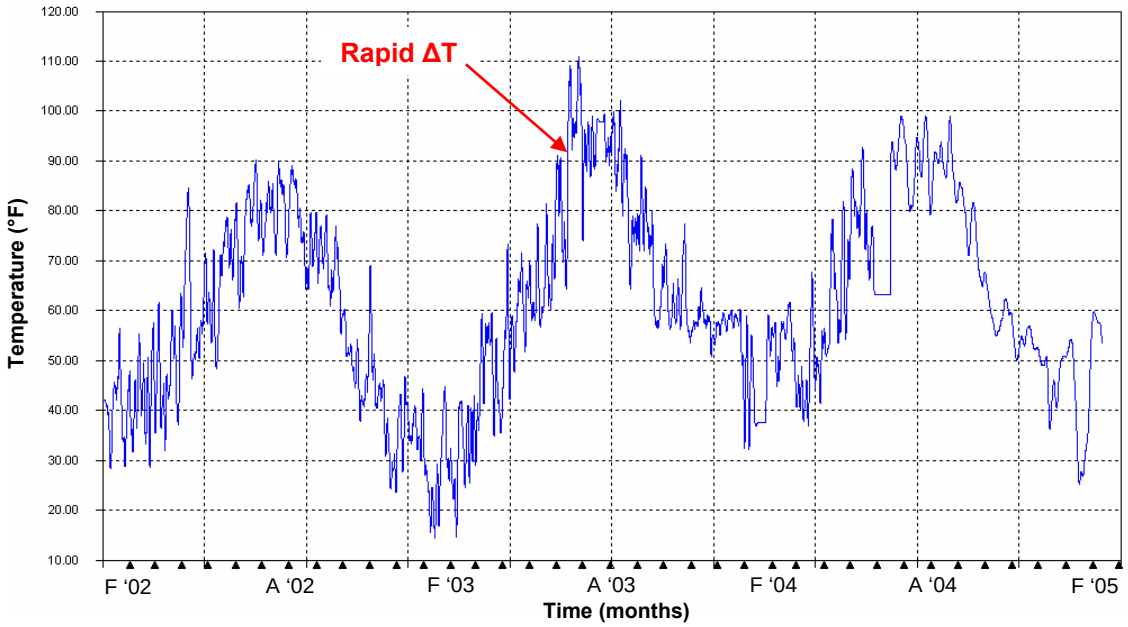

Figure 4.23: Temperature response of top gage of west cross of sway brace L9-U10 (TSB910WT)

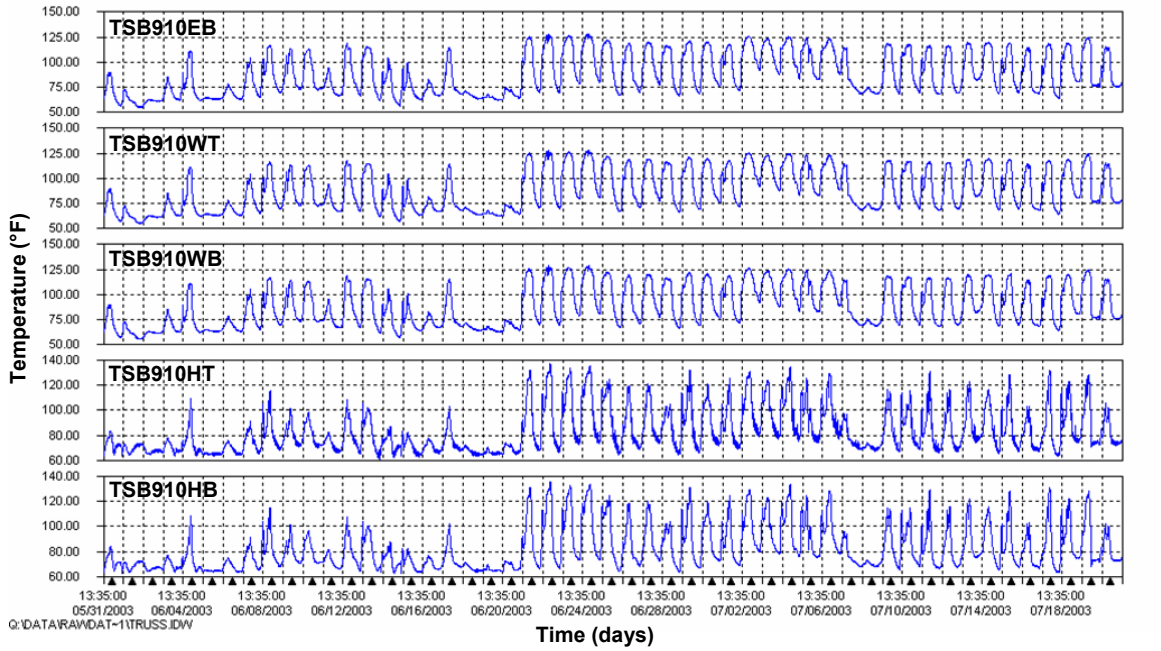

Figure 4.24: Portion of unfiltered temperature response of gages on sway brace L9-U10

The responses of both the top and bottom gages of the horizontal strut L9-L9 are shown in Figure 4.25. The figure indicates that the top and bottom face of the member exhibit nearly the same temperature response. The top gage is slightly warmer at some points due to greater sunlight exposure, but overall the behavior is the same. The member L9-L9 (W14 x 61) is much smaller than the lower chord members previously discussed. The temperature distribution would be expected to remain more uniform in a smaller member such as L9-L9 than in a larger box section (i.e., L25-L27). This behavior was also verified for the west cross of sway brace L9-U10. It could not be shown for the east cross of sway brace L9-U10 or any sway bracing members at U24-L25 due to the number of temperature gages that are not functioning properly (see Table 4.11). Hence, accurate conclusions could not be made for these members. However, it is reasonable to assume the temperature behavior of the sway bracing at U24-L25 is comparable to the sway bracing at L9-U10.

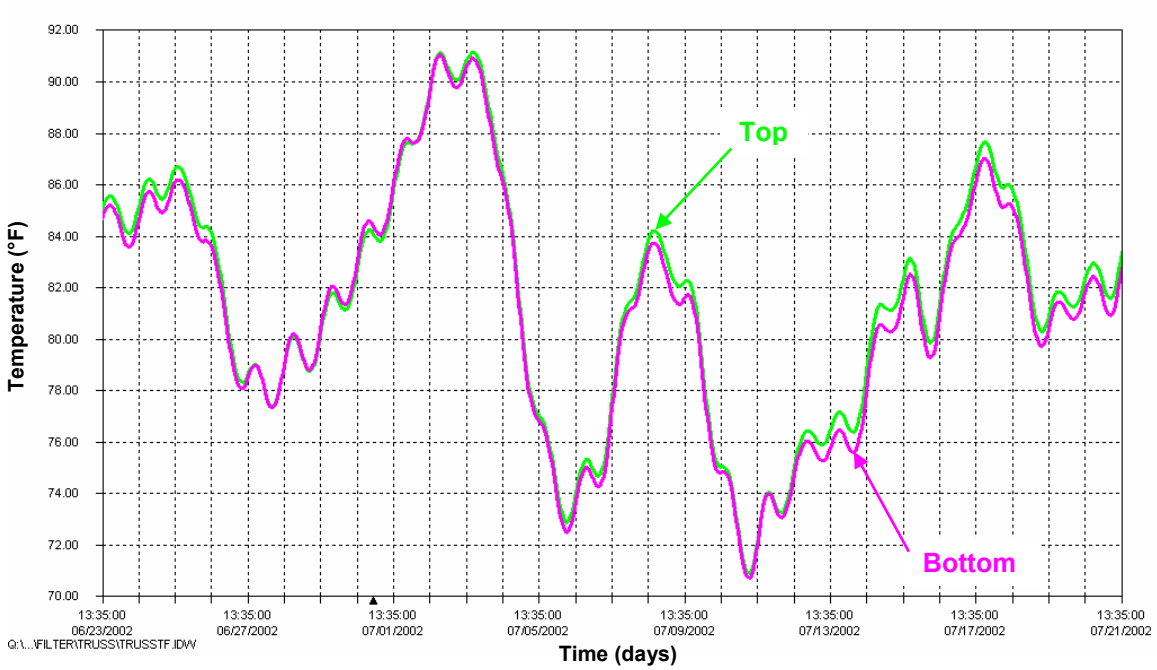

Figure 4.25: Portion of temperature response of both gages on the horizontal strut L9-L9

4.4.2 Strain Behavior

The vibrating wire strain gages installed on the sway bracing members and their functionality are presented in Table 4.12. An "X" signifies that the gage is not producing reliable data. The "?" denotes that accurate data were collected most of the time.

Gage Name	Location	Functionality
SSB910ET	East cross of sway brace Top face	OK
SSB910EB	East cross of sway brace Bottom face	OK
SSB910WT	West cross of sway brace Top face	X
SSB910WB	West cross of sway brace Bottom face	OK
SSB910HT	Horiz. strut of sway brace Top face	OK
SSB910HB	Horiz. strut of sway brace Bottom face	OK
SSB2425ET	East cross of sway brace Top face	OK
SSB2425EB	East cross of sway brace Bottom face	X
SSB2425WT	West cross of sway brace Top face	?
SSB2425WB	West cross of sway brace Bottom face	OK
SSB2425HT	Horiz. strut of sway brace Top face	X
SSB2425HB	Horiz. strut of sway brace Bottom face	OK

Table 4.12: Sway bracing vibrating wire strain gages and their functionality

Both the temperature and strain responses of the bottom gage of the east cross of sway brace L9-U10 are displayed in Figure 4.26. It is clear from the figure that this sway brace gage responds to changes in temperature similar to the lower chords. It experiences decreases in strain with increasing temperature and increases in strain with decreasing temperature. A similar relationship between temperature and strain was observed at locations SB910WB and SB2425WB.

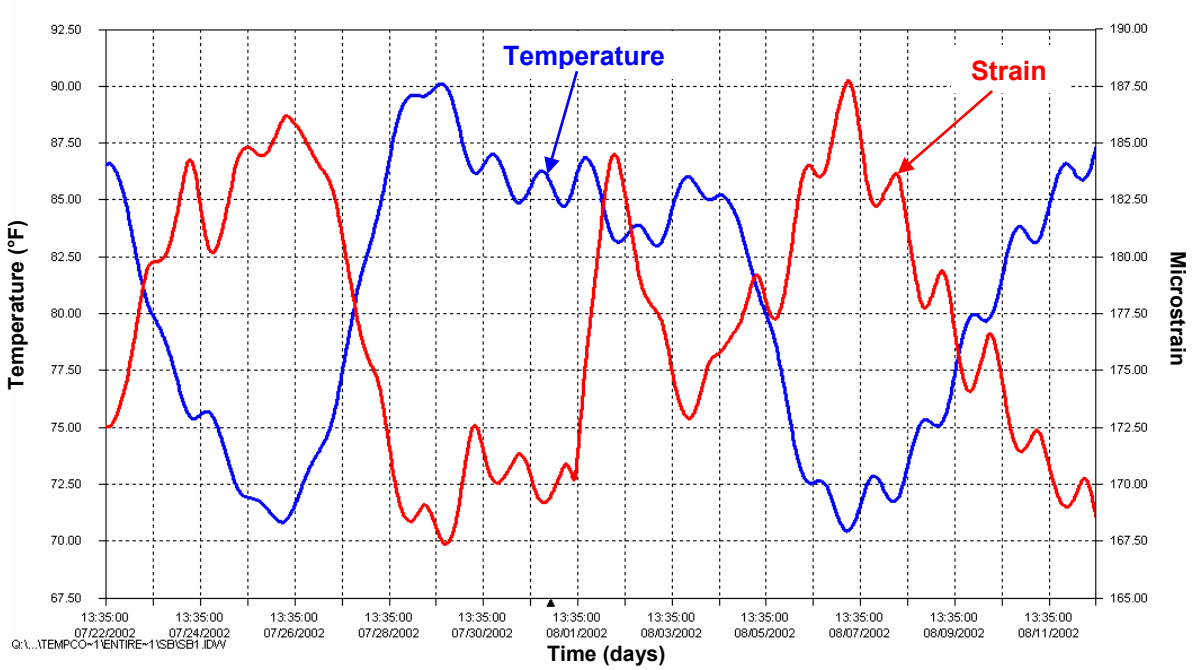

Figure 4.26: Portion of temperature and strain response of east cross of sway brace L9-U10 (SB910EB)

Figure 4.27 plots temperature and strain versus time for the top gage of the east cross of sway brace U24-L25. Unlike the previous gage (SSB910EB), this strain gage responds to increases in temperature with increases in microstrain. It was difficult to observe a consistent relationship between temperature and strain at locations SB910HT and SB910HB over the data collection period. Furthermore, assessments of overall sway bracing response could not be made due to the number of temperature and strain gages that were not functioning correctly. (It was not possible to observe the effects of differential heating on the sway bracing members in the simplified two-dimensional SAP2000 model since they were not included in the model.)

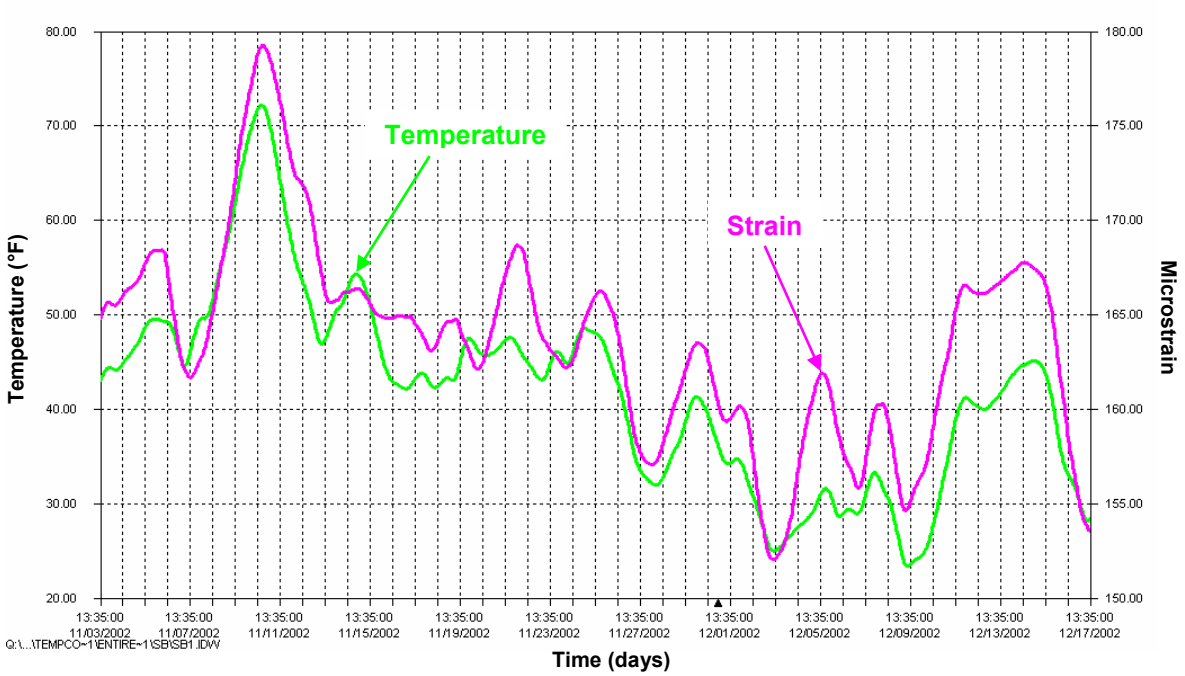

Figure 4.27: Portion of temperature and strain response of east cross of sway brace U24-L25 (SB2425ET)

The long-term temperature and strain response for the top gage of the east cross of sway brace U24-L25 is plotted in Figure 4.28. It should be noted that the long-term strain data for the sway bracing members was less reliable than the data for other members. The data contained noise spikes making it difficult to establish long-term trends in the strain behavior. It appears that there is neither an increase nor decrease in strain over time for this sway bracing location. In fact, some of the sway bracing gage locations appear to be experiencing a very slight decline in strain over time. This is illustrated in Figure 4.29 for the bottom gage of the east cross of sway brace L9-U10.

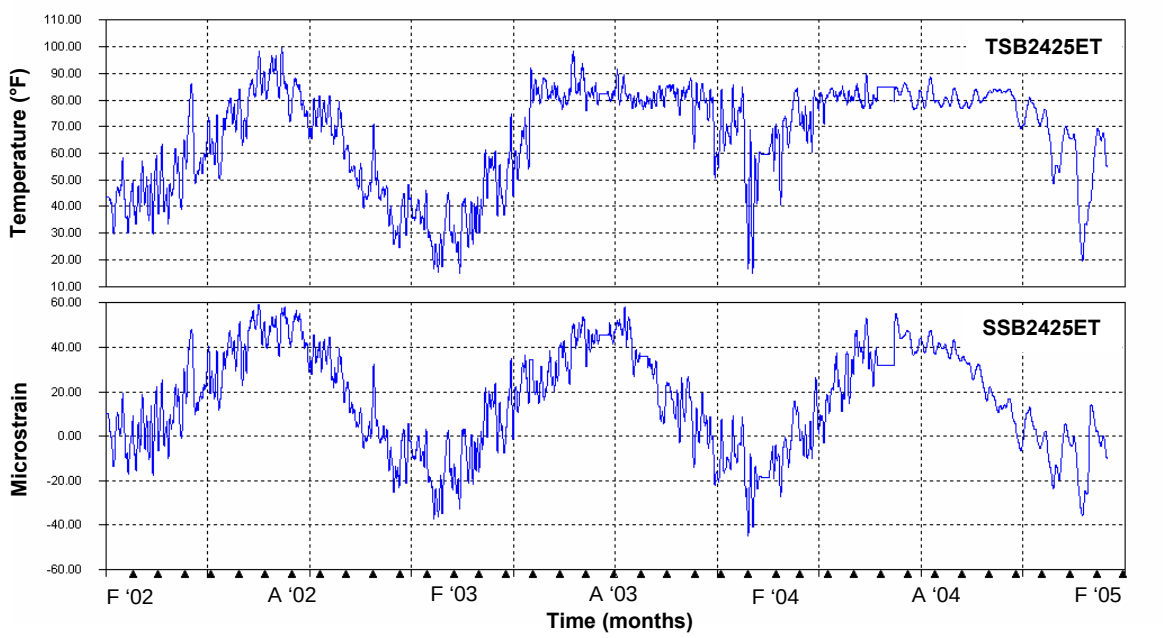

Figure 4.28: Long-term temperature and strain response of top gage of east cross of sway brace U24-L25

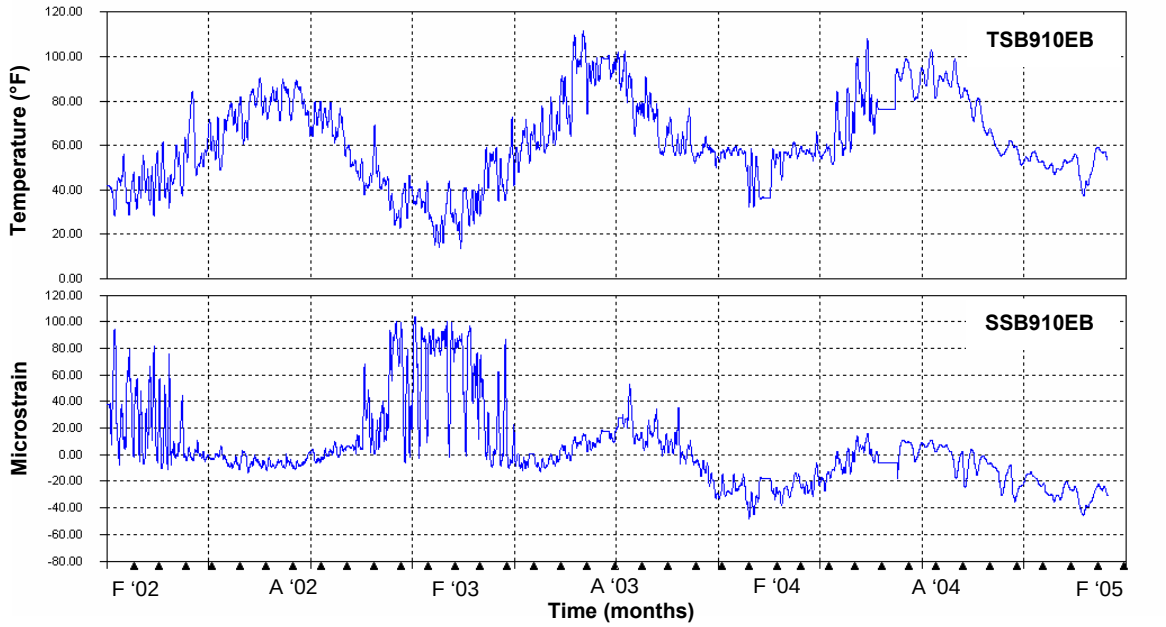

Figure 4.29: Long-term temperature and strain response of bottom gage of east cross of sway brace L9-U10

Changes in stress over time are presented in Table 4.13 for all functioning gages on the sway bracing members. There was not a consistent long-term response for all of the sway bracing. It appears that some of the members experienced a decrease in stress while others displayed little or no change in stress over time. The changes in stress from February, 2004 to December, 2004 were very small in magnitude (nearly all are less than

0.30 ksi). This is consistent with the long-term plots of the sway bracing depicted in Figure 4.28 and Figure 4.29.

Gage Name	Change in Stress (ksi)		
	Mar '02 to Apr '03	Apr '03 to Feb '04	Feb '04 to Dec '04
SSB910ET	0.24	-0.93	0.47
SSB910EB	-0.52	-0.87	0.04
SSB910WB	-0.47	-0.47	-0.05
SSB910HT	-1.30	-1.34	0.10
SSB910HB	-0.54	-1.05	0.29
SSB2425ET	0.23	-0.77	0.21
SSB2425WB	0.17	0.08	0.23
SSB2425HB	-0.78	-0.51	0.21

Table 4.13: Summary of changes in stress for sway bracing gages

4.5 Stringer Response

4.5.1 Temperature Behavior

Table 4.14 lists all temperature gages installed on the stringers between panel points U16 and U18. An "X" indicates that the gage is not functioning properly.

Gage Name	Location	Functionality
TS1TOC	Top flange of S1 18" N of U16	OK
TS1BOC	Bottom flange of S1 18" N of U16	OK
TS2TOC	Top flange of S2 18" N of U16	OK
TS2BOC	Bottom flange of S2 18" N of U16	OK
TS3TOC	Top flange of S3 18" N of U16	OK
TS3BOC	Bottom flange of S3 18" N of U16	OK
TS7TCL	Top flange of S7 27' N of U16	OK
TS7BCL	Bottom flange of S7 27' N of U16	X
TS8TCL	Top flange of S8 27' N of U16	OK
TS8BCL	Bottom flange of S8 27' N of U16	OK

Table 4.14: Stringer temperature gages and their functionality

The temperature response of a typical stringer gage is shown in Figure 4.30. Specifically, the top gage response of stringer 8 at midspan between U16 and U18 is plotted versus time. The gage behaves as anticipated with the member experiencing warmer temperatures in the summer and colder temperatures during the winter. Overall, the summer to summer temperature values and winter to winter readings are comparable. The rapid increase in temperature near June 20, 2003 is visible in Figure 4.30 and is typical of all functioning temperature gages on the stringers. This increase was also noticeable in almost all of the lower chords and all sway bracing members.

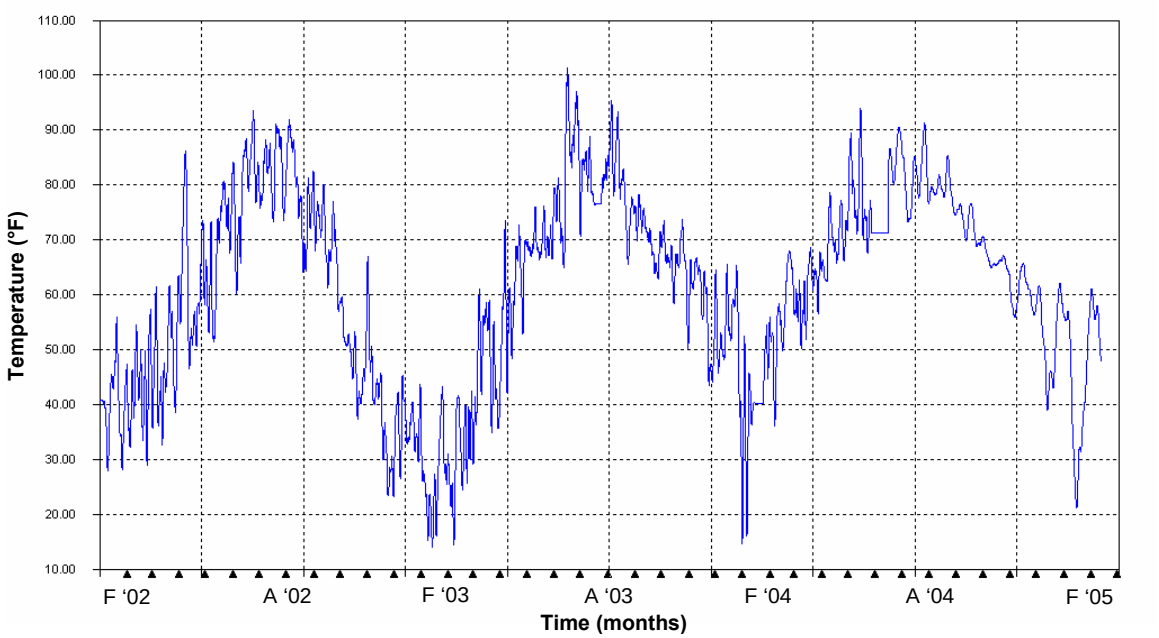

Figure 4.30: Temperature response of top gage of stringer 8 at midspan between U16 and U18 (TS8TCL)

The temperature responses of both top and bottom gages of stringer 1 are shown in Figure 4.31. These gages are located eighteen inches north of the floorbeam at U16. The plot shows that the temperature of the top gage is slightly warmer than the bottom gage by approximately 3 °F to 5 °F. The top gage is located closer to the concrete deck and the thermal mass of the deck has a greater effect on its temperature response. The deck gets warmer since it is directly exposed to the sun and also cools more slowly. This response could not be established for stringer 7 since its bottom gage (TS7BCL) was not functioning properly. However, this behavior was confirmed for all other instrumented stringers between U16 and U18.

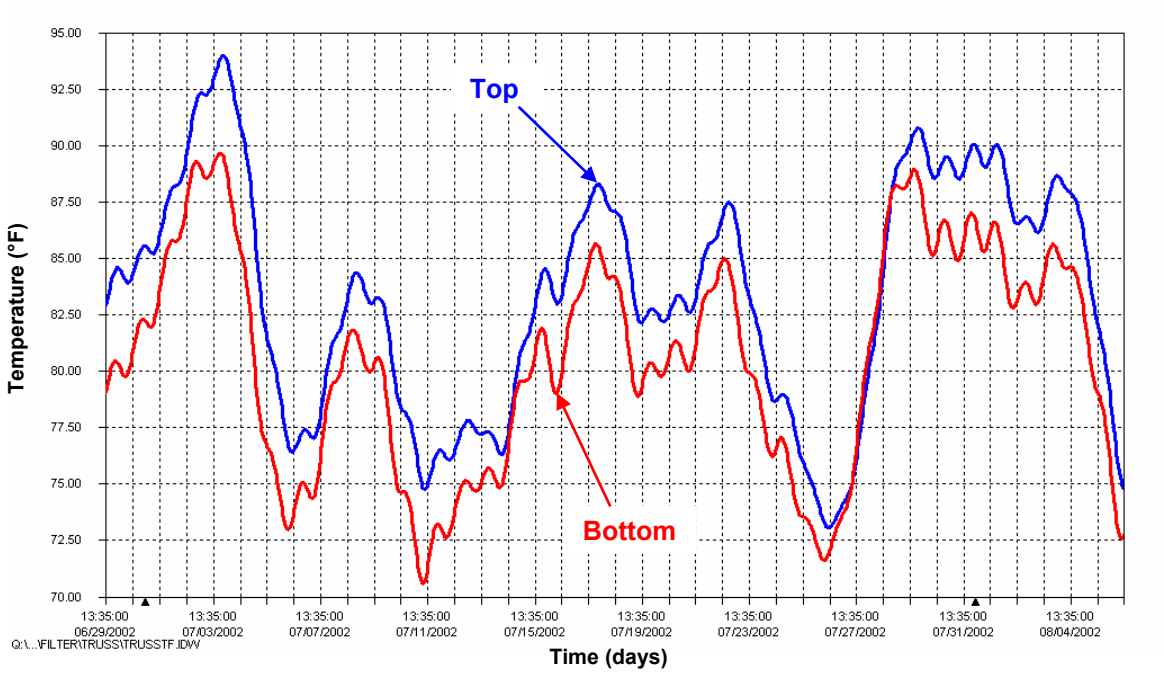

Figure 4.31: Portion of temperature response of both gages on stringer 1, 18" north of U16

4.5.2 Strain Behavior

The vibrating wire strain gages installed on the stringers between panel points U16 and U18 are listed in Table 4.15. Those not functioning properly are denoted by an "X" in the "Functionality" column. The symbol "?" signifies that accurate data were gathered for most of the data collection period.

Gage Name	Location	Functionality
SS1TOC	Top flange of S1 18" N of U16	OK
SS1BOC	Bottom flange of S1 18" N of U16	OK
SS2TOC	Top flange of S2 18" N of U16	OK
SS2BOC	Bottom flange of S2 18" N of U16	OK
SS3TOC	Top flange of S3 18" N of U16	?
SS3BOC	Bottom flange of S3 18" N of U16	OK
SS7TCL	Top flange of S7 27' N of U16	OK
SS7BCL	Bottom flange of S7 27' N of U16	OK
SS8TCL	Top flange of S8 27' N of U16	X
SS8BCL	Bottom flange of S8 27' N of U16	OK

Table 4.15: Stringer vibrating wire strain gages and their functionality

The relationship between temperature and strain for the stringers between U16 and U18 was not as consistent as the members previously discussed (i.e., upper chords and lower chords). Reliable data were obtained for a limited number of locations. It was decided that the gage locations near the floorbeam U16-U16 not be used for comparison to the upper chord gages which are at midspan of U16-U18. The comparison would be complicated by the complex interaction between the stringer and floorbeam at the

connection. Therefore, the locations at the midspan of stringer 7 and stringer 8 were chosen for comparison to the upper chords. However, the temperature gage on the bottom flange of stringer 7 (TS7BCL) and the strain gage on the top flange of stringer 8 (SS8TCL) were not functioning properly (see Table 4.14 and Table 4.15). This made it difficult to establish an overall temperature/strain relationship for locations at the stringer midspans.

The temperature and strain behavior for the top flange of stringer 7 located at midspan between U16 and U18 is shown in Figure 4.32. It should be noted that the relationship between temperature and strain was not as consistent as it was with previous members. However, the most noticeable trend over the data collection period was increasing strain with increasing temperature and a decrease in strain for a decrease in temperature. This response is comparable to the upper chords discussed in Section 4.1.2. The relationship between temperature and strain could not be determined for the top flange of stringer 8 since the vibrating wire strain gage (SS8TCL) was not functioning correctly.

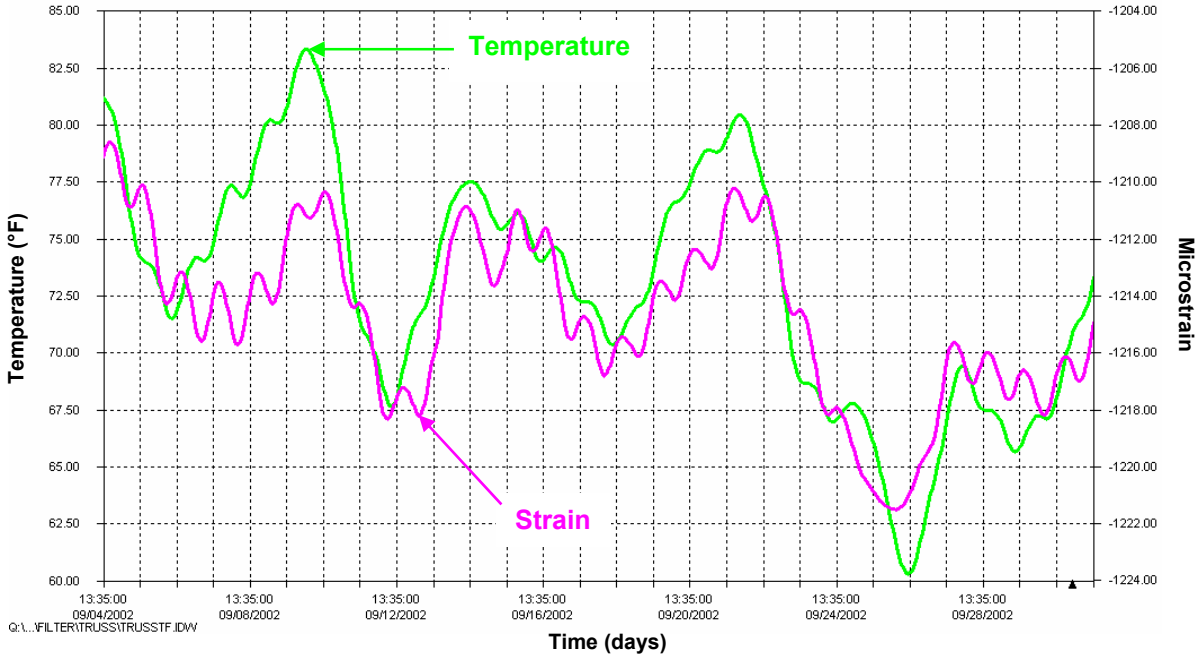

Figure 4.32: Portion of temperature and strain response of stringer 7 between U16 and U18 (S7TCL)

Figure 4.33 describes the relationship between temperature and strain for the bottom flange of stringer 8 at midspan between panel points U16 and U18. As stated previously, this relationship was not as consistent as shown for other members (i.e., upper chords and lower chords). The prevailing trend was an increase in strain with increasing temperature and vice versa as illustrated in Figure 4.33. This behavior is also consistent with the upper chord response. The strain gage for the top flange of stringer 8 (SS8TCL) was not functioning properly and the relationship between temperature and strain could not be verified. Therefore, the relationship could not be confirmed for both flanges on a single stringer member. The top flanges (or bottom flanges) of stringers 7 and 8 would

most likely exhibit a similar response to changes in temperature due to the location of gages on these members. However, the limited number of reliable gages prevented this assumption from being confirmed.

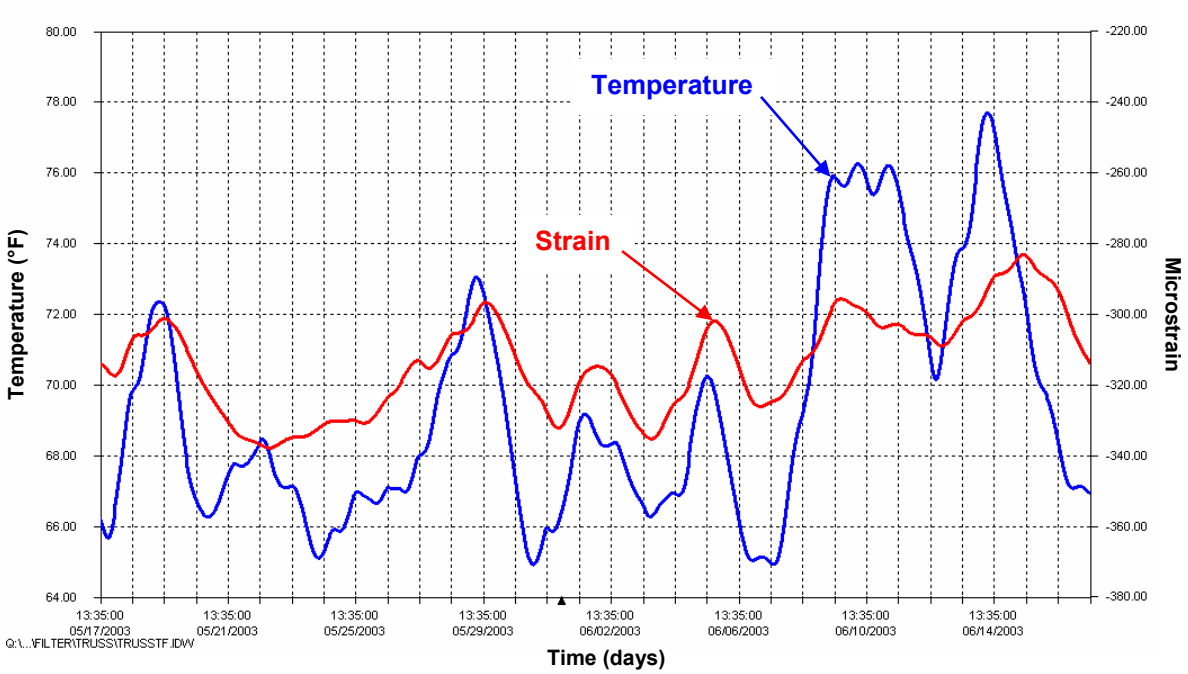

Figure 4.33: Portion of temperature and strain response of stringer 8 between U16 and U18 (S8BCL)

The correlation between temperature and strain for both gages on stringer 2 (S1TOC and S2BOC) was comparable to the stringers previously discussed. Although the relationship was not as consistent as other members, the primary behavior was increasing strain with increasing temperature and a decrease in strain with decreasing temperature. This trend was also verified for locations S1BOC and S3BOC. The strain gage on the top flange of stringer 3 (SS3TOC) was not functioning properly (see Table 4.15). The response of the top flange of stringer 1 (S1TOC) did not reveal a consistent pattern between temperature and strain. All of these gage locations discussed are located eighteen inches north of floorbeam U16-U16 and were not compared to the upper chords due to the complex interaction at the connection of the stringer and floorbeam.

The long-term temperature and strain response for the bottom flange of stringer 8 is plotted in Figure 4.34. This gage is located at midspan between panel points U16 and U18. It is apparent from the plot that the stringer is experiencing an increase in strain over time. The increasing trend also seems to be "leveling off" over time, consistent with expected creep behavior in concrete. The long-term response of the stringers is comparable to the response of the upper chords. The data for the long-term variation in strain for the top flange of stringer 1 (SS1TOC) contained many noise spikes and a reliable trend was not established. The remaining stringer strain gages that were functioning correctly (see Table 4.15) exhibited a similar increase in strain over the data collection period as shown in Figure 4.34. It should be noted that the top stringer gages were more susceptible to noise spikes in the data. However, a similar trend of increasing

strain over time was still visible. The long-term response for the top gage of stringer 2 is presented in Figure 4.35.

Both of the stringers discussed behave similarly to the upper chords over pier 2. Downward vertical deflection of the truss at midspan due to concrete creep causes tensile stresses in members located in the negative moment region. All of the instrumented stringers are located between panel points U16 and U18. Therefore, it would be expected that the stringers and upper chords in this region of the bridge experience a similar trend of increasing strain due to creep.

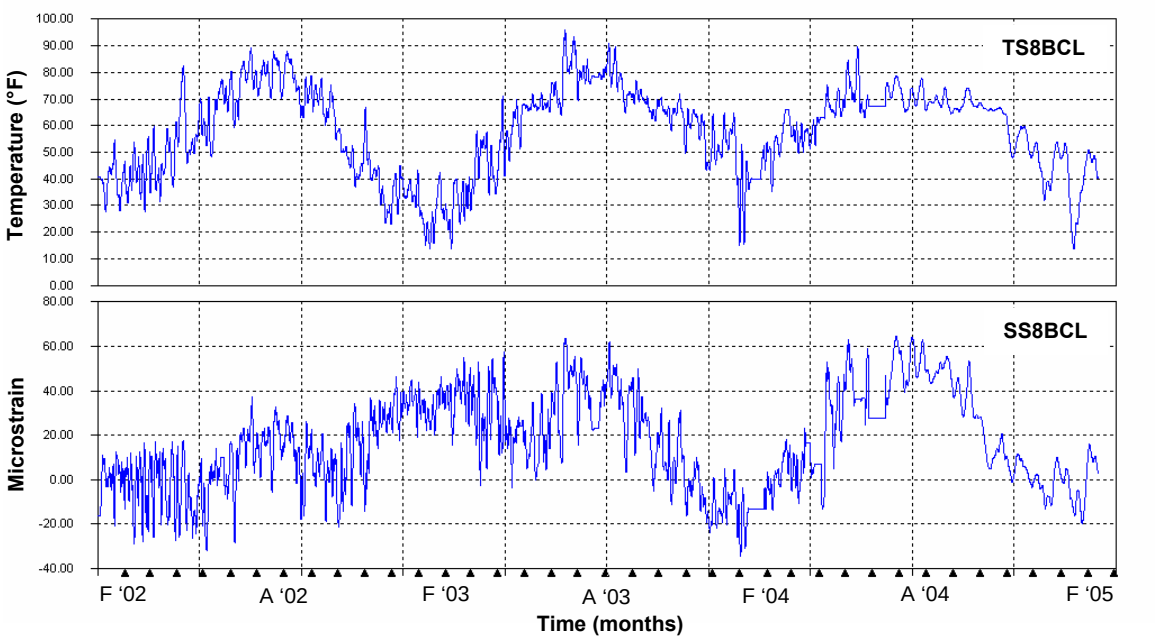

Figure 4.34: Long-term temperature and strain response of stringer 8 at midspan between U16 and U18

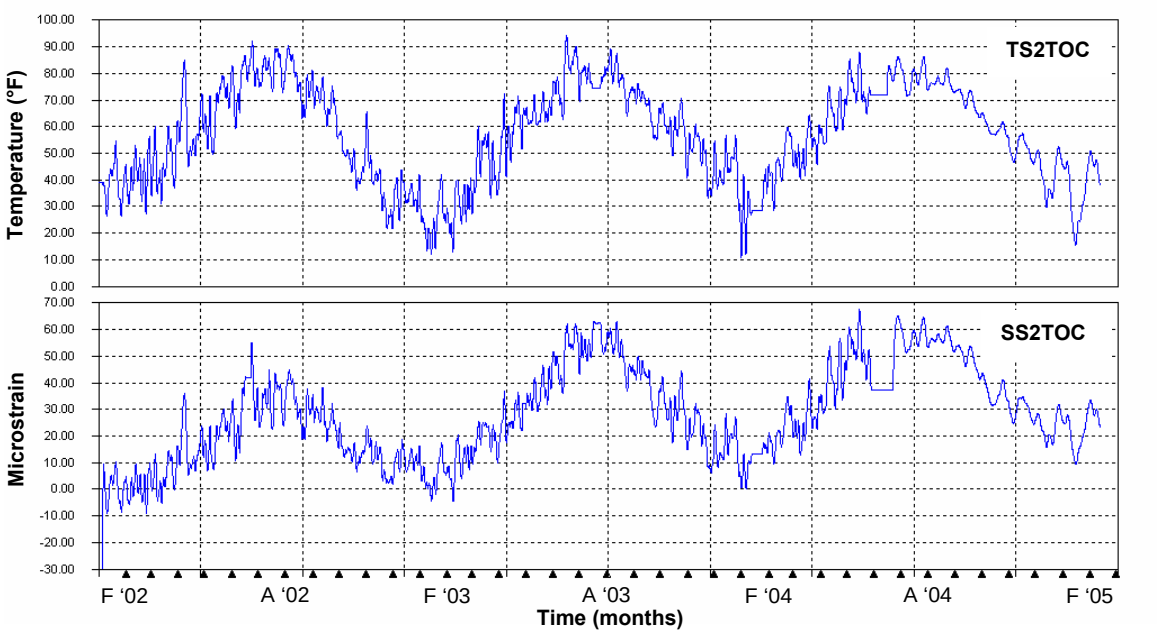

Figure 4.35: Long-term temperature and strain response of stringer 2, 18" north of U16

The changes in stress are summarized in Table 4.16 for the stringer gage locations that were producing reliable data. It appears that the largest increases in stress occurred early in the data collection period. Also, the stringers exhibited decreases in stress from March, 2003 to February, 2004. The magnitudes of stress change appear to have decreased as shown in the last column of Table 4.16. This response is consistent with behavior previously discussed for the upper chords and the plots shown in Figure 4.34 and Figure 4.35.

Gage Name	Change in Stress (ksi)		
	Mar '02 to Mar '03	Mar '03 to Feb '04	Feb '04 to Jan '05
SS1TOC	1.09	-1.57	0.31
SS1BOC	1.09	-0.10	0.58
SS2TOC	0.41	-0.03	0.24
SS2BOC	0.92	-0.10	0.27
SS3BOC	0.62	-0.70	0.22
SS7TCL	0.90	-0.37	0.24
SS7BCL	1.23	-0.91	0.28
SS8BCL	1.00	-1.16	0.16

Table 4.16: Summary of changes in stress for stringer gages

4.6 Tension Tie Plate Response

4.6.1 Temperature Behavior

The temperature response of the floorbeam tension tie plate on the east upper chord at U16 is shown in Figure 4.36. The temperatures increase during the summer months and decrease during the winter season. Temperatures for the summer months remained fairly consistent between years during the monitoring period. There was an

increase in temperature near June 20, 2003 which was verified by weather data. The low temperatures during the winter months are also comparable.

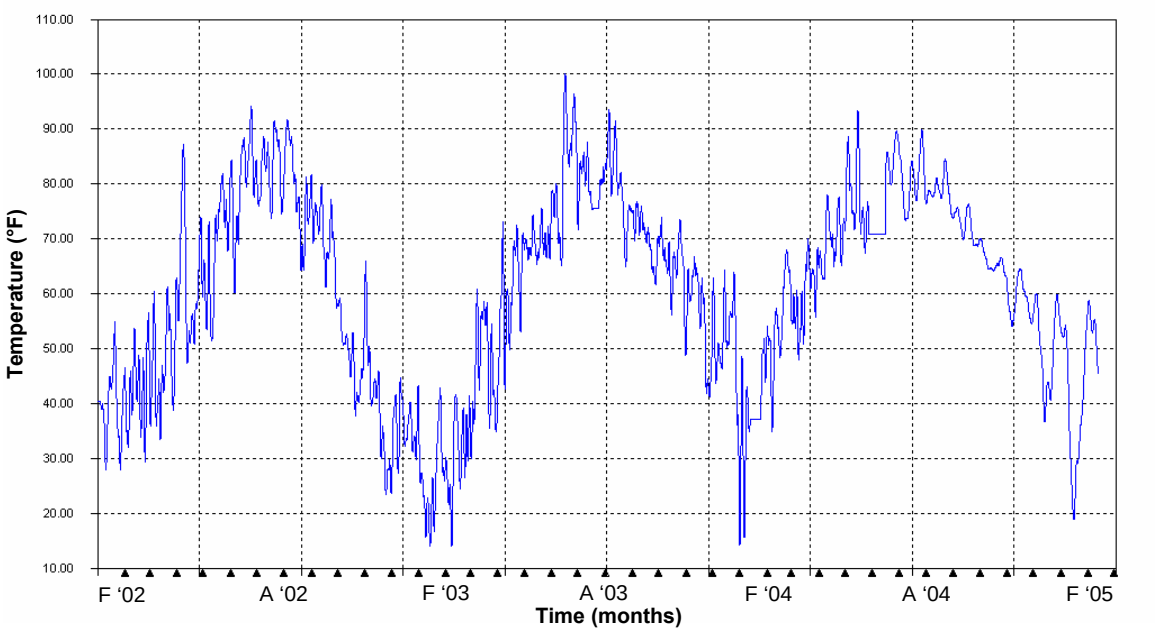

Figure 4.36: Temperature response of floorbeam tension tie plate (FBTPL)

4.6.2 Strain Behavior

Temperature and strain for the tie plate are plotted versus time in Figure 4.37. The figure illustrates that this tie plate behaves much like the upper chords due to changes in temperature. It experiences increases in strain with increasing temperature and decreases in strain with decreasing temperature.

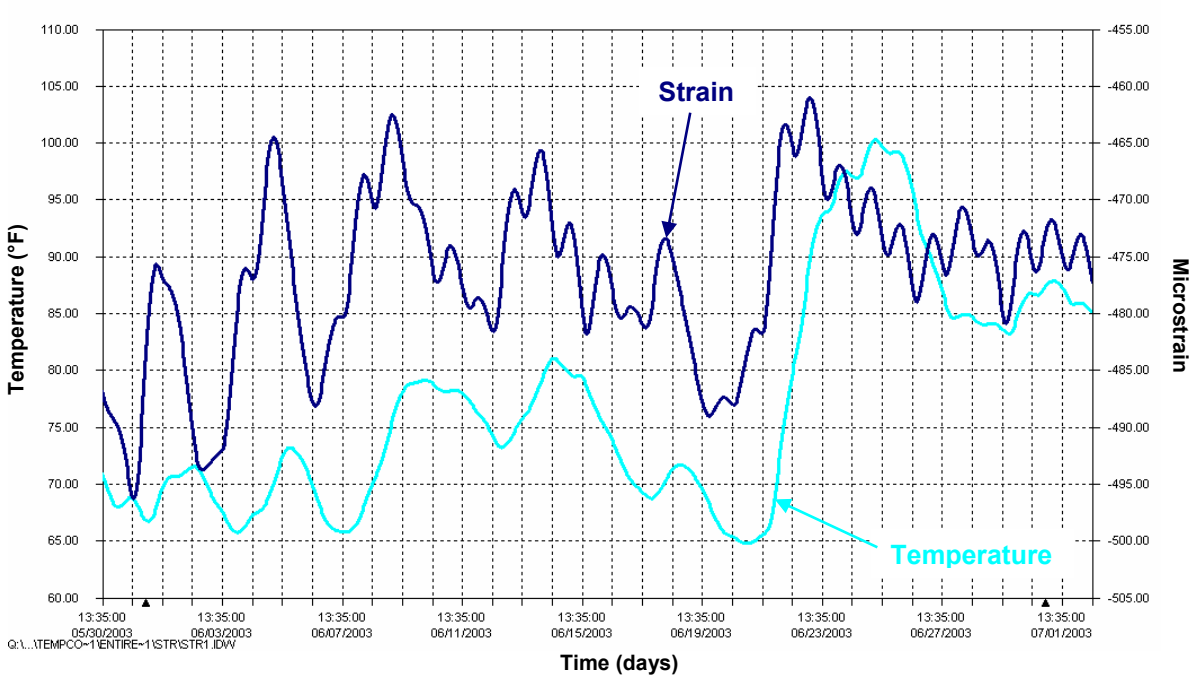

Figure 4.37: Portion of temperature and strain response of floorbeam tension tie plate (FBTPL)

For the 38-month data collection period, the temperature and strain responses of the tension tie plate are pictured in Figure 4.38. It is apparent from the plot that the tie plate is experiencing an increase in strain over time. The long-term strain response of the tie plate in the Interim Report identified a rapid increase in strain near May, 2003. As discussed for the lower chords, this erroneous offset was removed from the data as shown in Figure 4.38.

Creep in the concrete deck would be expected to cause the exterior floorbeams cantilevered outside of the truss to deflect downward vertically. Likewise, this type of deformation would put the tie plate in tension from the negative moment developed at the floorbeam to gusset plate connection. The response of the tie plate in Figure 4.38 is consistent with this behavior.

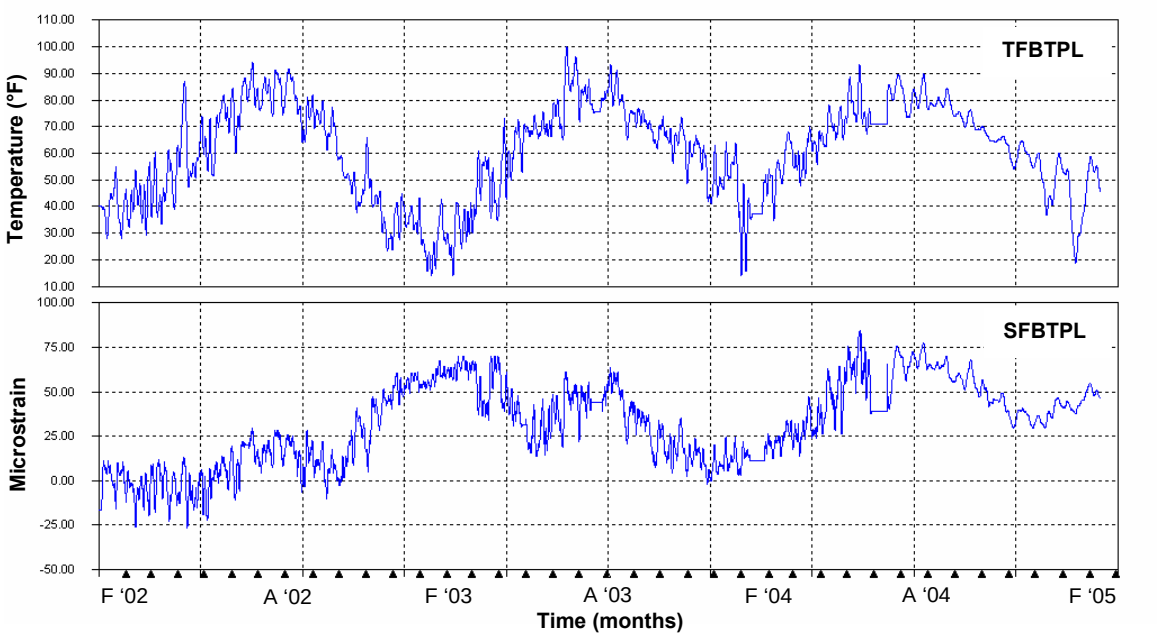

Figure 4.38: Long-term temperature and strain response of floorbeam tension tie plate

Calculated changes in stress are presented in Table 4.17 for the tension tie plate. The largest change occurred early during the collection period. The tie plate also experienced a decrease in stress from March, 2003 to February, 2004. The magnitude of increase in stress is smaller from February, 2004 to January, 2005. This is consistent with the long-term strain response of the tie plate illustrated in Figure 4.38.

Gage Name	Change in Stress (ksi)		
	Mar '02 to Mar '03	Mar '03 to Feb '04	Feb '04 to Jan '05
SFBTPL	1.63	-1.06	0.64

Table 4.17: Summary of changes in stress for tension tie plate

4.7 Deck Reinforcement Response

4.7.1 Temperature Behavior

The following deck reinforcement locations listed in Table 4.18 were instrumented with temperature gages. Gages not functioning properly are marked with an "X".

Gage Name	Location	Functionality
TS2WB	3’ W of S2 and 18” N of U16	OK
TS2EB	3’ E of S2 and 18” N of U16	OK
TS3WB	3’ W of S3 and 18” N of U16	X
TS3EB	3’ E of S3 and 18” N of U16	OK
TS7WB	3’ W of S7 and 27’ N of U16	X
TS7EB	3’ E of S7 and 27’ N of U16	X
TS8WB	3’ W of S8 and 27’ N of U16	OK
TS8EB	3’ E of S8 and 27’ N of U16	OK
TWU1618WB	4’ W of UC and 27’ N of U16	X
TWU1618CB	CL of UC and 27’ N of U16	OK
TWU1618EB	4’ E of UC and 27’ N of U16	OK
TEU1618WB	4’ W of UC and 27’ N of U16	OK
TEU1618CB	CL of UC and 27’ N of U16	OK
TEU1618EB	4’ E of UC and 27’ N of U16	OK

Table 4.18: Deck reinforcement temperature gages and their functionality

The temperature response of a typical deck reinforcement gage is shown in Figure 4.39. The response of the embedment gage located 3 feet east of stringer 8 at midspan between U16 and U18 is plotted versus time. Once again, a rapid increase in temperature occurred around June 20, 2003. This was consistent with weather data observed at this time. In Figure 4.39, the temperatures between summers are comparable. It also appears that the winters of 2003 and 2004 reached cooler temperatures than the winter of 2005 for this gage. The other functioning temperature gages on the rebar between U16 and U18 displayed similar behavior over the data collection period.

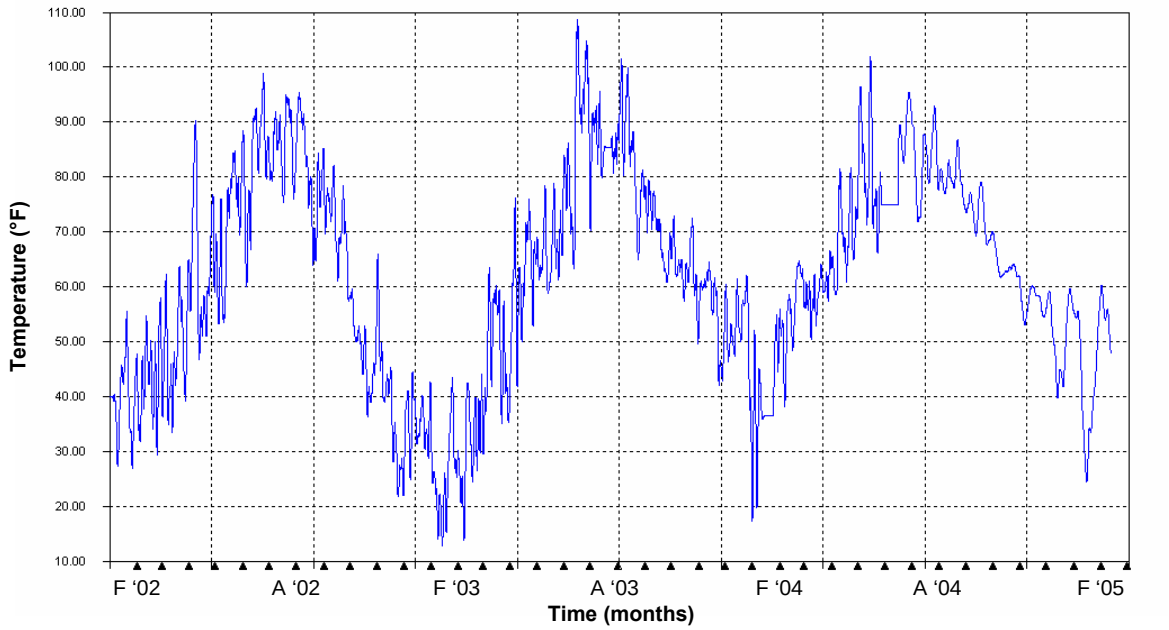

Figure 4.39: Temperature response of embedment gage east of stringer 8 between U16 and U18 (TS8EB)

The temperature responses of the three embedment gages near midspan of the east upper chord (U16-U18 East) are shown in Figure 4.40. These gages are located on rebar directly above the centerline of the upper chord and on either side of the upper chord at a 4-foot offset. The plot shows that the temperature response of all gages is very similar. A variation of approximately 2 °F to 3 °F occurs between these embedment gages. This is most likely due to the non-uniform heating and cooling of the large thermal mass of the concrete deck. The embedment gages near stringer 8 (TS8WB and TS8EB) also have nearly identical temperature responses. This response was observed in two of the gages near the west upper chord as well (TWU1618CB and TWU1618EB).

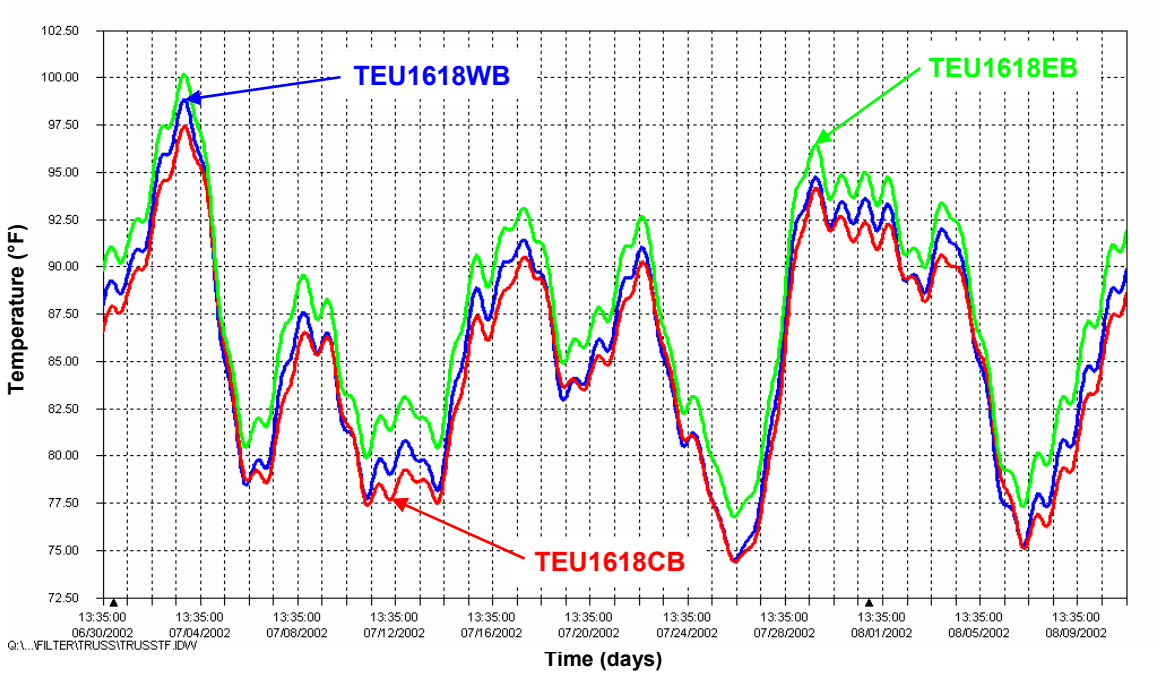

Figure 4.40: Portion of temperature response of all gages near the east upper chord between U16 and U18

4.7.2 Strain Behavior

Table 4.19 lists the location and functionality of vibrating wire strain gages installed on the deck reinforcement between panel points U16 and U18.

Gage Name	Location	Functionality
SS2WB	3’ W of S2 and 18” N of U16	OK
SS2EB	3’ E of S2 and 18” N of U16	X
SS3WB	3’ W of S3 and 18” N of U16	X
SS3EB	3’ E of S3 and 18” N of U16	X
SS7WB	3’ W of S7 and 27’ N of U16	OK
SS7EB	3’ E of S7 and 27’ N of U16	OK
SS8WB	3’ W of S8 and 27’ N of U16	OK
SS8EB	3’ E of S8 and 27’ N of U16	OK
SWU1618WB	4’ W of UC and 27’ N of U16	X
SWU1618CB	CL of UC and 27’ N of U16	OK
SWU1618EB	4’ E of UC and 27’ N of U16	X
SEU1618WB	4’ W of UC and 27’ N of U16	OK
SEU1618CB	CL of UC and 27’ N of U16	OK
SEU1618EB	4’ E of UC and 27’ N of U16	X

Table 4.19: Deck reinforcement vibrating wire strain gages and their functionality

Due to the number of deck reinforcement gages that were not functioning properly (see Table 4.18 and Table 4.19), temperature and strain could only be compared at a limited number of locations. The available locations were S2WB, S8WB, S8EB, WU1618CB, EU1618WB, and EU1618CB. Figure 4.41 shows the temperature and strain response of the gage on the rebar 3 feet west of stringer 2 and 18 inches north of U16. It is clear from the figure that this deck reinforcement behaves much like the lower chords due to changes in temperature. It experiences increases in strain with decreasing temperature and decreases in strain with increasing temperature.

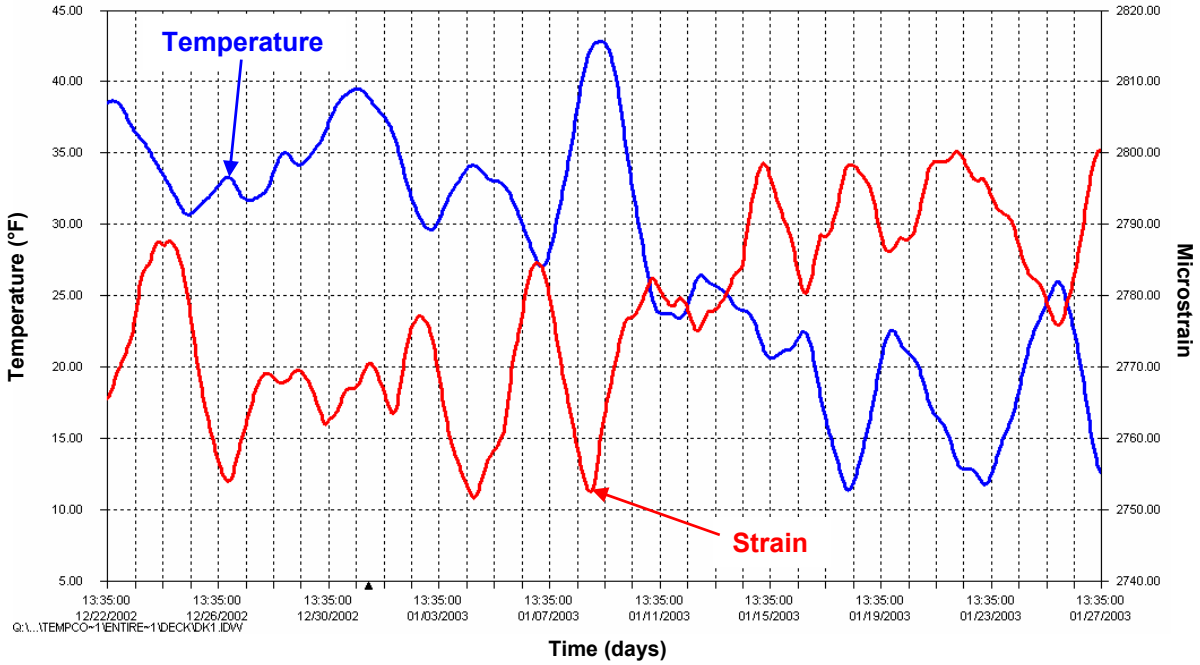

Figure 4.41: Portion of temperature and strain response of rebar west of stringer 2, 18” north of U16 (S2WB)

Also, the deck reinforcement at midspan between U16 and U18 exhibits a similar response. The temperature and strain response of the gage on the rebar 3 feet west of stringer 8 at the midspan between U16 and U18 is plotted in Figure 4.42. This gage experiences increases in strain with decreasing temperature and decreases in strain with increasing temperature. This relationship was confirmed at all other available locations previously listed. The simplified two-dimensional SAP2000 model did not include the deck reinforcement. The composite deck, upper chord and stringers were combined into a single frame element and assigned the equivalent area and moment of inertia at a cross-section near midspan of span 2.

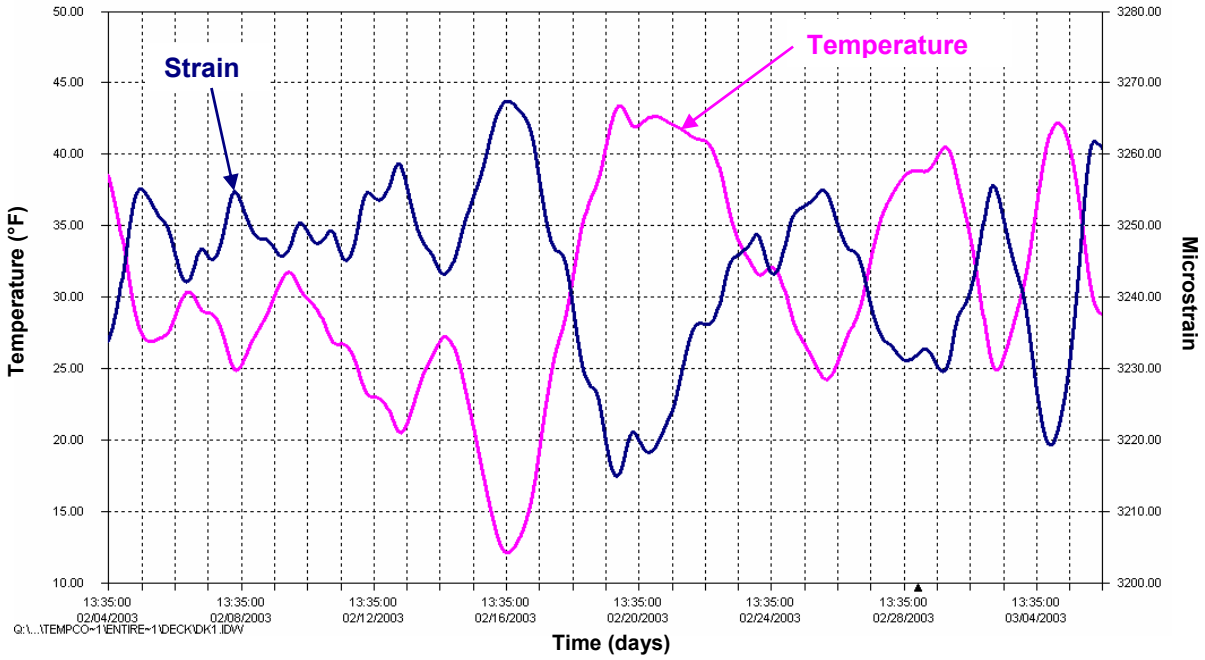

Figure 4.42: Portion of temperature and strain response of rebar west of stringer 8, 27' north of U16 (S8WB)

The response of the deck reinforcement gages opposes the response of the upper chords to changes in temperature. This behavior is shown in Figure 4.43 for the rebar above the west upper chord (SWU1618CB) and the bottom gage of U16-U18 West (SBU1618WB). Since the scales for each gage were different, the microstrain scale for the rebar is on the left axis and the scale for the upper chord is on the right axis. The figure illustrates that the microstrain responses for these gages oppose each other. This could not be verified for the east upper chord bottom gage (SBU1618EB) since it was not functioning properly. However, this behavior was confirmed for the east and west gages of U16-U18 East.

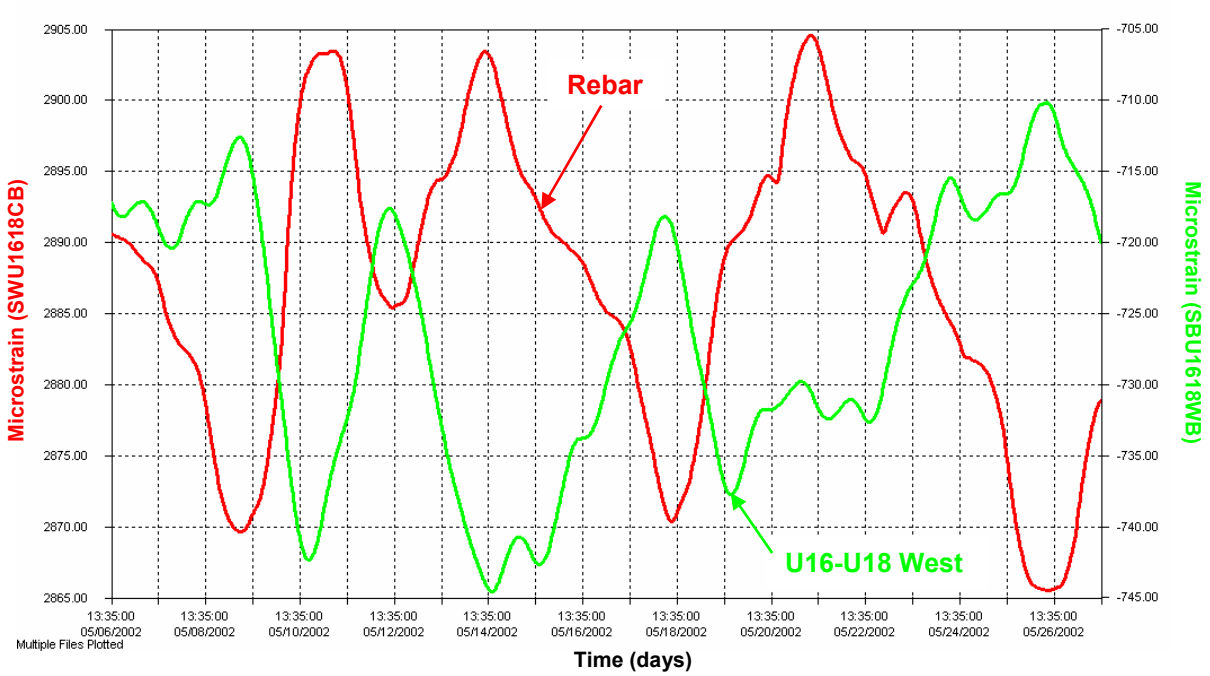

Figure 4.43: Portion of strain response of rebar above U16-U18 West and bottom gage of U16-U18 West

The long-term effects of strain for a rebar gage are shown in Figure 4.44. The response of the rebar gage 3 feet west of stringer 8 is plotted versus time. It is apparent from the plot that the rebar gage is experiencing an increase in strain over time. It should be noted that noise spikes occurred in the strain data for the deck reinforcement. This made interpretation of the long-term behavior difficult; however, a trend is still visible in the data. The gage (SS8WB) plotted in Figure 4.44 produced the most reliable data of the functioning deck reinforcement strain gages. The other gages contained more noise spikes and an apparent drift in strain near the end of the data collection period. Overall, the long-term response of the rebar illustrated in Figure 4.44 is comparable to the upper chord. It appears to be encountering an increase in microstrain that is "leveling off" over time. The behavior of the deck reinforcement is consistent with other members discussed in the negative moment region of the bridge and expected response from structural analysis.

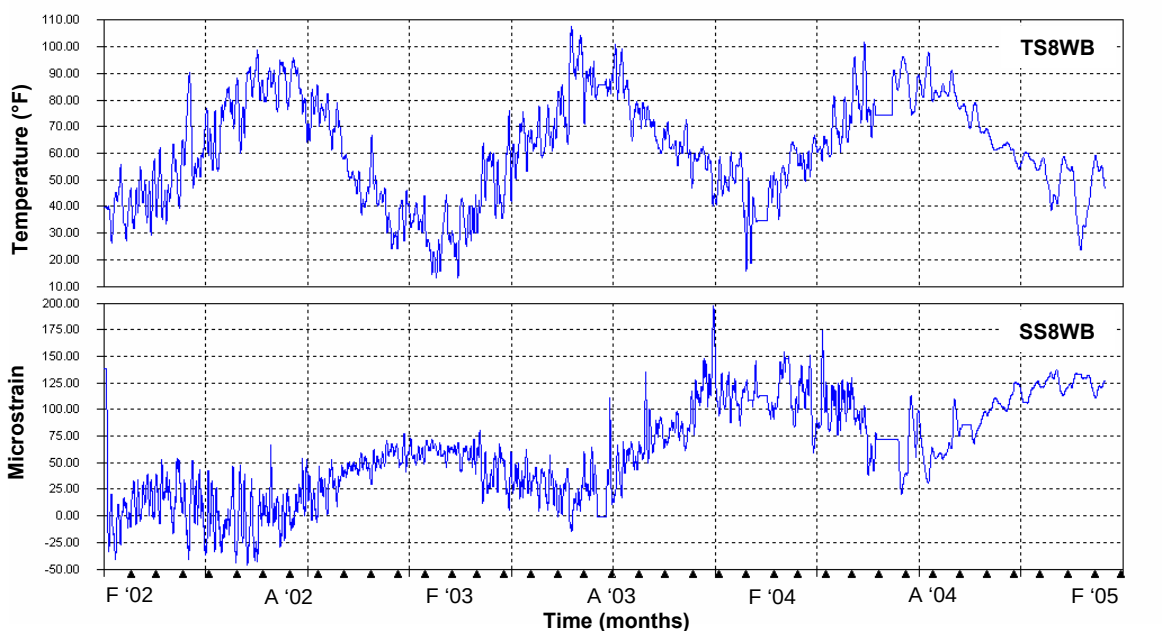

Figure 4.44: Long-term temperature and strain response of rebar gage west of stringer 8

A summary of stress variations over time is presented in Table 4.20 for reliable deck reinforcement gages. The largest increases in stress took place early in the data from January, 2002 to December, 2003 for the rebar gages. In almost all cases, the increase in stress decays substantially later in the data. Overall, the deck reinforcement is experiencing an increase in stress that is "leveling off" over time. This response is consistent with behavior illustrated for the upper chords and stringers located between panel points U16 and U18.

Gage Name	Change in Stress (ksi)		
	Jan '02 to Dec '02	Dec '02 to Dec '03	Dec '03 to Jan '05
SS2WB	2.33	0.51	0.49
SS7WB	1.38	0.94	0.67
SS7EB	3.13	0.59	0.52
SEU1618WB	3.47	0.91	0.60
SEU1618CB	2.81	0.48	0.58
SS8WB	2.05	1.59	0.41
SS8EB	3.01	0.49	0.72

Table 4.20: Summary of changes in stress for deck reinforcement gages

4.8 Summary of Long-Term Data

Overall, the long-term data behaved as expected. Temperature readings on the instrumented members increased during the summer months and decreased during the winters. Most truss members displayed fairly uniform temperature distributions. Gages shaded by either the member itself or the concrete read slightly lower values at times than gages more exposed to direct sunlight (i.e., a gage on the bottom web plate of the lower chord).

Almost all of the members experienced a gradual and slight increase in microstrain over the data collection period. The sway bracing members appeared to experience little change, if any, or slight declines in strain over time. The increase in microstrain for other members appeared to be "leveling off", comparable with the long-term characteristics of creep in concrete. The behavior of the members was also consistent with the expected long-term response of the truss to concrete creep. It was anticipated that creep would cause the structure to sag, much like the bridge acting under its own self-weight. Thus, the lower chords near midspan, the instrumented tension diagonals, and the members between panel points U16 and U18 (i.e., upper chords, stringers, and rebar) all experienced a gradual increase in strain. Calculations of strain variation were made and are consistent with the anticipated "leveling off" response of the members to creep.

5.0 Verification of Truss Response to Live Load

Uncontrolled live load data were collected on August 8, 2003. A group of truss members were selected to verify that the response of the bridge under vehicular live load was consistent with measurements made during Phase I. This data was collected for a period of approximately ten hours from 10:00 AM to 8:00 PM at a sampling rate of 100 Hz. Data could not be collected for a longer period of time due to the power demand it put on the batteries. Longer periods of uncontrolled live load monitoring have been collected and will be discussed in Section 6.0. Table 5.1 lists all gages that were monitored on August 8, 2003. An "X" denotes that the gage is not functioning properly.

Gage Name	Location	Functionality
BU2628EW	East U26-U28 West face	OK
BU2628EE	East U26-U28 East face	OK
BU2628EB	East U26-U28 Bottom face	OK
BU2628WW	West U26-U28 West face	OK
BU2628WE	West U26-U28 East face	OK
BU2628WB	West U26-U28 Bottom face	OK
S1TCL	Stringer 1 Top flange	OK
S1BCL	Stringer 1 Bottom flange	OK
S2TCL	Stringer 2 Top flange	OK
S2BCL	Stringer 2 Bottom flange	OK
S3TCL	Stringer 3 Top flange	OK
S3BCL	Stringer 3 Bottom flange	OK
S4TCL	Stringer 4 Top flange	OK
S4BCL	Stringer 4 Bottom flange	OK
S5TCL	Stringer 5 Top flange	OK
S5BCL	Stringer 5 Bottom flange	OK
BL2527ET	East L25-L27 Top face	X
BL2527EB	East L25-L27 Bottom face	OK
BL2527WB	West L25-L27 Bottom face	OK
BL2729ET	East L27-L29 Top face	X
BL2729EB	East L27-L29 Bottom face	OK
BL2729WT	West L27-L29 Top face	X
BL2729WB	West L27-L29 Bottom face	OK
BU1618EW	East U16-U18 West face	X
BU1618EB	East U16-U18 Bottom face	OK
BU1618EE	East U16-U18 East face	OK
BU1618WB	West U16-U18 Bottom face	OK
BU1618WE	West U16-U18 East face	OK
DW1819EW	East U18-L19 West face	OK
DW1819EE	East U18-L19 East face	OK
DW1819WW	West U18-L19 West face	X
DW1819WE	West U18-L19 East face	OK
DW2021EW	East U20-L21 West face	OK
DW2021EE	East U20-L21 East face	OK
DW2021WW	West U20-L21 West face	X
DW2021WE	West U20-L21 East face	OK

Table 5.1: Live load gages monitored on 8/8/03 and their functionality

5.1 Upper Chord Response

The upper chords between U26 and U28 near the midspan of span 2 and the upper chords between U16 and U18 above pier 2 were monitored. The response of these members is seen in the following figures. Figure 5.1 plots the response of the bottom gage of U26-U28 East. The large spikes in the plot are due to truck traffic while the smaller spikes are from cars and other light vehicles, or vehicles in other lanes.

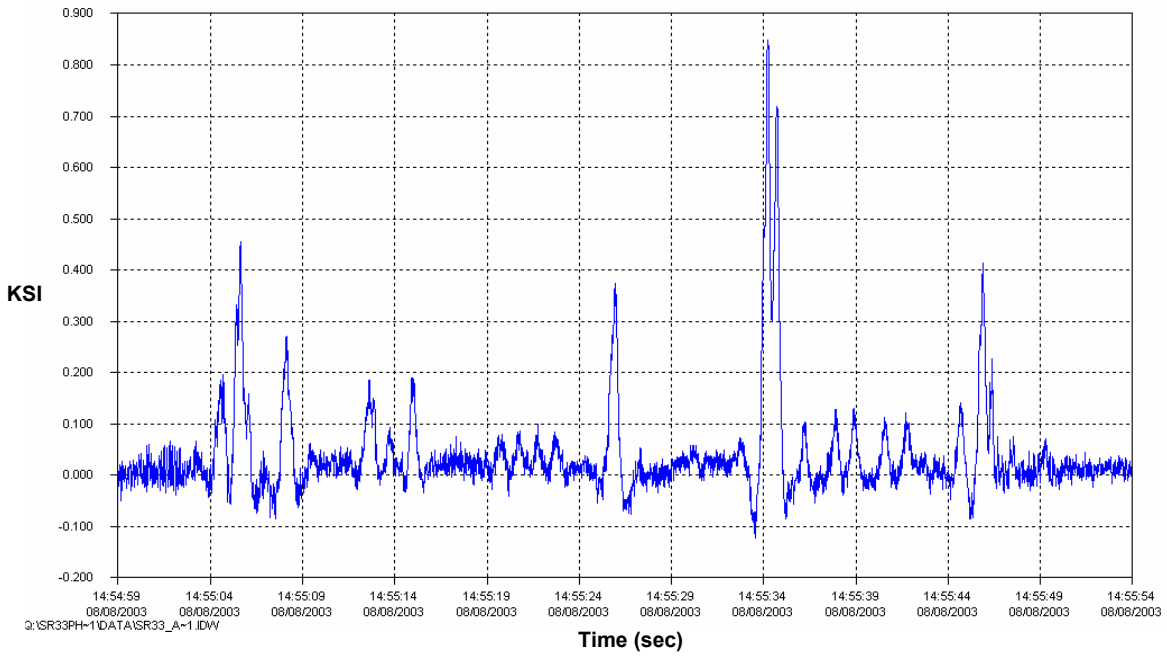

Figure 5.1: Typical response of bottom gage of U26-U28 East (BU2628EB)

The upper chord gages on U26-U28 exhibit identical behavior as observed in ATLSS Report 02-07 for U16-U18 (Connor and Santosuosso, 2002). The gages on the side flange plates respond similarly to live load. The bottom web plate is subjected to higher stresses than the gages on the side flange plates due to bending of the upper chord. This behavior is shown in Figure 5.2 for U26-U28 West.

Overall, the response of the upper chords is dominated by a local bending response. This local bending is seen in Figure 5.2 as the short period of compression, the reversal to much greater tension, and a final small reversal to compression. The global response of the upper chord U26-U28 is not clear from the figure. Due to the variability of loads on the bridge, the global response defined by the slight rise in compression as the load moves along the bridge cannot be seen in Figure 5.2. The global response for U16-U18 was verified during controlled load tests, however, in ATLSS Report 02-07 (Connor and Santosuosso, 2002). Above pier 2, the upper chords (U16-U18) experience a slight rise in tension as the load traverses spans 1 and 2. The magnitude of the global response for U26-U28 during the uncontrolled live load test in Figure 5.2 is minimal compared to the magnitude of the response for U16-U18 during the controlled load test.

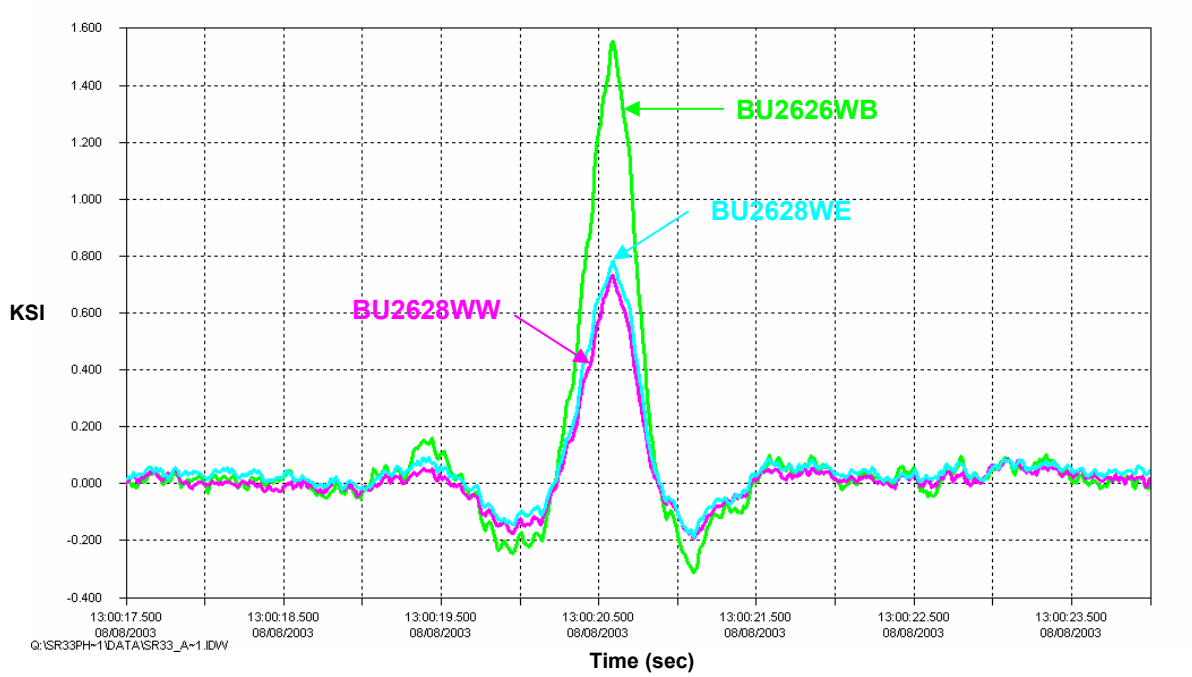

Figure 5.2: Response of all gages on U26-U28 West

As noted in ATLSS Report 02-07, the upper chords at U16-U18 do not equally share loads located in a given single lane. For example, if the primary portion of the northbound lane is loaded, the upper chord on the east truss carries the load. This behavior was verified during the controlled live load testing for the upper chords at U16-U18. Figure 5.3 demonstrates the same behavior for the bottom gages of the upper chords between U26 and U28. It is clear that when one upper chord responds locally to traffic, the other upper chord has little local response. This should not be confused with the global response of the upper chord. The unequal distribution discussed is purely a local phenomenon.

In fact, as the vehicle moves away from the location of the members, both upper chords begin to share the global response more equally. Extensive finite element models were used to investigate the lateral load distribution of the bridge in the vicinity of pier 2 (Santosuosso, 2002). A load placed at midspan of span 2 produced a very uniform strain distribution in the upper chords and stringers between U16 and U18. This suggests that the upper chords, stringers, and deck act together similar to the top flange of a box girder in bending with the lower chords representing the bottom flange.

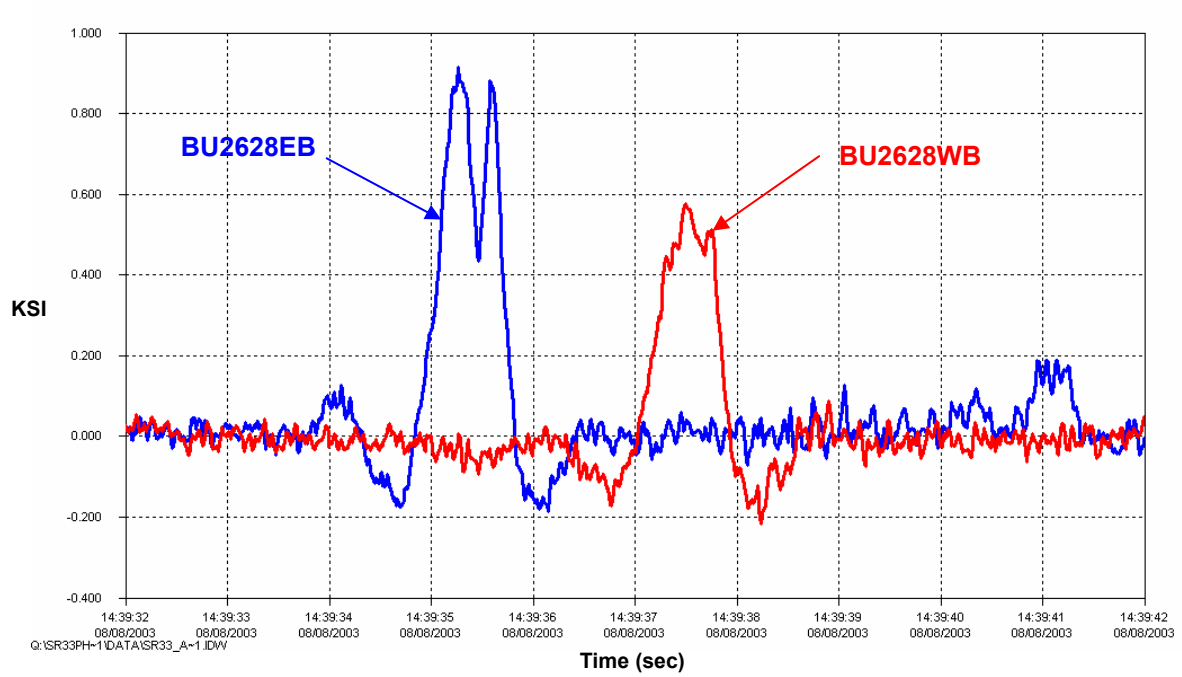

Figure 5.3: Response of bottom gages on U26-U28 East and U26-U28 West

Figure 5.4 describes the response of gages on U16-U18 West above pier 2. One of the side gages (BU1618WW) was not operational during monitoring and was therefore not plotted. The member behaves as expected with the bottom gage experiencing a higher stress than the side gage under live load. This response for U16-U18 was also shown in ATLSS Report 02-07 (see Figure 2.8).

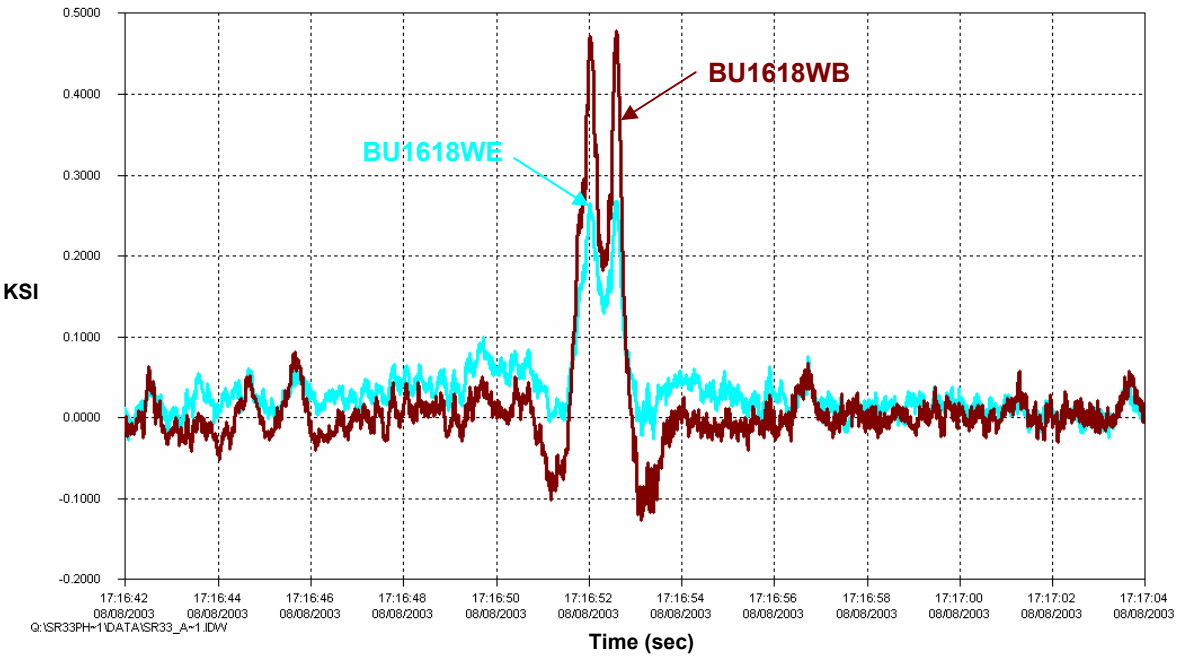

Figure 5.4: Response of gages on U16-U18 West

5.2 Lower Chord Response

The lower chords L25-L27 and L27-L29 of span 2 were monitored under traffic load. It should be noted that the data for the lower chords was noisier than the upper chords. However, reliable data were obtained. Figure 5.5 is a plot of both lower chord bottom gages for L25-L27. It can be seen from the plot that both lower chords carry a portion of the load when either lane is loaded.

From controlled load tests conducted in January of 2002, the lower chords were determined to behave primarily as axial members. However, this could not be verified for the uncontrolled live load monitoring of August 8, 2003, since the top gages on the lower chords were damaged some time when construction was being completed and are not functioning properly. However, it is reasonable to assume that the lower chords are still exhibiting primarily a global and axial response to live load.

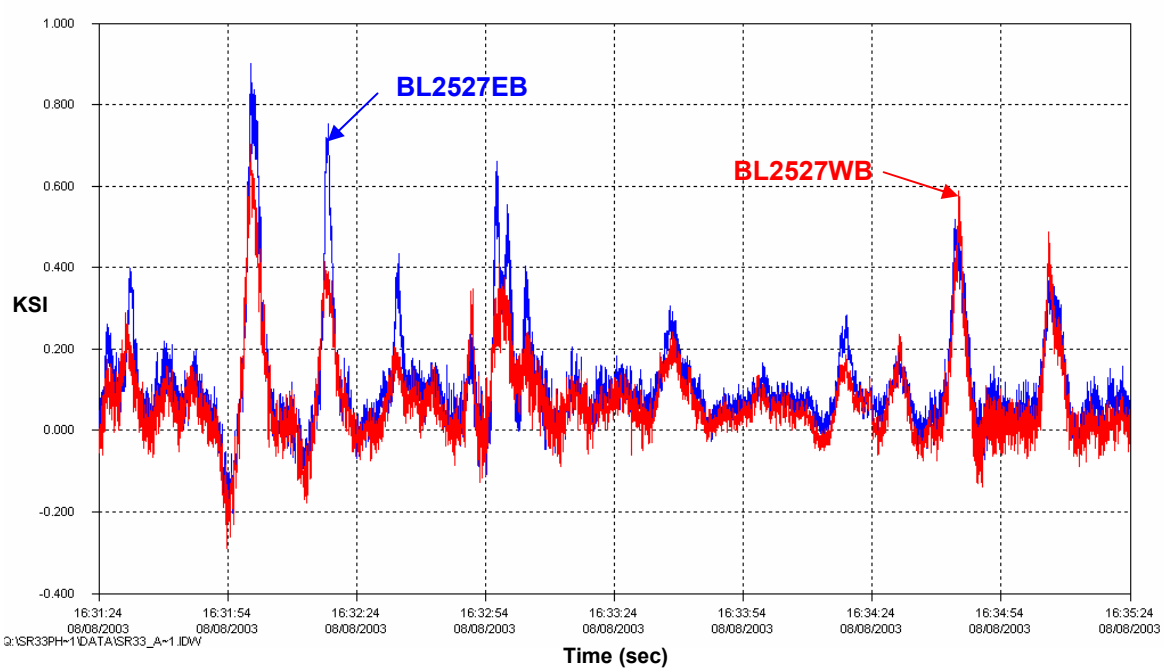

Figure 5.5: Response bottom gages on L25-L27 East and L25-L27 West

5.3 Diagonal Response

The diagonals U18-L19 and U20-L21 were monitored under random traffic. The diagonals were observed to behave mainly as axial members. This response is consistent with data collected from controlled load tests. In the previous study, it was shown that the diagonals experience a small out-of-plane bending component when the shoulder lanes were loaded during the controlled load testing.

Figure 5.6 describes the response of U18-L19 East. Both gages on the centerlines of the flanges experience the same stress due to the vehicular live load. This implies that the diagonal behaves primarily as an axial member. The diagonal members experience noticeable vibration after a load passes. The region circled in red in Figure 5.6 is shown in Figure 5.7 and illustrates the vibration of U18-L19 East. The diagonal experiences reversals in tension and compression for a period of time after a vehicle passes. Similar behavior can be seen for other instrumented diagonals.

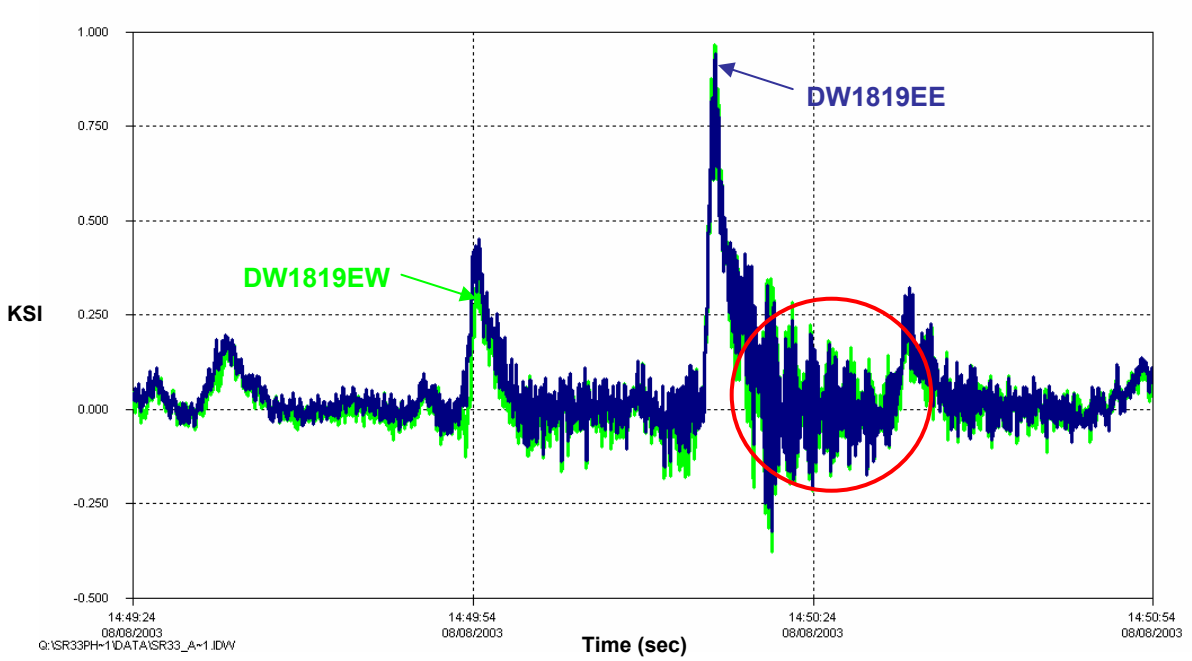

Figure 5.6: Response of both gages on U18-L19 East

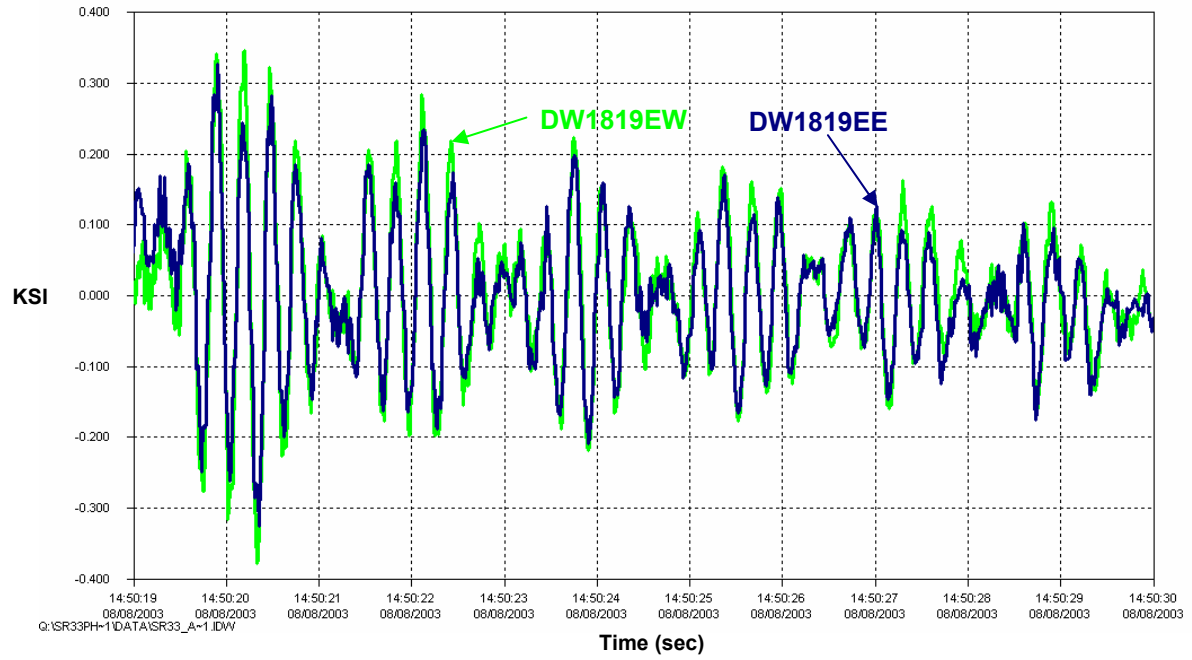

Figure 5.7: Vibration response of U18-L19 East

The response of U20-L21 East is shown in Figure 5.8. As expected, this diagonal exhibits a similar response to live load as U18-L19. Both gages on the centerlines of the flanges output similar stresses. This implies that the diagonal U20-L21 East exhibits a predominant axial response. It was not possible to verify the axial response of the diagonals U18-L19 West and U20-L21 West. One of the gages on each of these

members was not functioning properly (see Table 5.1). However, it is reasonable to believe that these members are still exhibiting primarily an axial response under live load.

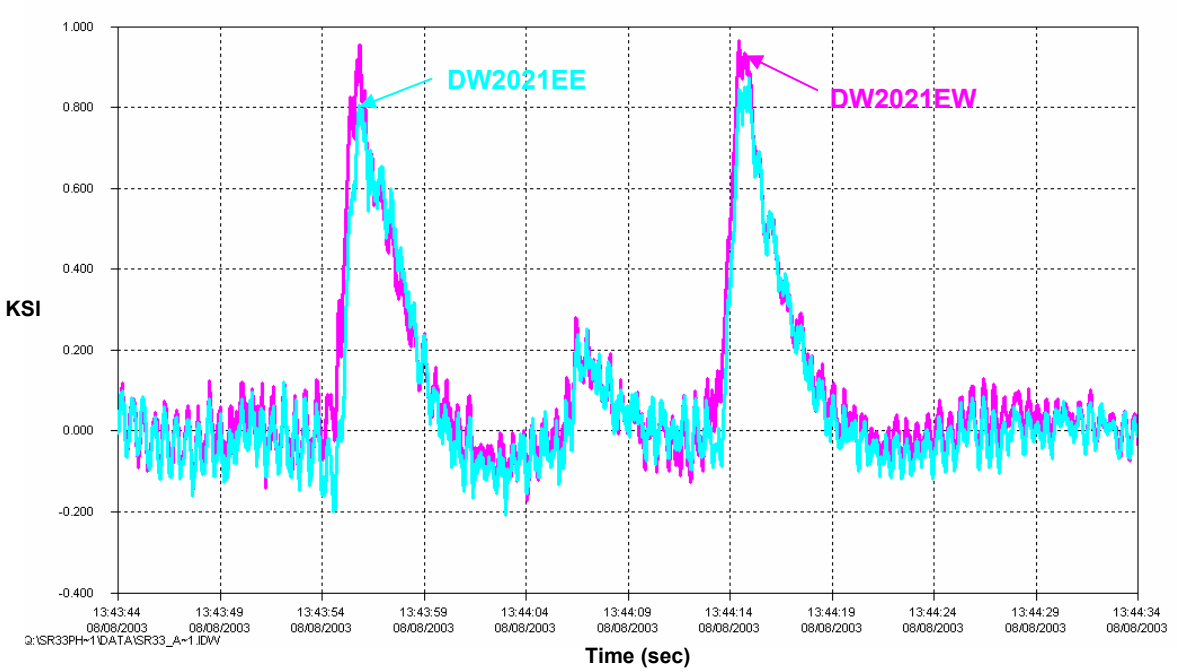

Figure 5.8: Response of U20-L21 East

Figure 5.9 exhibits the response of diagonals on opposite sides of the bridge. The diagonals at U18-L19 are shown in this figure. The bottom gages of stringers 2, 3 and 4 between U26 and U28 are plotted to verify transverse truck position. When stringers 2 (S2BCL) and 3 (S3BCL) respond, the truck is traveling southbound in Lane 2 (see Figure 2.6). It is apparent from the figure that the diagonal under the loaded lane carries the majority of the load. The diagonal of the west truss (DW1819WE) responds to the load from the vehicle after the stringers because of its longitudinal position on the truss. The diagonal on the east truss (DW1819EE) has a much smaller response to a load in the southbound lane. Similarly, the diagonal on the west truss has little response to a load in the northbound lane. Approximately 84% of the load was distributed to U18-L19 West and 16% to U18-L19 East for the response shown in Figure 5.9.

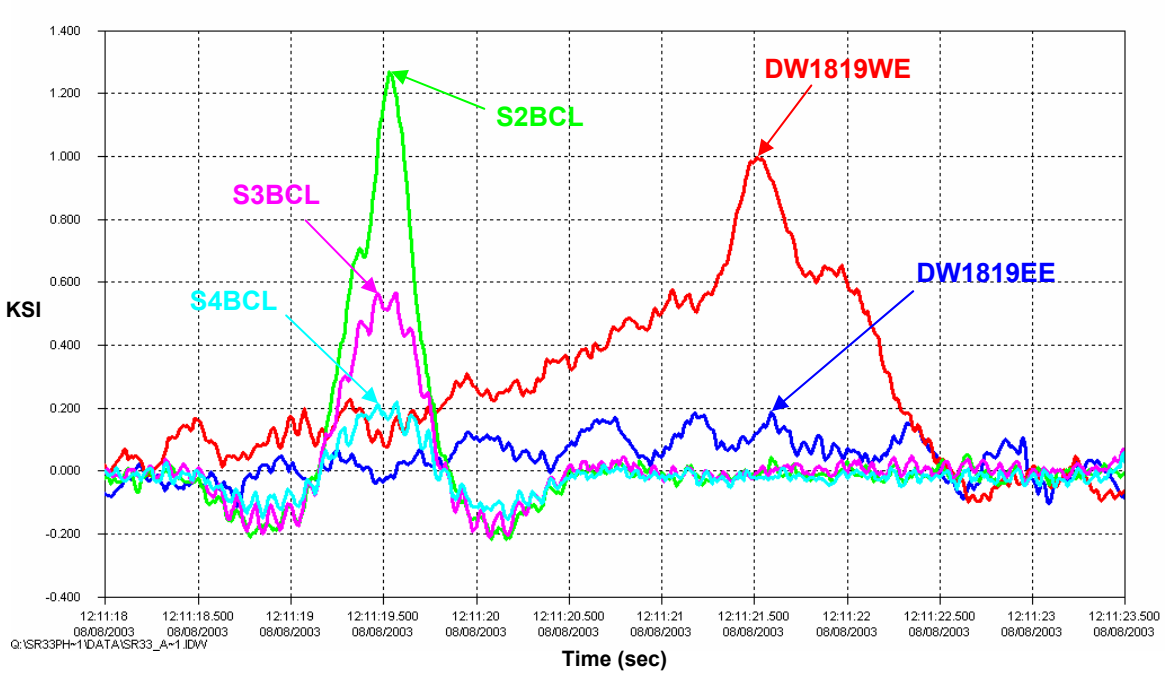

Figure 5.9: Response of U18-L19 East and U18-L19 West (Lane 2 loaded)

On the other hand, the diagonals on opposite sides share the load more equally when the vehicle is traveling closer to the bridge centerline. This behavior is illustrated for the diagonals at U18-L19 in Figure 5.10. The bottom gages of stringers 2, 3, and 4 are again plotted to verify transverse truck position. When stringers 3 (S3BCL) and 4 (S4BCL) respond, the vehicle is traveling southbound in Lane 3. Both diagonals have a significant response to the load. The west diagonal (DW1819WE) has a higher response since it is under the loaded lane, but it is clear from the figure that both diagonals respond more equally. Approximately 63% of the load was distributed to U18-L19 West and 37% to U18-L19 East.

Similar distributions occurred between opposite diagonals at U20-L21 for vehicles traveling in lanes 2 and 3, respectively. It should be noted that the instrumented diagonals (U18-L19 and U20-L21) are close to pier 2. The distribution between diagonals near midspan of span 2 could not be determined from the measurements taken at U18-L19 and U20-L21.

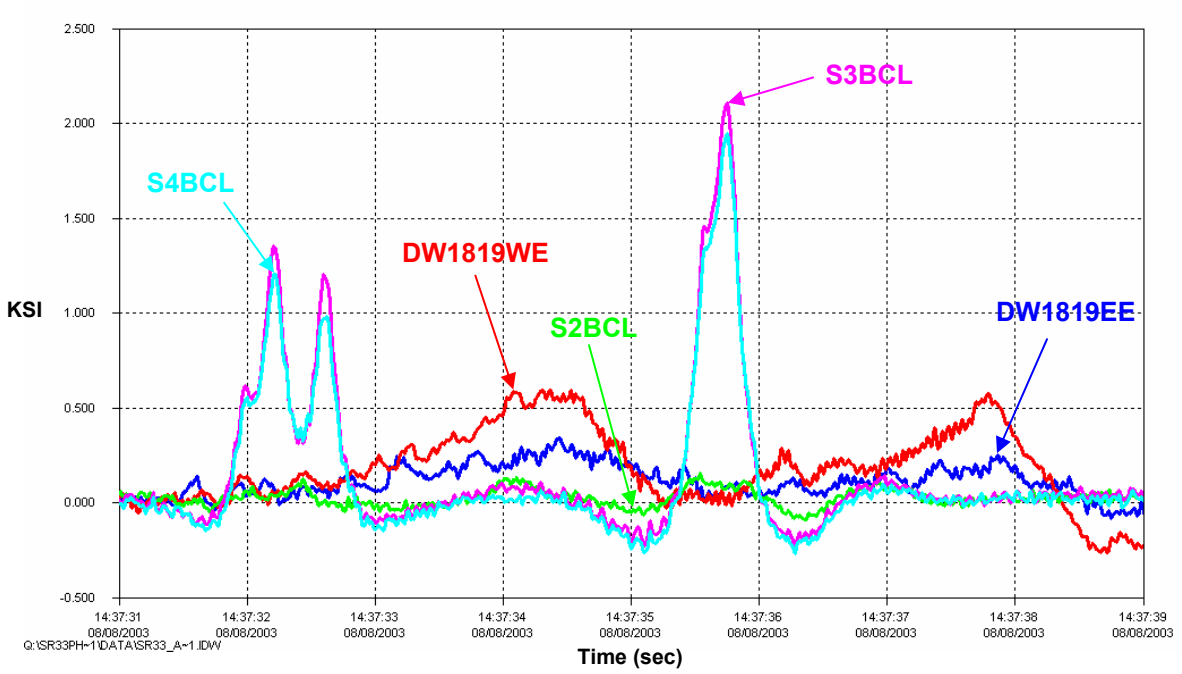

Figure 5.10: Response of U18-L19 East and U18-L19 West (Lane 3 loaded)

5.4 Stringer Response

The stringers recently instrumented in July of 2003 between U26 and U28 were monitored under live load. It was decided that only the stringers on the southbound lane be instrumented due to the symmetry of the bridge. The response of members symmetrical about the bridge centerline was verified and determined to be independent of direction of travel during Phase I. The stringers exhibit primarily a local bending behavior and respond primarily to direct loading as expected.

A typical stringer response can be seen in Figure 5.11 for stringer 3 which is approximately underneath the middle of the two southbound traffic lanes. It can be seen that the response of the top gage (S3TCL) remains close to zero throughout the live load time history. It was shown in ATLSS Report 02-07 that the neutral axis of the composite stringer and concrete deck is near the interface of the stringer top flange and concrete deck. This agrees with the top flange gage output which is located on the bottom face of the stringer top flange. The bottom gage experiences distinct peaks corresponding to the axle loads of the truck passing over the gage at midspan of the member. It is clear from the response of the bottom gage that the behavior of the stringers at midspan is primarily local bending. Due to its transverse location, stringer 3 is highly loaded by traffic traveling in either of the two southbound lanes. The bottom gages of the stringers will be used to determine transverse load position since the top gages experience little response (see Figure 5.11).

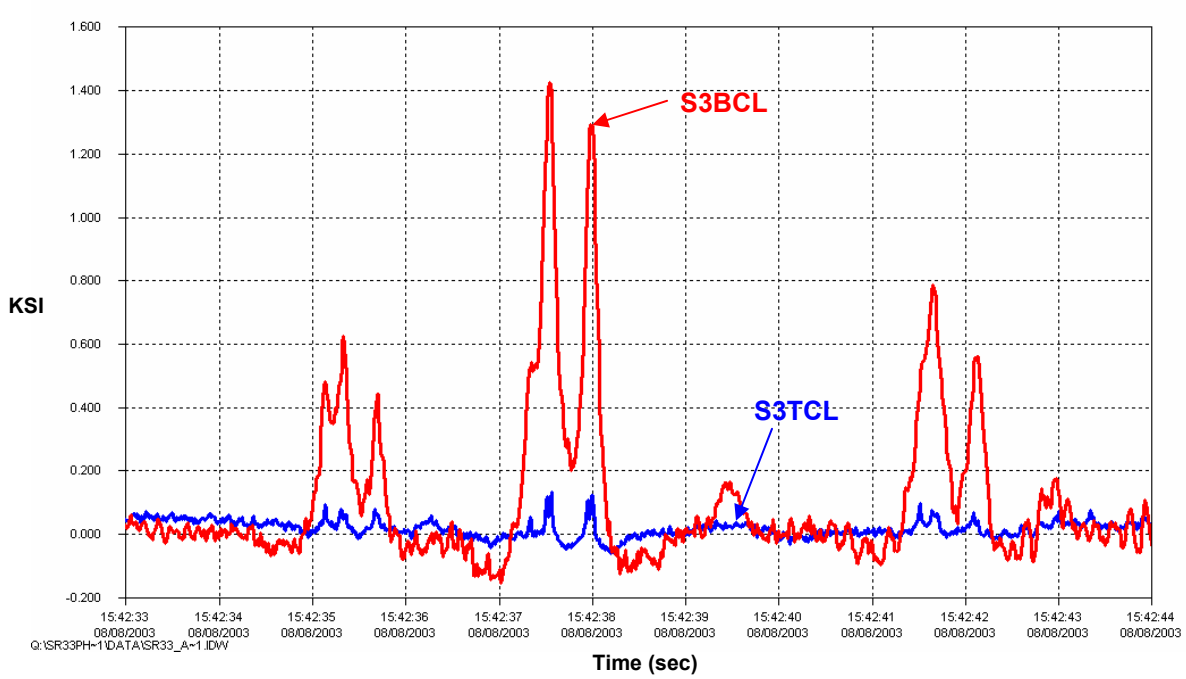

Figure 5.11: Typical stringer response between panel points U26 and U28 (Stringer 3)

The transverse distribution of traffic load can be seen in Figure 5.12 and Figure 5.13. These figures show the response of stringers 1, 2, 3 and 4 between U26 and U28 of the truss to live load. The results are in agreement with the layout of the members. The results of Figure 5.12 suggest the truck was traveling in Lane 2 (see Figure 2.6 for lane demarcation). Stringers 1 and 2, which are cantilevered outside the truss, experience significant stress compared to stringer 4 which is closer to the bridge centerline. Stringer 3 experiences stress due to its proximity to Lane 2. Figure 5.13 would suggest the vehicle was traveling in Lane 3. Stringers 3 and 4, which are directly underneath Lane 3, experience significant stress compared to stringers 1 and 2. Stringers 1 and 2 have very little response to the vehicle in Lane 3 since they are outside of the truss.

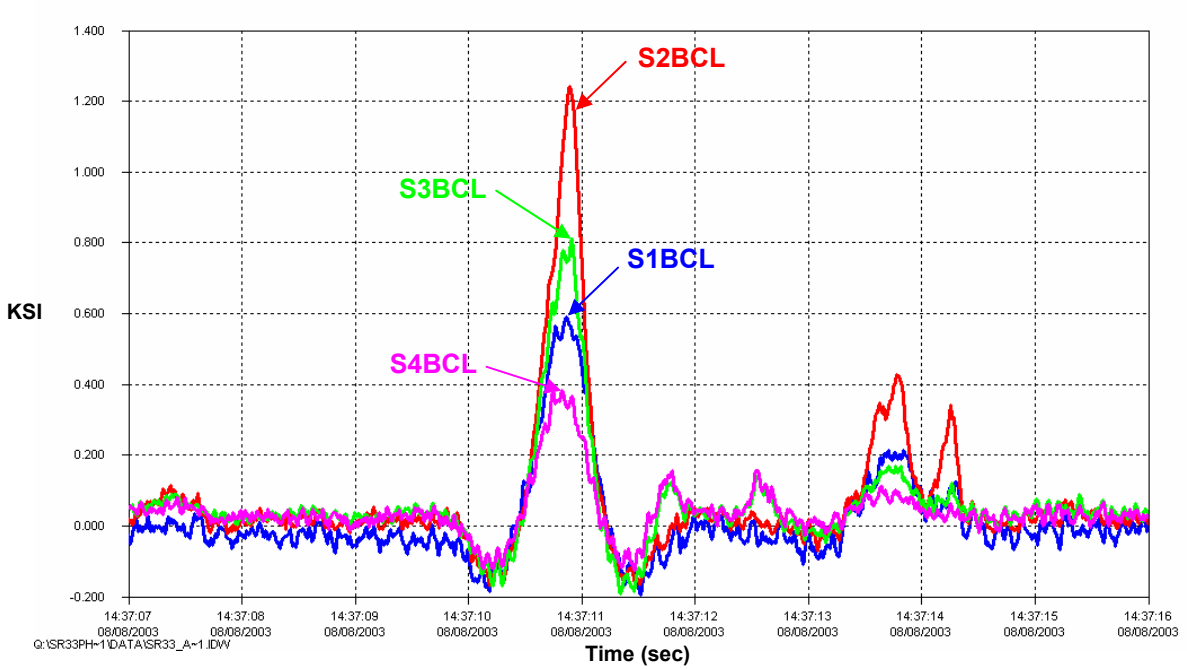

Figure 5.12: Response of stringers under southbound lanes between panel points U26 and U28 (Lane 2 loaded)

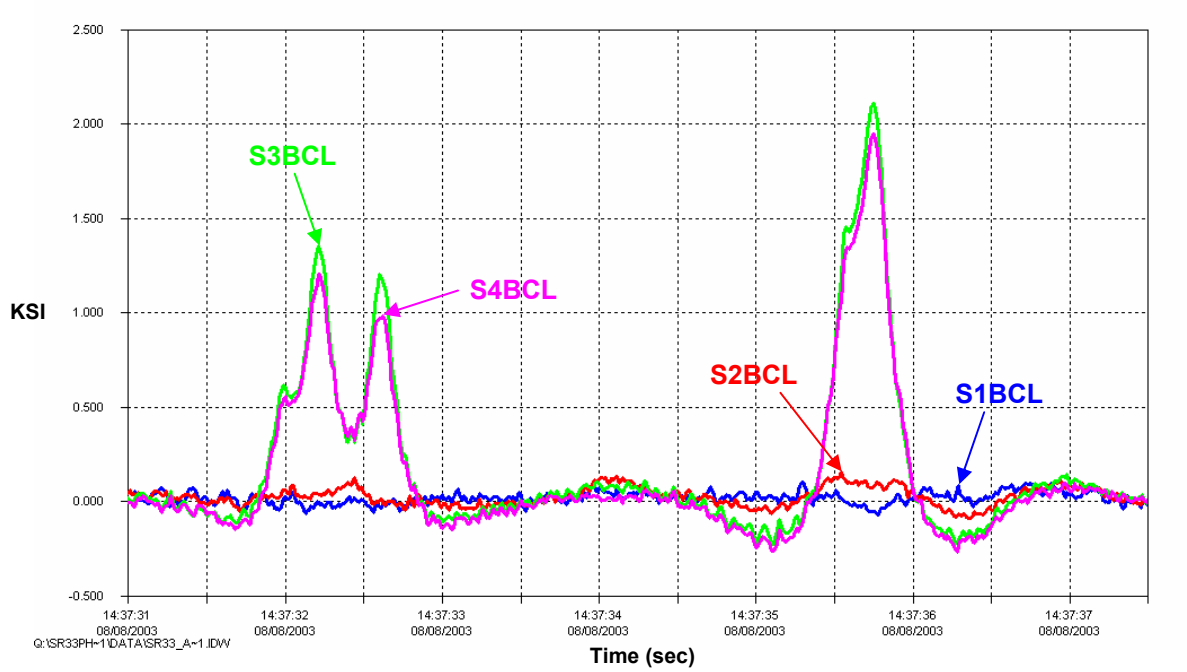

Figure 5.13: Response of stringers under southbound lanes between panel points U26 and U28 (Lane 3 loaded)

5.5 Overall Response

The response of a lower chord, upper chord, and two stringers to a load traveling southbound is shown in Figure 5.14. The global response of the lower chord can be seen from its early response to the load. It gradually increases its response as the load traverses the main river span and peaks when the truck is above L27-L29. The local responses of the upper chord and stringers are seen by their more abrupt response when the load is directly above these members. The upper chord and stringers primarily exhibit local bending. Furthermore, transverse lane position can be determined from this figure. Stringers 3 and 4 have a significant response to the first two stress cycles indicating that the vehicles are traveling in Lane 3. These two stringers are directly beneath this lane of traffic. The next stress cycle indicates that the vehicle is positioned in Lane 2. The upper chord and lower chord, which are both beneath this lane of traffic, have more significant responses.

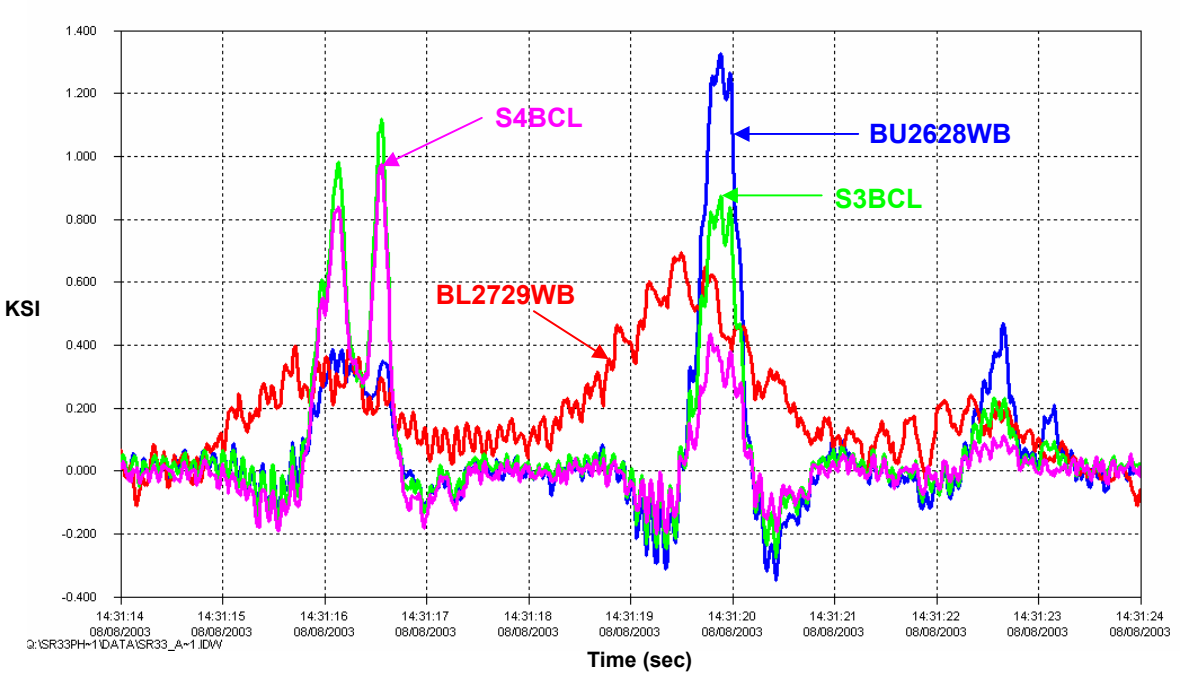

Figure 5.14: Overall response to vehicles traveling southbound

6.0 Long-Term Uncontrolled Live Load Monitoring

A remote monitoring program was conducted to study the long-term effects of live load on the Lehigh River Bridge. Various members of the steel superstructure were selected to assess the future fatigue performance of the bridge.

In order to have both the CR5000 and CR9000 data loggers running simultaneously, modifications needed to be made to both data logger programs. It was found while collecting live load data that the CR5000 introduced spurious noise spikes in the live load data. This occurred at 5 minute intervals, the sampling rate for the vibrating wire strain gages. Every time the AVW100 vibrating wire interface sent a signal to the vibrating wire strain gages, locations with both a vibrating wire and uniaxial resistance strain gage contained noise spikes in the live load "response". Figure 6.1 displays the response of the bottom gage of U16-U18 West containing noise spikes from the vibrating wires. A closer view of the noise spike circled in Figure 6.1 is shown in Figure 6.2. It can be seen from the figure that the duration for this particular noise spike is very short (less than 1.0 second). Other gages experienced interference from the vibrating wire interface for durations up to 1.0 second.

This interference problem needed to be resolved so that noise spikes from the vibrating wire gages would not be counted as stress cycles in the long-term live load monitoring program. The solution to this problem was as follows. The sampling rate for the vibrating wire strain gages was reduced from every 5 minutes to every 3 hours. After a review of more than two years worth of data, the researchers were confident that this new sampling rate would still capture the long-term response of the truss members to concrete creep, shrinkage, and thermal/seasonal effects. It takes the vibrating wire interface approximately 1 minute to cycle through all 59 vibrating wire strain gages. The CR9000 data logger is turned off 15 seconds before the AVW100 begins its cycle through the 59 vibrating wire strain gages and is then turned back on 15 seconds after the cycle has completed. Therefore, live load data is not recorded for a total of 90 seconds each time the CR5000 polls data from the vibrating wires. This occurs 8 times each day so that 12 minutes of live load data are not recorded each day. This will have a negligible effect on assessing the fatigue performance of the bridge.

Two separate periods of data were collected and analyzed to evaluate the long-term live load characteristics of the Lehigh River Bridge. The first period was during the summer of 2004 from June 21st to August 30th. This was not a continuous period of data collection. There were times when communication was lost with the CR9000 data logger and data were not recorded. All calculations were made taking these factors into account. The second phase consisted of data collected from February 7th to February 18th of 2005.

For each monitoring phase, calculations were made in order to quantify the long-term behavior of the bridge. These calculations included the maximum stress range, effective stress range, cycles per day, cycles greater than the constant amplitude fatigue limit (CAFL), and remaining life of the detail. The maximum stress range is the largest stress cycle that the gage experiences. The effective stress range is calculated using the following formula:

$$SR_{eff} = (\Sigma \alpha_i SR_i^3)^{1/3}$$

The coefficient α_i is the frequency of stress cycles in the i^{th} bin. SR_i is the i^{th} stress range bin. For example, for cycles counted between 2.5 and 3.0 ksi, $SR_i = (2.5 + 3.0)/2 = 2.75$ ksi. The frequency is multiplied by the cube of the stress range bin and summed over all bins. Finally, the cube root is taken to determine the effective stress range. Cycles per day were counted as the number of cycles greater than or equal to 1.0 ksi divided by the number of days. It is reasonable to ignore cycles less than 1.0 ksi since they do not contribute to fatigue damage, and they tend to skew the effective stress range to a smaller value. There were no cycles greater than the CAFL found in this research which suggests infinite fatigue life for the members investigated.

Stress cycles were counted using the rainflow cycle counting method (Downing and Socie, 1982). This algorithm is built into the CR9000 data logger. The algorithm searches for peaks and valleys in the long-term data and counts the number of cycles in each specified stress range bin. A peak and valley that comprises a specific stress range does not necessarily have to occur during the same stress cycle. In fact, they may occur hours apart from each other. In other words, an individual truck may not have generated the maximum stress range for a gage location shown in the tables of this chapter. However, the maximum stress ranges identified in the tables can almost always be traced back to an individual truck by searching through the triggered time history data. For the long-term remote monitoring of the Lehigh River Bridge, ten (10) bins of 0.5 ksi were specified. The largest bin size was from 4.5 ksi to 5.0 ksi. The rainflow analysis algorithm was also programmed to ignore any stress range less than 0.5 ksi. All long-term live load data were collected at a sampling rate of 50 Hz for the two data collection phases.

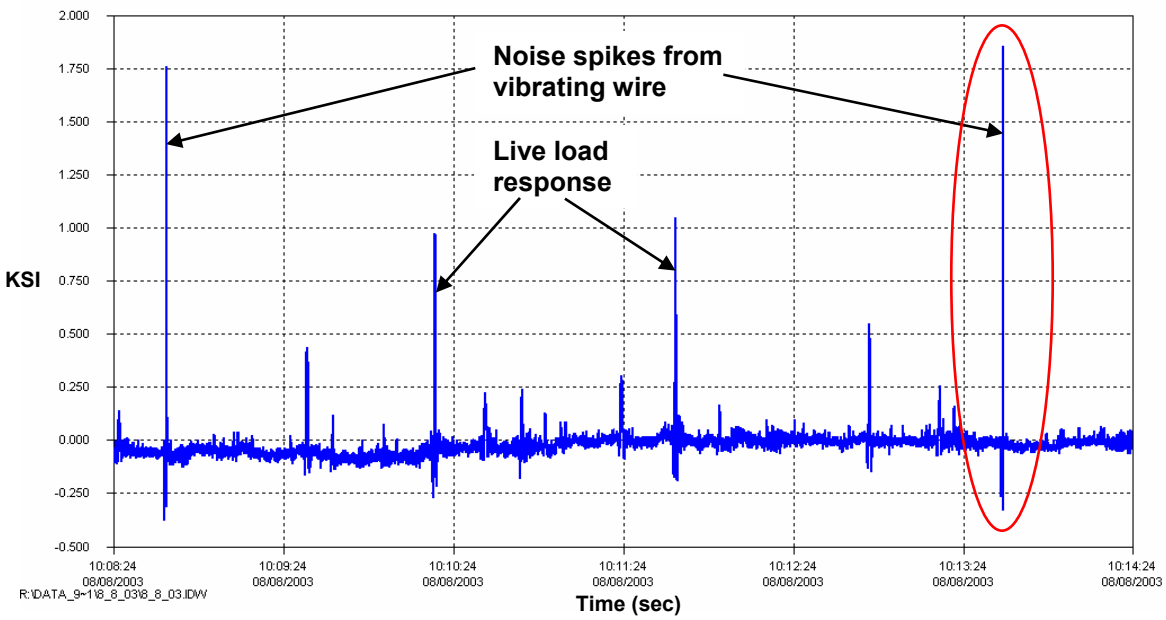

Figure 6.1: Response of bottom gage of U16-U18 West containing vibrating wire noise spikes (BU1618WB)

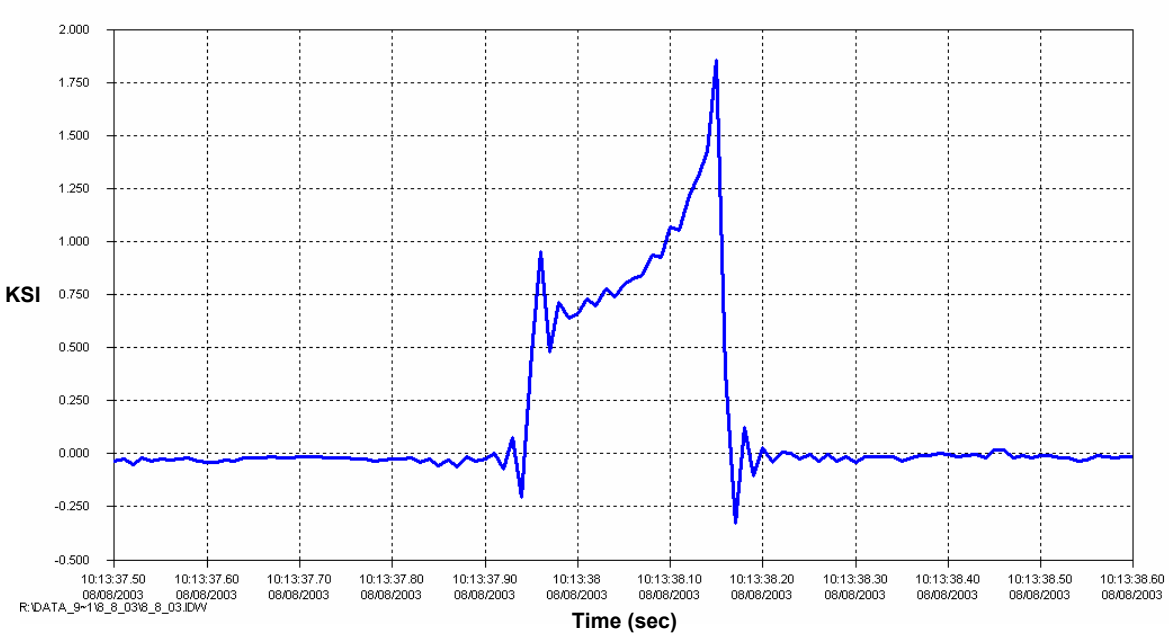

Figure 6.2: Close up view of noise spike in resistance strain gage signal caused by vibrating wire gage on BU1618WB

6.1 Long-Term Monitoring During Summer 2004

Table 6.1 lists the gages that were chosen for the long-term remote monitoring from June 21st to August 30th of 2004. Reliable data could not be obtained for BL2729EB and S9BCL due to failure of these gages.

Gage Name	Location	Functionality
BU1618EB	East U16-U18 Bottom face	OK
BU1618WB	West U16-U18 Bottom face	OK
BU1618WE	West U16-U18 East face	OK
DW1819EE	East U18-L19 East face	OK
DW1819WE	West U18-L19 East face	OK
DW2021EW	East U20-L21 West face	OK
DW2021WE	West U20-L21 East face	OK
BL2527EB	East L25-L27 Bottom face	OK
BL2527WB	West L25-L27 Bottom face	OK
BL2729EB	East L27-L29 Bottom face	X
BL2729WB	West L27-L29 Bottom face	OK
S6BCL	Bottom flange of S6 27' N of U16	OK
S7BCL	Bottom flange of S7 27' N of U16	OK
S8BCL	Bottom flange of S8 27' N of U16	OK
S9BCL	Bottom flange of S9 27' N of U16	X
BU2628EE	East U26-U28 East face	OK
BU2628EB	East U26-U28 Bottom face	OK
BU2628WE	West U26-U28 East face	OK
BU2628WB	West U26-U28 Bottom face	OK
S1BCL	Bottom flange of S1 27' N of U26	OK
S2BCL	Bottom flange of S2 27' N of U26	OK
S3BCL	Bottom flange of S3 27' N of U26	OK
S4BCL	Bottom flange of S4 27' N of U26	OK
S5BCL	Bottom flange of S5 27' N of U26	OK

Table 6.1: Gages included in long-term remote monitoring during summer of 2004

The following stringer members listed in Table 6.2 were used as triggers to capture significant responses to live load. Data from the triggers were necessary to find maximum stress ranges and identify spurious stress cycles in the data caused by noise. The trigger value for each stringer, direction of travel, and associated traffic lane are described. These stringers were chosen to capture the response of a vehicle traveling in one of the four traffic lanes outlined in Figure 2.6. It should be noted that stringers 6 and 8 are located above pier 2 (between U16 and U18) and stringers 2 and 4 are located near midspan of span 2 (between U26 and U28).

Gage Name	Trigger Value (ksi)	Direction of Travel	Traffic Lane
S2BCL	1.25	Southbound	Lane 2
S4BCL	2.00	Southbound	Lane 3
S6BCL	1.75	Northbound	Lane 4
S8BCL	1.00	Northbound	Lane 5

Table 6.2: Stringers used as triggers during summer of 2004

6.1.1 Upper Chord Response

A total of seven (7) upper chord gages were monitored during the summer of 2004. These gages are located on the upper chords above pier 2 (U16-U18) and near midspan of span 2 (U26-U28). A summary of the maximum and effective stress ranges observed for the upper chord gages is presented in Table 6.3. It is evident from the results in the table that the upper chords monitored have infinite fatigue life. Measurements indicated that there were no stress cycles even near the constant amplitude fatigue limit (CAFL) of the member.

It is noted that due to the shear studs installed on the top surface of the upper chords, these members would be evaluated for fatigue as category C. However, the controlled and uncontrolled live load data confirms that the neutral axis of the member is very high and near the concrete/steel interface and that the primary stress component in the upper chords is the result of local bending as the upper chord acts as a beam spanning between panel points. Since this is the controlling load case and due to the composite behavior of the member, stresses in the top plate are almost negligible. The only stresses of significance are at the bottom of the member and are due to bending. At this location, the worst fatigue category is the web to flange weld which is classified as category B. Hence, the member was evaluated as category B. The gages on the side flange plates should actually be evaluated as base metal or category A, but were conservatively assigned category B.

The table also illustrates that the upper chords near midspan of span 2 (U26-U28) experience stress cycles of greater magnitude and a larger frequency of stress cycles in excess of 1.0 ksi each day. This can be attributed directly to the smaller gross cross-sectional area of U26-U28 (125.13 in^2 compared to 275.14 in^2 for U16-U18). A stress-range histogram is presented in Figure 6.3 for the bottom gages on U26-U28 East and West. From the histogram, it appears that U26-U28 East experiences more stress cycles in the 1.0-1.5 ksi bin than U26-U28 West. However, this could not be confirmed for the lower chords or stringers. The stringers under the southbound lanes (Lanes 2 and 3) experience significantly more stress cycles than the stringers under the northbound lanes (Lanes 4 and 5). This can be attributed to the smaller cross-sectional area of the bridge near midspan (the stringers are discussed in more detail in Section 6.1.4). The response of the lower chords is global, and the direction of travel and lane loaded become less influential on these members. On the other hand, the local bending response of the upper chords can be attributed to direct wheel loading when a vehicle is positioned above the member. Transverse vehicle position (i.e., lane of travel) also play a significant role in the response of the upper chord.

Channel	Fatigue Life Calculation Summary						
	SR_{max} ksi	Cycles > CAFL #	Cycles > CAFL %	SR_{eff} ksi	Cycles/day	Remaining Life (years)	Category
BU1618EB	1.8	0	0	1.3	27	Infinite	B
BU1618WB	1.9	0	0	1.3	33	Infinite	B
BU1618WE	1.0	0	0	1.3	1	Infinite	B
BU2628EB	3.1	0	0	1.3	360	Infinite	B
BU2628EE	1.5	0	0	1.3	3	Infinite	B
BU2628WB	2.8	0	0	1.4	167	Infinite	B
BU2628WE	1.4	0	0	1.3	4	Infinite	B

Note:
1. The effective stress range and cycles per day calculations ignore cycles less than 1.0 ksi
2. The CAFL for a category B detail is 16.0 ksi
3. It is conservative to consider the side flange plate gages category B (typically base metal, category A)

Table 6.3: Summary of maximum and effective stress ranges for upper chord gages (Summer 2004)

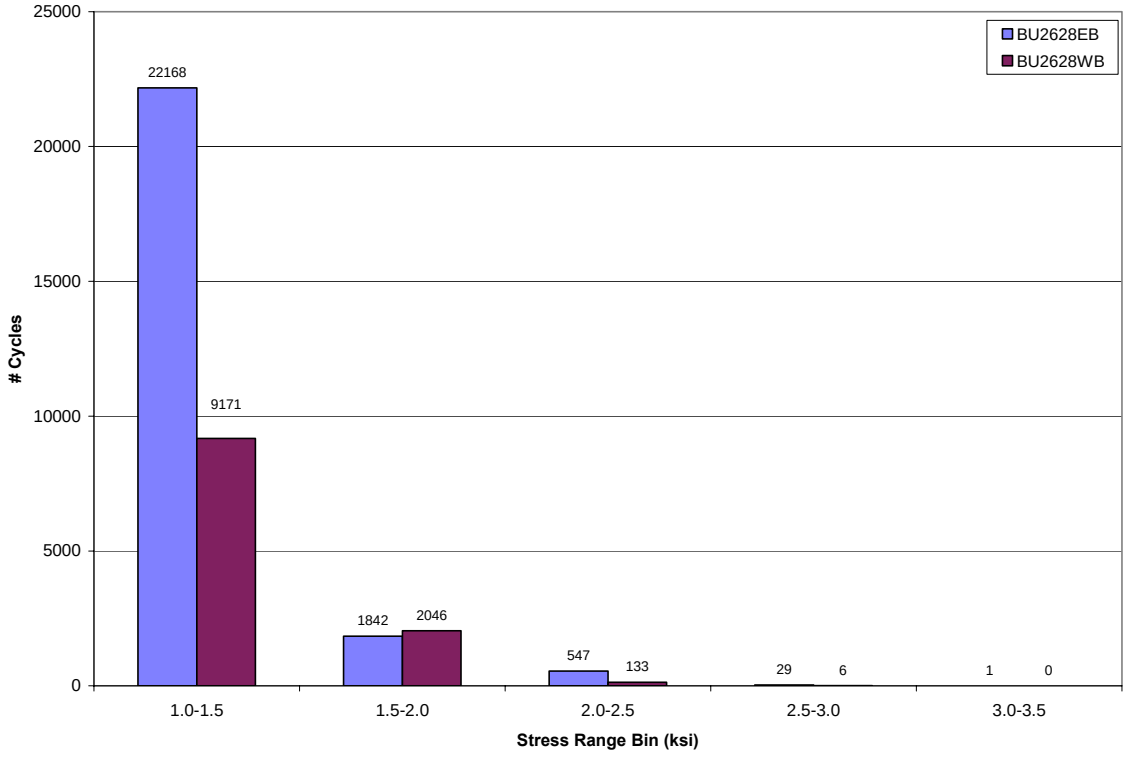

Figure 6.3: Stress-range histogram for BU2628EB and BU2628WB (Summer 2004)

The peak stress range responses for BU2628EB and BU2628EE are illustrated in Figure 6.4. This response occurred on July 22, 2004 at 12:19 PM for a vehicle traveling northbound in Lane 5 and was obtained from triggered time history data. Recall that a vehicle in Lane 5 is positioned directly above the upper chord. The bottom gage of the upper chord experienced a stress cycle of approximately 3.1 ksi while the side flange

plate gage experienced a cycle of 1.5 ksi. Even though this was the largest cycle observed, the magnitude was well below the CAFL of the member.

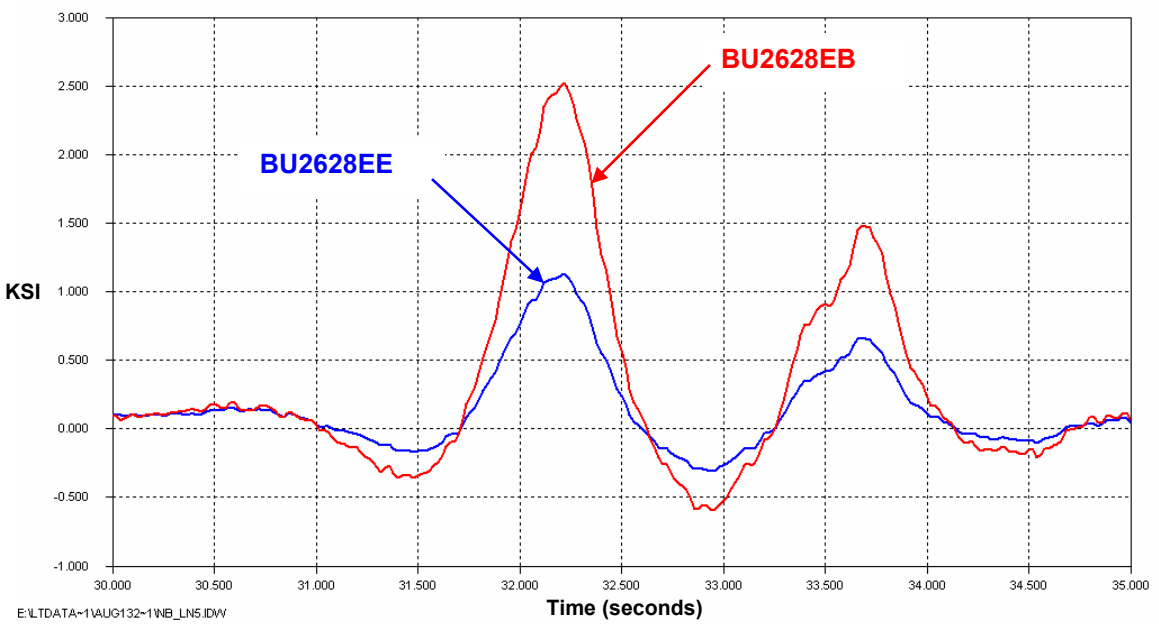

Figure 6.4: Maximum stress cycle for gages on U26-U28 East (Summer 2004)

6.1.2 Diagonal Response

Four gages installed on diagonal members were monitored. These diagonals are U18-L19 and U20-L21, the large tension diagonals located near pier 2 of the bridge. It should be noted that these diagonal gages did not produce reliable data over the entire data collection period. Unfortunately the rainflow algorithm stopped counting stress cycles at various times. However, sufficient amounts of accurate data were obtained and all calculations take into account the periods of time for which reliable data were collected.

A summary of maximum stress ranges and effective stress ranges is presented in Table 6.4. Each diagonal encountered a maximum stress range of 2.1 ksi and had a corresponding effective stress range of 1.3 ksi. The number of cycles per day larger than 1.0 ksi is distributed fairly evenly between opposing diagonals. Furthermore, no stress cycles were measured greater than the CAFL of the member (Category B). The stress-range histogram for DW1819EE and DW1819WE is shown in Figure 6.5. Unlike the upper chords near midspan of span 2, there is not a large discrepancy between cycles within each stress bin. The upper chords have a more significant response to direct loading. The concentration of truck traffic on one side of the bridge would be expected to influence the upper chord. On the other hand, the diagonals exhibit more of a global response to live load. Vehicles traveling in either the northbound or southbound lanes produce significant responses in these diagonals.

Channel	Fatigue Life Calculation Summary						
	SR_{max} ksi	Cycles > CAFL		SR_{eff} ksi	Cycles/day	Remaining Life (years)	Category
		#	%				
DW1819EE	2.1	0	0	1.3	183	Infinite	B
DW1819WE	2.1	0	0	1.3	185	Infinite	B
DW2021EW	2.1	0	0	1.3	298	Infinite	B
DW2021WE	2.1	0	0	1.3	284	Infinite	B

Note:
1. The effective stress range and cycles per day calculations ignore cycles less than 1.0 ksi
2. The CAFL for a category B detail is 16.0 ksi

Table 6.4: Summary of maximum and effective stress ranges for diagonal gages (Summer 2004)

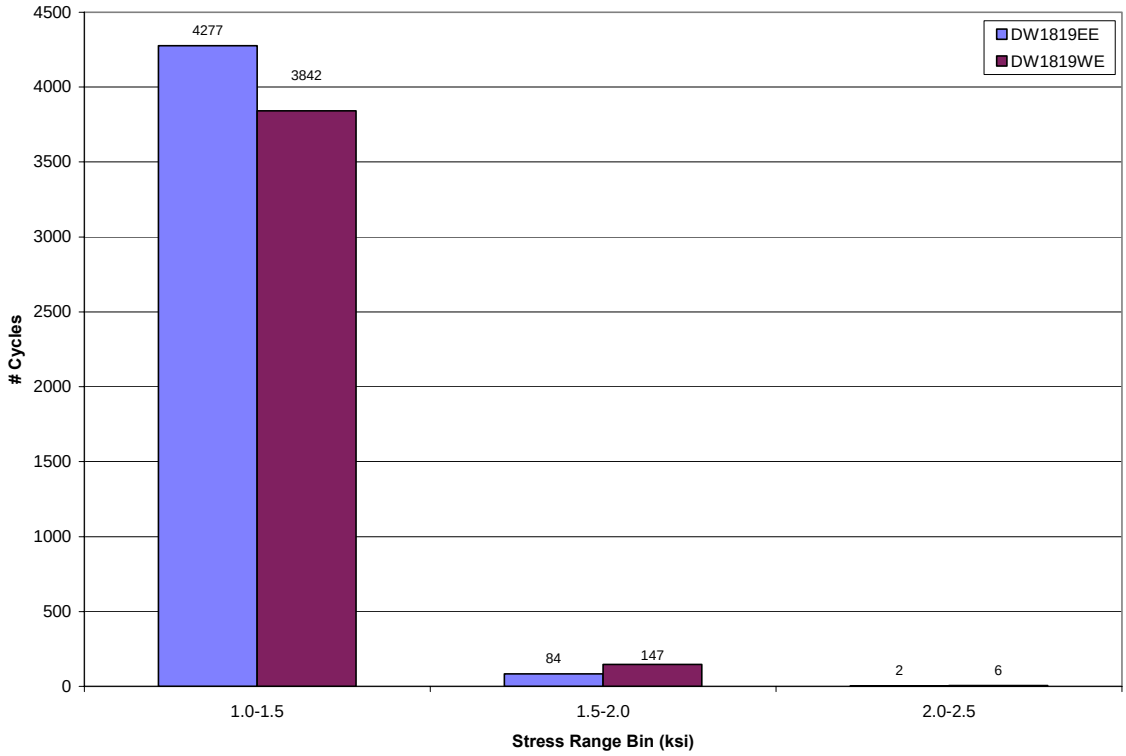

Figure 6.5: Stress-range histogram for DW1819EE and DW1819WE (Summer 2004)

The gage on the west flange plate of U20-L21 East (DW2021EW) experienced a maximum stress cycle of 2.1 ksi. This response is shown in Figure 6.6 along with a significant response for DW1819EE. This event occurred on August 3, 2004 at 6:45 AM and was triggered by a vehicle traveling northbound in Lane 5 as confirmed from data from the stringers. Once again, Lane 5 is located directly above the east truss line. The response of the diagonals tends to be greatest in magnitude when a vehicle is positioned directly over the truss (Lane 2 or Lane 5).

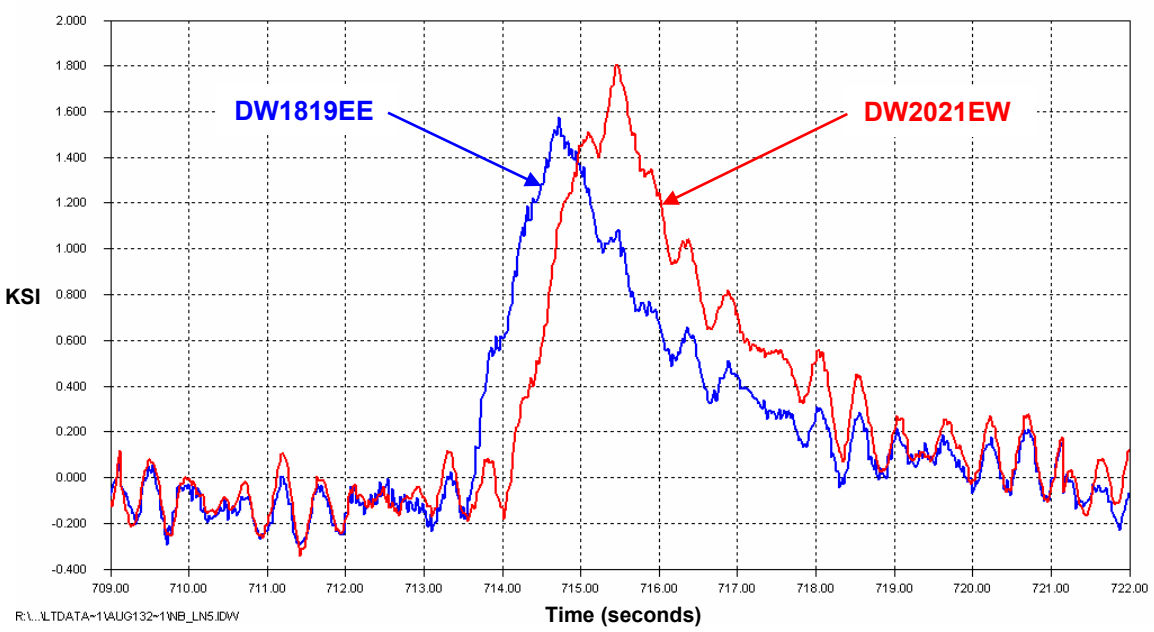

Figure 6.6: Maximum stress cycle for DW2021EW (Summer 2004)

6.1.3 Lower Chord Response

A gage from each of the four (4) instrumented lower chords was chosen to be monitored. The data for the lower chords were less reliable than the data for other members. All calculations consider the durations of time for which these member produced accurate data. The gage on L27-L29 East (BL2729EB) was not functioning properly and is identified in Table 6.1.

The maximum and effective stress ranges for the functioning lower chord gages are presented in Table 6.5. The maximum stress cycle each lower chord experienced was approximately 2.0 ksi with an effective stress range of 1.3 ksi. No cycles greater than the CAFL were reported for the lower chords and this suggests an infinite fatigue life for the members investigated. Figure 6.7 displays the stress-range histogram for L25-L27 East and L25-L27 West. It appears that the west lower chord experienced more stress cycles in the 1.0-1.5 ksi bin. There were more cycles for the east lower chord in the other stress range bins. This inconsistency with the upper chord data was noted. However, these members have different responses to live load. The lower chords exhibit primarily a global response to live load and respond to vehicles traveling in both directions. Therefore, it is not uncommon for these trends to appear in the data.

Channel	Fatigue Life Calculation Summary						
	SR_{max} ksi	Cycles > CAFL #	Cycles > CAFL %	SR_{eff} ksi	Cycles/day	Remaining Life (years)	Category
BL2527EB	2.0	0	0	1.3	106	Infinite	B
BL2527WB	2.0	0	0	1.3	148	Infinite	B
BL2729EB	-	-	-	-	-	-	B
BL2729WB	2.0	0	0	1.3	66	Infinite	B

Note:
1. The effective stress range and cycles per day calculations ignore cycles less than 1.0 ksi
2. The CAFL for a category B detail is 16.0 ksi

Table 6.5: Summary of maximum and effective stress ranges for lower chord gages (Summer 2004)

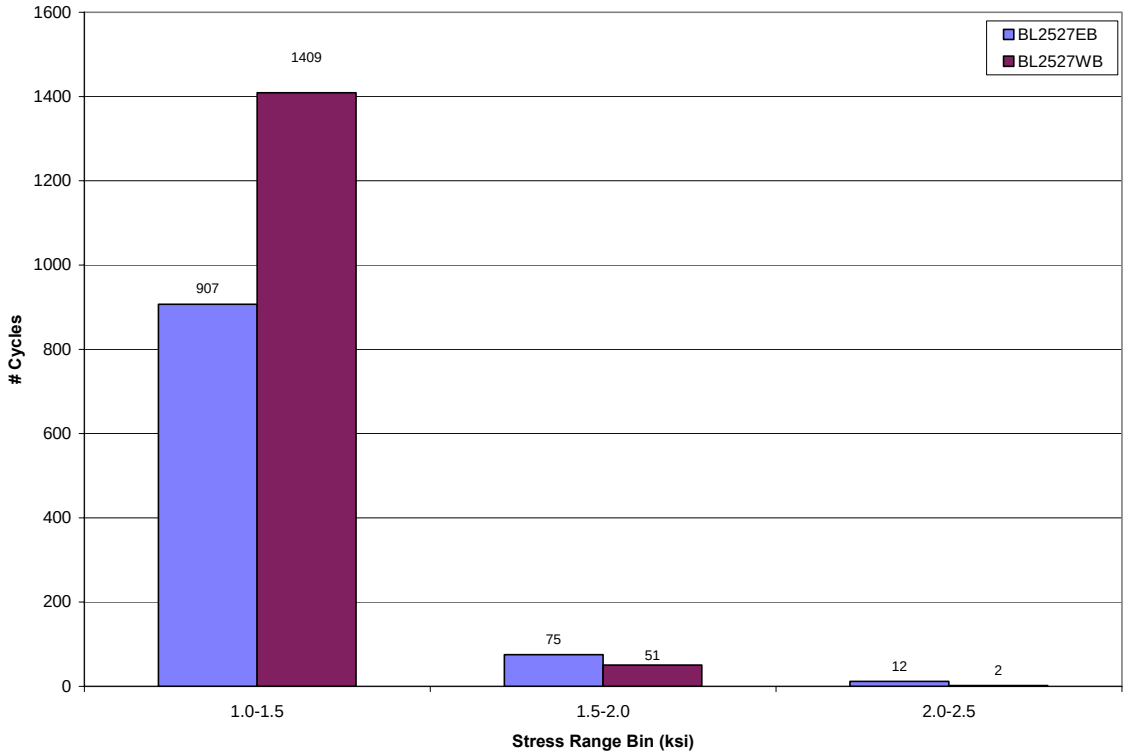

Figure 6.7: Stress-range histogram for BL2527EB and BL2527WB (Summer 2004)

A plot of the maximum stress cycle for BL2527WB is illustrated in Figure 6.8. The response of BL2729WB is also shown for reference. In this figure, BL2527WB experiences a stress cycle of approximately 2.0 ksi. This response occurs on August 17, 2004 at 11:17 AM and was caused by two (2) vehicles traveling southbound in Lane 2. Each vehicle is identified in the figure by the local bending response of U26-U28 West (BU2628WB) and stringer 2 (S2BCL) under Lane 2.

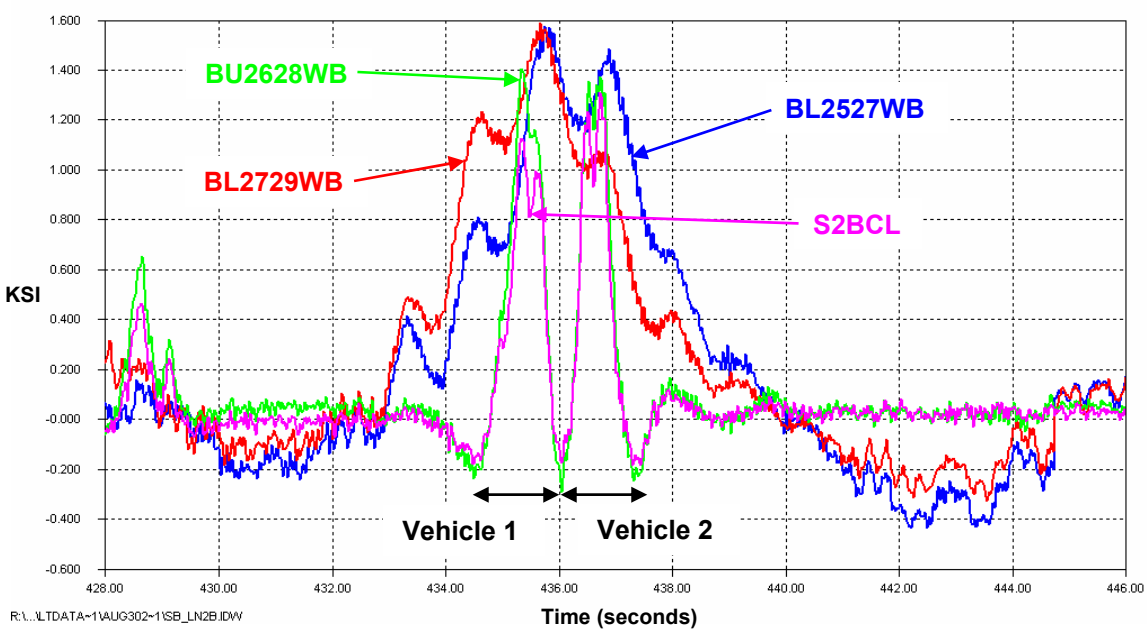

Figure 6.8: Maximum stress cycle for BL2527WB (Summer 2004)

6.1.4 Stringer Response

The stringers between U16 and U18 and between U26 and U28 were monitored under long-term vehicular live load. The gages on these stringers are all located along the centerline of the bottom flange at midspan of the member. It was determined that the instrumentation on stringer 9 between U16 and U18 was not functioning properly. Therefore, data for this stringer are not reported.

Maximum and effective stress ranges were calculated for the stringers and these values are presented in Table 6.6. It is evident from the table that the stringers near midspan of span 2 (S1BCL to S5BCL) experience larger stress ranges and more cycles greater than 1.0 ksi each day. With the exception of S1BCL, all of these stringers are W30 x 108 sections. However, the area of the entire bridge cross-section is smaller at midspan of span 2 (U26 to U28) than over pier 2 (U16 to U18). The upper chords between U26 and U28 have considerably less gross cross-sectional area than those between U16 and U18 as previously discussed. Also, the concrete deck near midspan is 8" thick compared to 8.5" thick over pier 2. Therefore, the stiffness of the entire cross-section is less near midspan of span 2. This causes the bottom flanges of the stringers to compensate by experiencing larger tensile stresses under live load for local bending.

There were no stress cycles greater than the CAFL reported for the stringer members. This indicates an infinite fatigue life for these members. A stress-range histogram for two of the more highly stressed stringers, stringers 3 and 4, is shown in Figure 6.9. It is clear from the histogram that stringer 3 is exposed to a larger number of stress cycles than stringer 4. The location of stringer 3 in the cross-section of the bridge exposes the member to direct wheel loading more often. Vehicles in either Lane 2 or Lane 3 typically generate significant responses for stringer 3 (see Figure 5.12 and Figure 5.13). Significant responses for stringer 4 generally occur only for a vehicle traveling in Lane 3.

Channel	Fatigue Life Calculation Summary						
	SR_{max} ksi	Cycles > CAFL #	Cycles > CAFL %	SR_{eff} ksi	Cycles/day	Remaining Life (years)	Category
S6BCL	2.7	0	0	1.5	110	Infinite	C
S7BCL	2.6	0	0	1.5	149	Infinite	C
S8BCL	2.1	0	0	1.3	20	Infinite	C
S9BCL	-	-	-	-	-	-	C
S1BCL	1.6	0	0	1.3	5	Infinite	C
S2BCL	2.4	0	0	1.4	84	Infinite	C
S3BCL	4.0	0	0	1.5	1280	Infinite	C
S4BCL	3.9	0	0	1.5	925	Infinite	C
S5BCL	2.4	0	0	1.3	79	Infinite	C

Note:
1. The effective stress range and cycles per day calculations ignore cycles less than 1.0 ksi
2. The CAFL for a category C detail is 10.0 ksi

Table 6.6: Summary of maximum and effective stress ranges for stringer gages (Summer 2004)

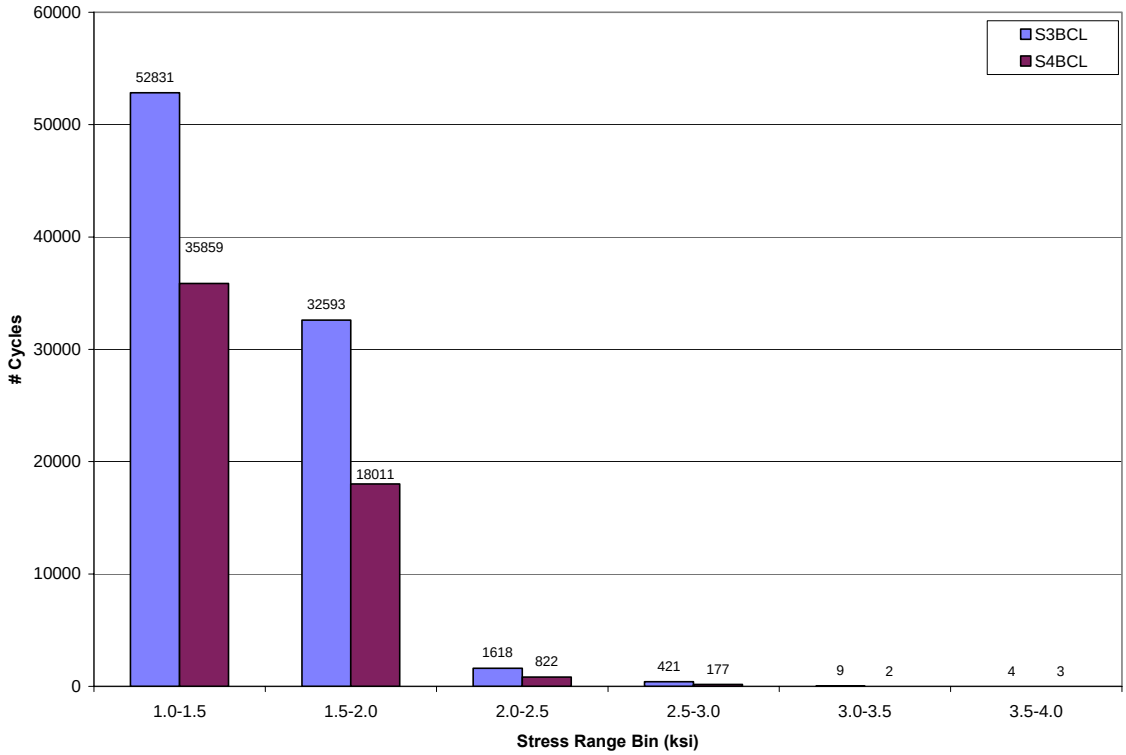

Figure 6.9: Stress-range histogram for S3BCL and S4BCL (Summer 2004)

The peak stress responses for stringers 3 and 4 were caused by the same vehicle on June 30, 2004 at 7:00 AM. The responses are shown in Figure 6.10. The bottom flange of stringer 3 (S3BCL) experienced a stress cycle of 4.0 ksi while the bottom flange of stringer 4 (S4BCL) experienced a cycle of 3.9 ksi. These responses were caused by a vehicle traveling southbound in Lane 3.

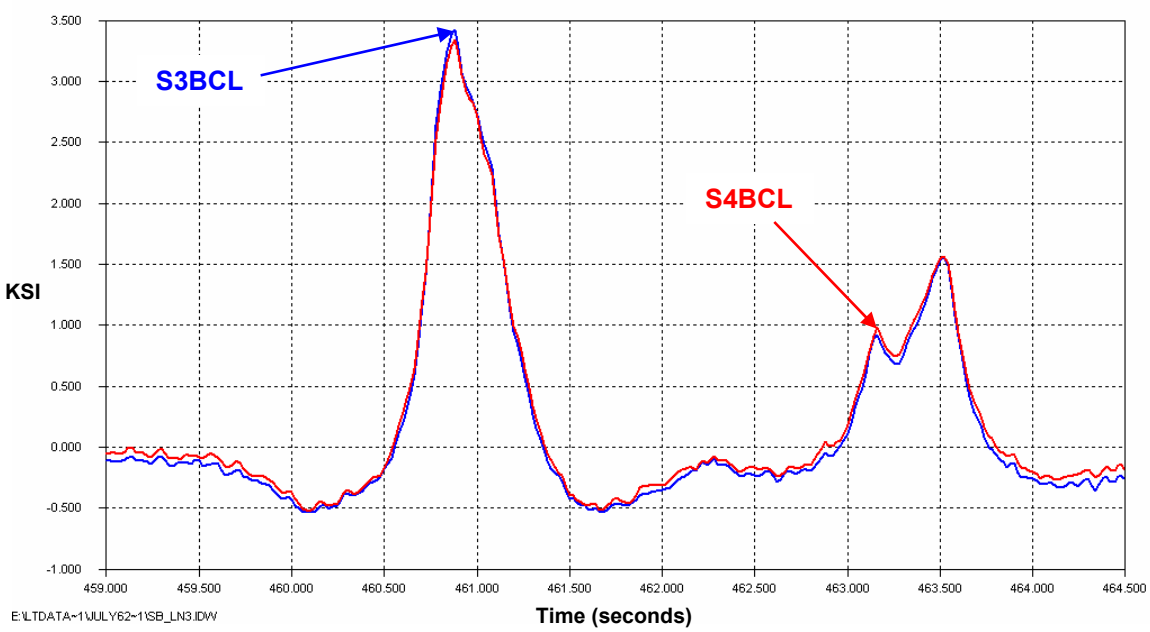

Figure 6.10: Maximum stress cycles for S3BCL and S4BCL (Summer 2004)

6.2 Long-Term Monitoring During Winter 2005

The following gages listed in Table 6.7 were monitored for a period of approximately eleven (11) days during February 2005. Of the 24 gages selected for this period of monitoring, six (6) of the gages were not producing reliable data. These gages are identified in Table 6.7.

Gage Name	Location	Functionality
BU1618EB	East U16-U18 Bottom face	OK
BU1618WB	West U16-U18 Bottom face	OK
DW1819EE	East U18-L19 East face	OK
DW1819WE	West U18-L19 East face	OK
DW2021EW	East U20-L21 West face	OK
DW2021WE	West U20-L21 East face	X
BL2527ET	East L25-L27 Top face	X
BL2527WB	West L25-L27 Bottom face	X
BL2729EB	East L27-L29 Bottom face	X
BL2729WB	West L27-L29 Bottom face	X
SB2425ET	East cross of sway brace Top face	OK
SB2425WB	West cross of sway brace Bottom face	OK
SB2425HB	Horiz. strut of sway brace Bottom face	X
S3BOC	Bottom flange of S3 18" N of U16	OK
S6BCL	Bottom flange of S6 27' N of U16	OK
S7BCL	Bottom flange of S7 27' N of U16	OK
S8BCL	Bottom flange of S8 27' N of U16	OK
BU2628EB	East U26-U28 Bottom face	OK
BU2628WB	West U26-U28 Bottom face	OK
S1BCL	Bottom flange of S1 27' N of U26	OK
S2BCL	Bottom flange of S2 27' N of U26	OK
S3BCL	Bottom flange of S3 27' N of U26	OK
S4BCL	Bottom flange of S4 27' N of U26	OK
S5BCL	Bottom flange of S5 27' N of U26	OK

Table 6.7: Gages included in long-term remote monitoring during winter of 2005

The same stringers used as triggers to capture significant live load response during the summer of 2004 were used for this monitoring phase. The trigger values were slightly adjusted to decrease the size of data files. These stringers are listed in Table 6.8.

Gage Name	Trigger Value (ksi)	Direction of Travel	Traffic Lane
S2BCL	1.50	Southbound	Lane 2
S4BCL	2.00	Southbound	Lane 3
S6BCL	2.00	Northbound	Lane 4
S8BCL	1.25	Northbound	Lane 5

Table 6.8: Stringers used as triggers during winter of 2005

6.2.1 Upper Chord Response

The gages located on the bottom web plates of four (4) upper chords were monitored during the winter of 2005. These included the upper chords above pier 2 (U16 to U18) and the upper chords near midspan of span 2 (U26 to U28). In order to allow for

the monitoring of other gages, it was decided that the side flange plate gages be disconnected for this period. The gages on the bottom web plates experience higher levels of stress due to local bending of the upper chord.

The maximum and effective stress ranges for these four upper chords are displayed in Table 6.9. No cycles greater than the CAFL of the member were reported. The larger stress ranges and greater number of cycles per day in excess of 1.0 ksi for the upper chords near midspan is consistent with data from the previous time interval. This can be attributed to the much smaller cross-sectional area of the upper chords near midspan. A stress-range histogram for BU2628EB and BU2628WB is presented in Figure 6.11. Data for this histogram is consistent with data from the previous monitoring phase (see Figure 6.3). The east upper chord appears to experience more stress cycles from truck traffic. As discussed earlier, the upper chords respond more significantly to direct loading (i.e., local bending response). The distribution of truck traffic between northbound and southbound lanes would be expected to affect these members.

Channel	Fatigue Life Calculation Summary						
	SR_{max} ksi	Cycles > CAFL		SR_{eff} ksi	Cycles/day	Remaining Life (years)	Category
		#	%				
BU1618EB	1.4	0	0	1.3	26	Infinite	B
BU1618WB	1.6	0	0	1.3	25	Infinite	B
BU2628EB	2.6	0	0	1.4	338	Infinite	B
BU2628WB	2.2	0	0	1.4	135	Infinite	B

Note:
1. The effective stress range and cycles per day calculations ignore cycles less than 1.0 ksi
2. The CAFL for a category B detail is 16.0 ksi

Table 6.9: Summary of maximum and effective stress ranges for upper chord gages (Winter 2005)

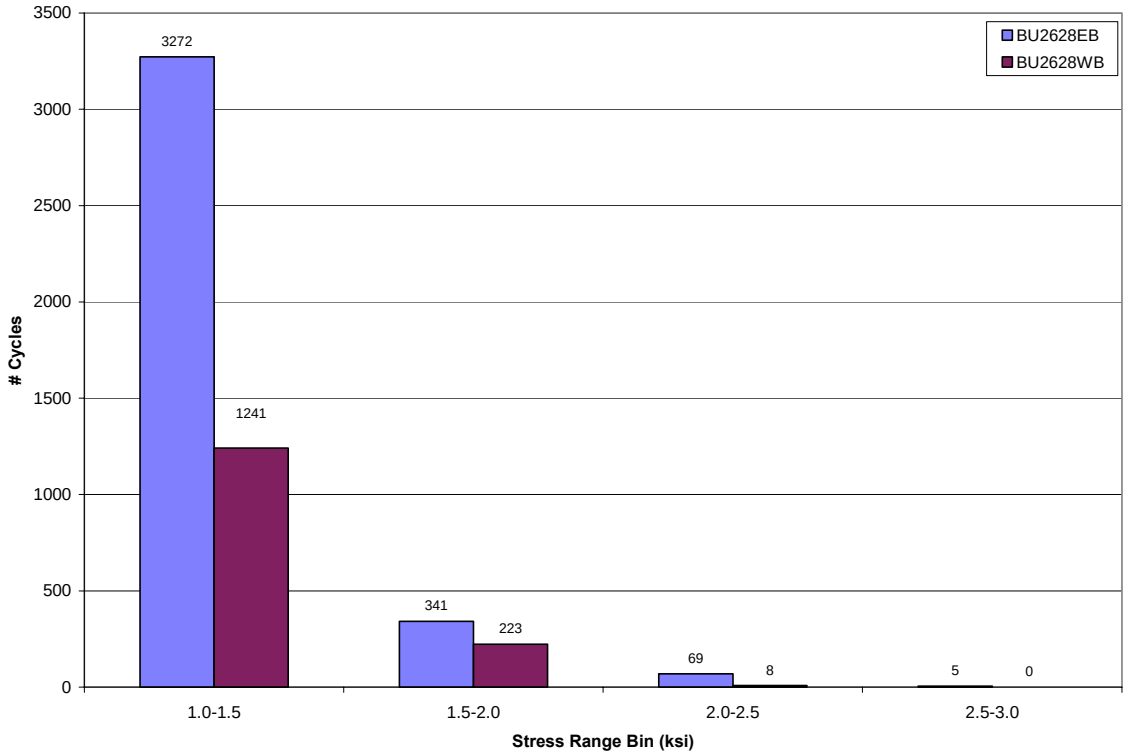

Figure 6.11: Stress-range histogram for BU2628EB and BU2628WB (Winter 2005)

6.2.2 Diagonal Response

A gage from each instrumented diagonal was monitored during the winter of 2005. These diagonals are located near pier 2 between panel points U18 and L19 and between U20 and L21. As noted in Table 6.7, the gage on the east flange plate of U20-L21 West (DW2021WE) was not producing reliable data. Most gages were installed nearly four years ago, and it was expected that some of them would become defective.

Table 6.10 summarizes the calculated maximum stress range and effective stress range for each of the three functioning diagonal gages. Similar to previous data collected, no cycles greater than the CAFL were reported. Both the east and west diagonals between U18 and L19 experience a similar number of cycles greater than 1.0 ksi each day. It is reasonable to assume an infinite fatigue life for these diagonals. A stress-range histogram for the diagonals is shown in Figure 6.12. DW1819EE and DW1819WE have a similar number of stress cycles in each bin, consistent with previous data. It appears that DW2021EW has more significant cycles than the diagonals at U18-L19.

Channel	Fatigue Life Calculation Summary						
	SR_{max} ksi	Cycles > CAFL #	Cycles > CAFL %	SR_{eff} ksi	Cycles/day	Remaining Life (years)	Category
DW1819EE	2.4	0	0	1.3	183	Infinite	B
DW1819WE	2.1	0	0	1.3	183	Infinite	B
DW2021EW	2.0	0	0	1.3	323	Infinite	B
DW2021WE	-	-	-	-	-	-	B

Note:
1. The effective stress range and cycles per day calculations ignore cycles less than 1.0 ksi
2. The CAFL for a category B detail is 16.0 ksi

Table 6.10: Summary of maximum and effective stress ranges for diagonal gages (Winter 2005)

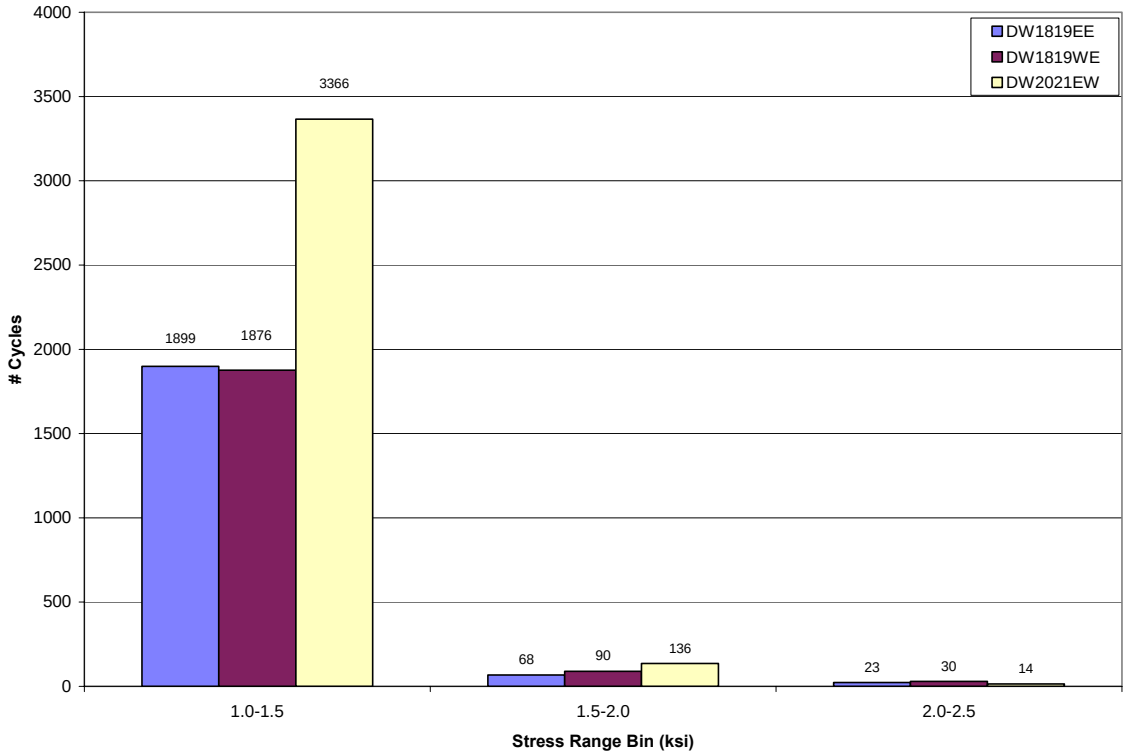

Figure 6.12: Stress-range histogram for DW1819EE, DW1819WE, and DW2021EW (Winter 2005)

The peak stress range response for DW2021EW is displayed in Figure 6.13. The diagonal experienced a stress cycle of 2.0 ksi caused by a vehicle traveling northbound in Lane 4 at 8:42 AM on February 8, 2005.

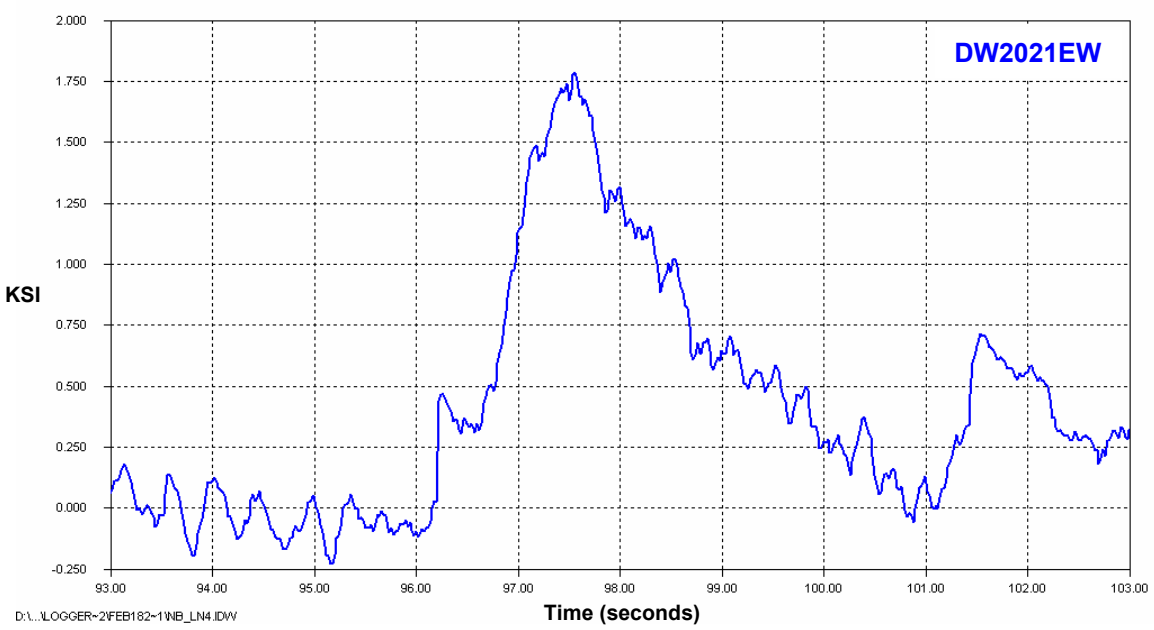

Figure 6.13: Maximum stress cycle for DW2021EW (Winter 2005)

6.2.3 Lower Chord Response

Unfortunately the quality of the lower chord gages has deteriorated to the point where reliable data is no longer available. These gages are identified in Table 6.7. This could be due to the very long wire lengths and nearly four years of exposure to rain, snow, and other weather-related elements. Although no dependable data could be reported for the lower chords during this monitoring period, it is reasonable to assume from previous data and the behavior of the other members (i.e., upper chords and diagonals) that these members will have infinite fatigue life.

6.2.4 Stringer Response

A total of nine (9) stringers were monitored during the winter of 2005. These included stringers above pier 2 between panel points U16 and U18 and stringers near midspan of span 2 between U26 and U28. Fatigue life calculations for these stringers are presented in Table 6.11. Similar to the previous data collection interval for the summer of 2004, no stress cycles greater than the CAFL were discovered. Furthermore, the stringers near midspan (S1BCL to S5BCL) appear to experience more stress cycles greater than 1.0 ksi. This is consistent with previous data and the smaller cross-sectional area of the bridge near midspan of span 2. A stress-range histogram for S6BCL and S7BCL is reported in Figure 6.14. Stringer 7 appears to have more significant stress cycles. This is consistent with data for stringers 3 and 4 near midspan (see Figure 6.9). The location of stringer 7 allows for more considerable responses to vehicles traveling in either Lane 4 or Lane 5. On the other hand, stringer 6 is more susceptible to loading in Lane 4.

Channel	Fatigue Life Calculation Summary						
	SR_{max} ksi	Cycles > CAFL		SR_{eff} ksi	Cycles/day	Remaining Life (years)	Category
		#	%				
S3BOC	1.1	0	0	1.3	12	Infinite	C
S6BCL	3.4	0	0	1.5	115	Infinite	C
S7BCL	2.7	0	0	1.4	152	Infinite	C
S8BCL	1.7	0	0	1.4	16	Infinite	C
S1BCL	1.4	0	0	1.3	2	Infinite	C
S2BCL	2.4	0	0	1.3	60	Infinite	C
S3BCL	2.7	0	0	1.5	1073	Infinite	C
S4BCL	2.5	0	0	1.4	813	Infinite	C
S5BCL	1.8	0	0	1.3	56	Infinite	C

Note:
1. The effective stress range and cycles per day calculations ignore cycles less than 1.0 ksi
2. The CAFL for a category C detail is 10.0 ksi

Table 6.11: Summary of maximum and effective stress ranges for stringer gages (Winter 2005)

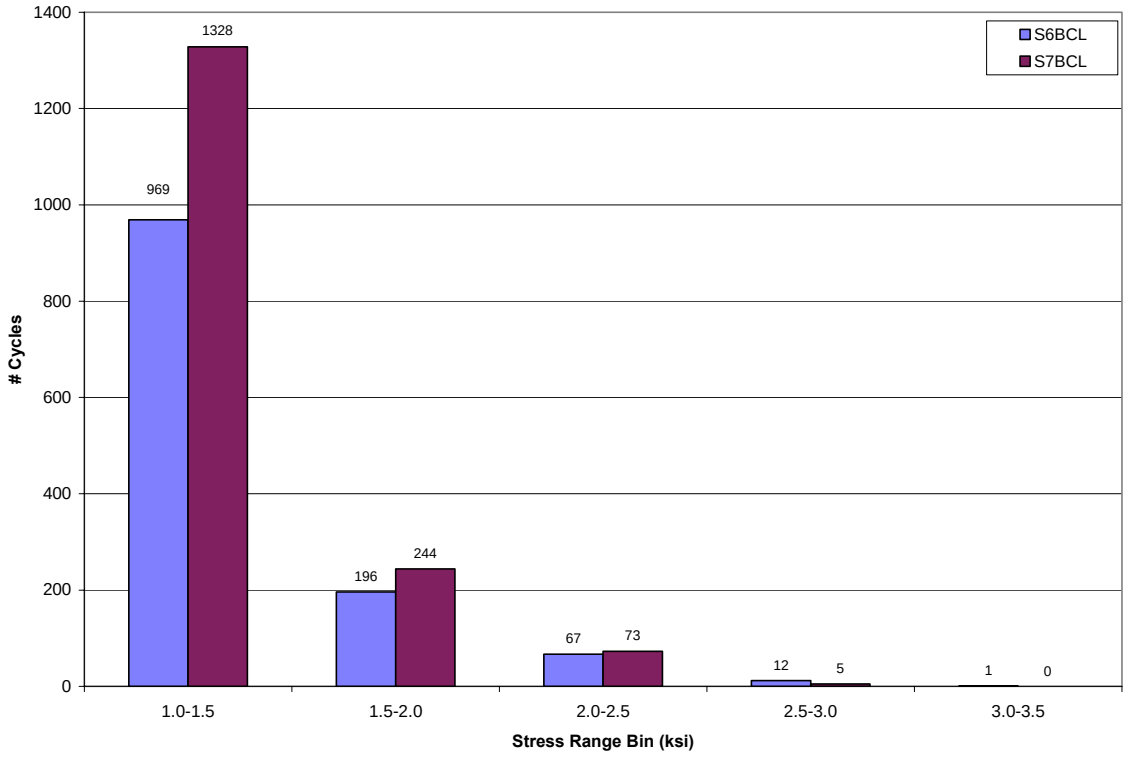

Figure 6.14: Stress-range histogram for S6BCL and S7BCL (Winter 2005)

Stringer 6 experienced a maximum stress range of 3.4 ksi during this data collection period. This response and the response of stringer 7 are shown in Figure 6.15. A vehicle traveling northbound in Lane 4 caused the responses of the stringers shown in Figure 6.15 on February 10, 2005 at 7:23 AM. Both stringers 6 and 7 are located directly underneath Lane 4, and the transverse vehicle position along with the magnitude of the axle loads triggered this significant local bending response.

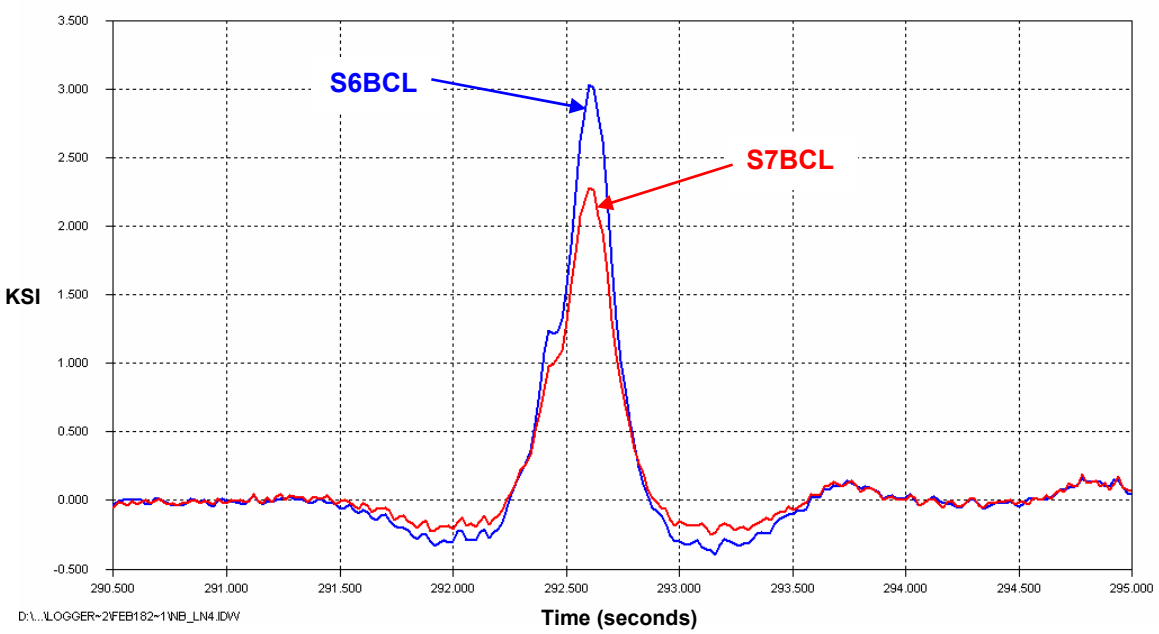

Figure 6.15: Maximum stress cycle for S6BCL (Winter 2005)

6.2.5 Sway Bracing Response

The long-term response of three (3) sway bracing gages were monitored. These members are located near midspan of span 2 between panel points U24 and L25 of the truss. The gage on the bottom flange of the horizontal strut at L25 (SB2425HB) was not producing reliable data. The fatigue life calculation summary for the sway bracing is reviewed in Table 6.12. No cycles greater than the CAFL of the members were discovered during this monitoring period. Therefore, infinite fatigue life for the sway bracing studied is expected. Both crosses of the sway bracing at U24-L25 experience a similar number of cycles larger than 1.0 ksi per day. The stress-range histogram for SB2425ET and SB2425WB is shown in Figure 6.16. Both functioning sway brace gages have nearly identical number of cycles in each stress range bin. Similar to the lower chords, the response of the sway bracing to live load is independent of the direction of traffic on the bridge (i.e., northbound or southbound). This is illustrated for both SB2425ET and SB2425WB in Figure 6.17.

Channel	Fatigue Life Calculation Summary						
	SR_{max} ksi	Cycles > CAFL #	Cycles > CAFL %	SR_{eff} ksi	Cycles/day	Remaining Life (years)	Category
SB2425ET	1.8	0	0	1.3	179	Infinite	B
SB2425WB	1.7	0	0	1.3	172	Infinite	B
SB2425HB	-	-	-	-	-	-	B

Note:
1. The effective stress range and cycles per day calculations ignore cycles less than 1.0 ksi
2. The CAFL for a category B detail is 16.0 ksi

Table 6.12: Summary of maximum and effective stress ranges for sway bracing gages (Winter 2005)

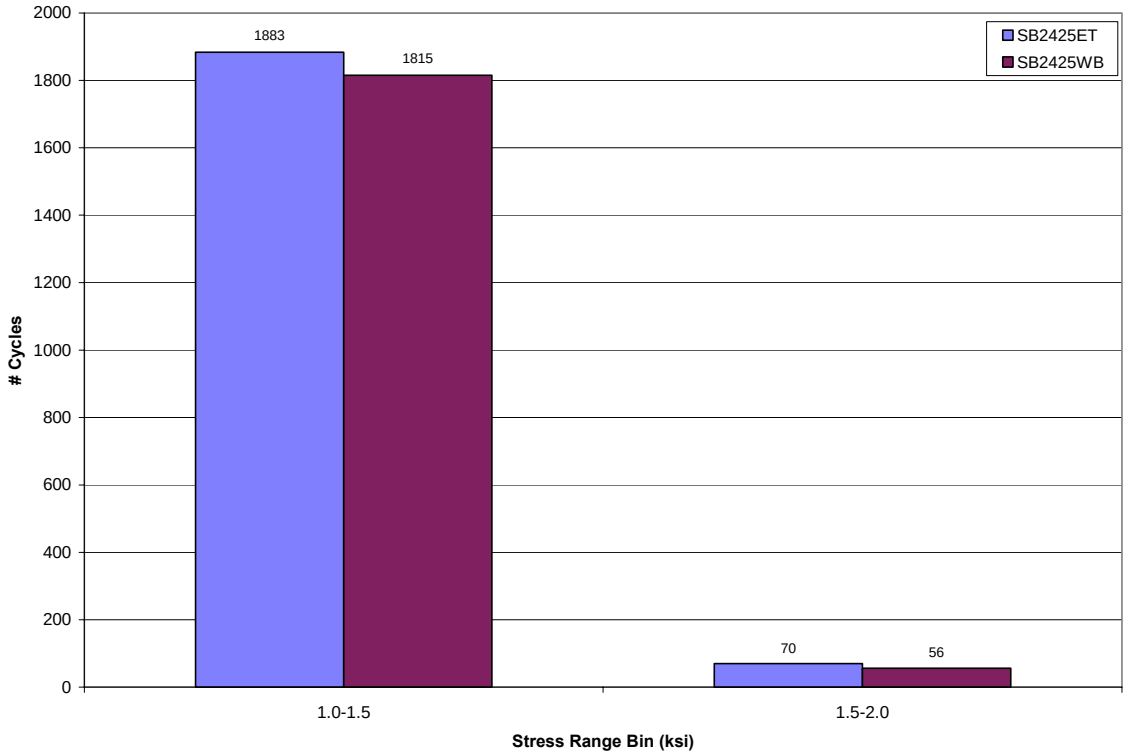

Figure 6.16: Stress-range histogram for SB2425ET and SB2425WB (Winter 2005)

The gage on the bottom flange of the west cross of the sway brace (SB2425WB) experienced a maximum stress range of 1.7 ksi. This was caused by a vehicle traveling southbound in Lane 2 and occurred on February 10, 2005 at 1:11 PM. This response and the response of SB2425ET are portrayed in Figure 6.17.

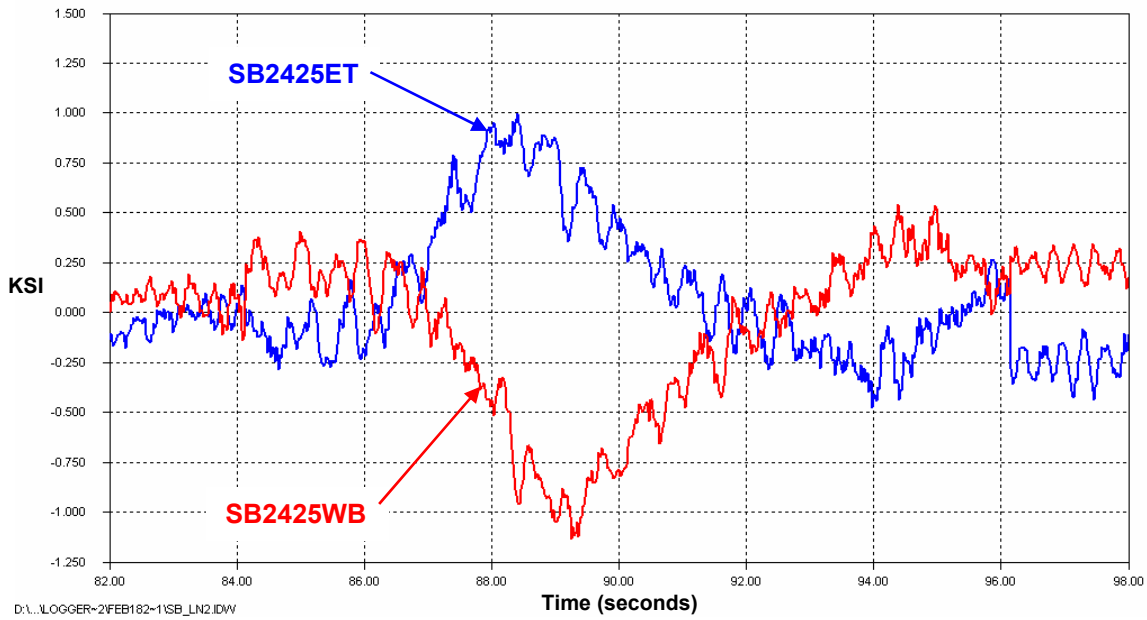

Figure 6.17: Maximum stress cycle for SB2425WB (Winter 2005)

6.3 Summary of Long-Term Live Load Monitoring

Two periods of data were collected and analyzed to study the long-term behavior of selected truss members subjected to live load. The first time period consisted of data from June 21, 2004 to August 30, 2004. The second period included data from February 7, 2005 to February 18, 2005. A comparison of fatigue life calculations for gages common between the two monitoring phases is presented in Table 6.13. There are little differences, if any, in the calculated effective stress ranges for each of the gages common to the two monitoring periods. The most notable differences are in the cycles per day in excess of 1.0 ksi. However, this can be attributed to the different times of year for which data were collected. Also, the shorter duration of monitoring in February 2005 (11 days) could also have an effect on the discrepancies in cycles per day.

Channel	Summer 2004		Winter 2005	
	SR_{eff} (ksi)	Cycles/day	SR_{eff} (ksi)	Cycles/day
BU1618EB	1.3	27	1.3	26
BU1618WB	1.3	33	1.3	25
BU2628EB	1.3	360	1.4	338
BU2628WB	1.4	167	1.4	135
DW1819EE	1.3	183	1.3	183
DW1819WE	1.3	185	1.3	183
DW2021EW	1.3	298	1.3	323
S6BCL	1.5	110	1.5	115
S7BCL	1.5	149	1.4	152
S8BCL	1.3	20	1.4	16
S1BCL	1.3	5	1.3	2
S2BCL	1.4	84	1.3	60
S3BCL	1.5	1280	1.5	1073
S4BCL	1.5	925	1.4	813
S5BCL	1.3	79	1.3	56

Note:
1. The effective stress range and cycles per day calculations ignore cycles less than 1.0 ksi

Table 6.13: Comparison of fatigue life calculations for the two long-term monitoring periods

Overall, the data collected over the two monitoring phases suggests that the structure will have infinite fatigue life for the members instrumented and analyzed. No stress cycles greater than the constant amplitude fatigue limit (CAFL) were recorded for each respective member.

7.0 Summary and Conclusions

Additional instrumentation has been installed on the SR-33 truss bridge near midspan of span 2 (U26-U28) as discussed in Section 3.2 of this Final Report. This instrumentation was utilized to help researchers further understand behavior of the bridge under vehicular live load. The power upgrade utilizing the bridge lighting system has been completed and allowed researchers to collect longer periods of live load data.

The effects of temperature and strain on instrumented truss members were investigated for a 38-month period beginning in January 2002 (the bridge was opened to traffic in January 2002). The temperature behavior for instrumented members was as expected. Temperatures increase in the summer months and decrease during the winter. Gages more directly exposed to sunlight exhibit a higher temperature response than those shaded by the deck or the member itself. The temperature response of multiple gages on a single member is very similar as anticipated. The truss experiences differential heating as revealed through the instrumentation. Certain members (i.e. upper chords) heat up and cool down at different rates than other members (i.e. diagonals and lower chords). Rapid increases in temperature occurred for some members in the data and their validity was confirmed by weather station temperature data.

The relationship between temperature and strain was not consistent for all instrumented members throughout the period of data retrieval. The upper chords and lower chords were observed to be the most consistent members in this respect. Unfortunately, an overall behavior was not determined for other members such as the stringers or sway bracing due to the number of gages which were not producing reliable data. Overall, most instrumented members appear to have experienced a gradual and slight increase in microstrain over time. The increases in microstrain appear to be "leveling off", consistent with expected long-term (first 1-3 years) behavior of concrete due to creep.

Limited live load data were collected for a period of time on August 8, 2003. The data were collected to verify that the behavior of instrumented members was consistent with the behavior determined in Phase I. It was found that the response of the members was consistent with the results of the controlled live load testing (Connor and Santosuosso, 2002). The upper chords above pier 2 (U16-U18) and the newly instrumented upper chords near midspan of span 2 (U26-U28) exhibited primarily a local bending response to live load. The axial response of the lower chords observed in Phase I could not be verified. However, it is reasonable to assume the lower chords continue to display predominantly a global axial response to live load. The instrumented diagonals portrayed an axial response to live load as expected. The stringers between U26 and U28 exhibited a local bending response under live load, similar to the stringers between U16 and U18.

Stress-range histograms were developed for various members of the bridge superstructure. The data collected suggest that the bridge experiences very small stress ranges due to live load. No stress ranges greater than the CAFL of the members investigated were found. Therefore, the bridge should have infinite fatigue life against anticipated design loads (i.e., in-plane live loading) for the members studied.

Acknowledgements

This work was conducted for the Pennsylvania Department of Transportation as part of the construction contract for SR-33 Lehigh River Bridge built by Dick Corporation of Pittsburgh, PA and American Bridge of Coraopolis, PA. Funding was provided by the Pennsylvania Department of Transportation (Penn DOT), the Federal Highway Administration (FHWA), and the Pennsylvania Infrastructure Technology Alliance (PITA).

Thanks are due to Mr. Vince Delmonte with Dick Corporation, American Bridge Corporation, and Structural Services Inc. for their support during the on-site field work portions of the research. The technical input of Mr. John Lang, P.E. and Mr. John Tarquinio, P.E. of URS Corporation, Mr. Tom Macioce, P.E. of Penn DOT Central Office Bridge Division, and Mr. Karl Kroboth, P.E. and Mr. Kamlesh Ashar, P.E. of Penn DOT District 5-0 are greatly appreciated. The authors would also like to thank Mr. Mike Adams of Campbell Scientific, Inc. with regards to technical input on the CR5000 and CR9000 data loggers.

The authors would like to recognize Mr. Carl Bowman, ATLSS Instrumentation Technician; Mr. Ian Hodgson, S.E., P.E., ATLSS Research Engineer; Mr. Michael Urban, ATLSS Graduate Research Assistant; Mr. Brian Santosuosso, former ATLSS Graduate Research Assistant; and Mr. Bob Alpago, P.E., ATLSS Associate Director; for their efforts related to field instrumentation, data reduction, project coordination and development of the data acquisition system.

The authors would also like to acknowledge the efforts of Penn DOT crane operators Mr. Mark Civitarese and Mr. John Pearson for their professional workmanship, adherence to safety, and making additional instrumentation of the bridge possible. The cooperation of Ms. Paula Burke and all the security staff at Summit Property Management with regards to instrumentation on Martin Tower are also appreciated.

References

Connor, Robert J. and Santosuosso, Brian J., "Field Measurements and Controlled Load Testing of the Lehigh River Bridge (SR-33)", Lehigh University, ATLSS Report 02-07, October 2002.

Downing, S.D., Socie, D.F., "Simple Rainflow Counting Algorithms", International Journal of Fatigue, January 1982.

Santosuosso, Brian J., "Analytical Investigation of Assumptions Used to Design the SR 33 Lehigh River Bridge", Thesis completed in September 2002 in partial fulfillment of MS degree requirements, Lehigh University, Bethlehem, PA, supervised by Prof. Stephen Pessiki

Smith, Steven W., "The Scientist's and Engineer's Guide to Digital Signal Processing", 2nd Edition, California Technical Publishing, San Diego, CA, 1999.